Energy transfer in Photosystem II

DISSERTATION
zur Erlangung des akademischen Grades des
Doktors der Naturwissenschaften
(Dr. rer. nat.)

eingereicht am
Fachbereich Biologie, Chemie, Pharmazie

FREIE UNIVERSITÄT BERLIN

vorgelegt von
Magister Grzegorz Raszewski
aus Warschau

Juni 2008

1. Gutachter: Dr. Thomas Renger, FU Berlin

2. Gutachter: Prof. Dr. Ernst-Walter Knapp, FU Berlin

Disputation am 18.09.2008

Contents

Chapter 1

Introduction

Photosystems are complex biological systems that are able to convert light into an electrochemical potential. Among all of photosystems, photosystem II (PS2) is unique in the sense that it is able to create such high redox potential that it is capable of oxidizing water to molecular oxygen. PS2 is a very large protein complex that is located in the thylakoid membrane of higher plants, algae and cyanobacteria. The PS2 core complex consists of several subunits, of which only 3 harbor chlorophylls (Chls) and phephytins (Pheos). These three subunits are: the reaction center (RC) and the 2 antenna complexes CP43 and CP47. The RC harbors 6 Chls and 2 Pheos, while CP43 contain 13 Chls and CP47 16 Chls. Two Chls of the RC (P_{D1} and P_{D2}) create the so called "special pair", which due to the relatively small distance between the pigments ($\sim$8Å) is the strongest coupled pigment pair in the whole PS2 core complex. The overall arrangement of pigments in the PS2 is shown in figure 1.1. Pigments in the antenna are organized in a two layer structure, one layer on the lumenal and one layer on the stromal part of the thylakoid membrane. Pigments in the RC creating two almost perfectly symmetrical branches D1 and D2 as indicated in the Fig. 1.2. The D1 is an "active" branch, in the meaning that only pigments belonging to this branch transfer electrons.

Antenna complexes CP43 and CP47 are responsible for absorption of light and transfer of the excitation energy to the RC. In the RC the excited state so-called $P680^*$ is created, that leads to the charge separation. An electron released from the primary electron donor is transferred to the Pheo of the active branch ($Pheo_{D1}$). From $Pheo_{D1}$ the electron is transferred to the plastoquinone Q_A. The hole stabilizes on P_{D1}, creating the $P680^+$ state, that is subsequently reduced via the redox-active tyrosine Tyr_Z by an electron from the manganese cluster. The latter catalyzes the oxidation of water to oxygen. The electron from Q_A is transferred to the plastoquinone Q_B, and after two cycles, the doubly reduced and protonated Q_B is released to the thylakoid membrane.

Although the overall reaction scheme is clear, the molecular identities of some of the functional states and the mechanistic and kinetic details are not. These aspects will be discussed in detail later in this work. Here I just want to highlight the most important issues.

Both antenna complexes as well as the RC complex of PS2 can be biochemically separated from each other. Such treatment allows to measure their spectroscopic properties separately and consequently makes an interpretation of optical spectra easier. Nevertheless the spectroscopic properties of PS2 are not fully understood yet. The main problem is that due to the excitonic coupling between the pigments, a pigment has contribution in more than one optical band and it is not clear how the local protein environment tunes the transition energies of the pigments, the so-called site energies. Site energies are energies at which the pigments would absorb if they were not coupled to other pigments. Due to the delocalization caused by the excitonic coupling, the pigments can however absorb at different energies than their site energies. To determine site energies one can apply a theory of optical spectra and treat the site energies as

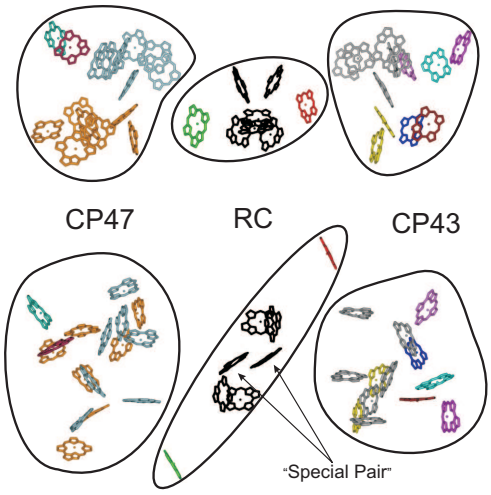

Figure 1.1: Arrangement of pigments in the PS2. *Top* View from the side of the thylakoid membrane on the PS2 pigments. Stroma is on the top, lumen on the bottom. Pigments of the antenna complexes CP43 (right) and CP47 (left) create a clearly visible two layer structure. *Bottom* View form the top of the thylakoid membrane on the PS2 pigments. Stroma is in front of the figure, lumen is in the back of the figure.

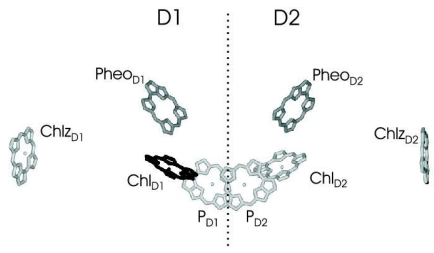

Figure 1.2: Arrangement of pigments in the RC. Active D1-branch is on the left side of the figure, while inactive D2-branch on the right side.

free parameters that are fitted to the experimental data. This procedure proved to be a very successful. In principle one can also determine site energies directly from the atomic structure of the protein, indeed first successful attempts of such treatment have been made (Müh et al., 2007). Understanding of the spectroscopic properties of the PS2 allows to answer fundamental questions regarding the mechanism of energy and electron transfer in PS2. The most important of these questions are: which pigment(s) act(s) as primary electron donor(s) in PS2 and what is the *bottleneck* of the decay of excited state i.e. in which way energy transfer from antenna to the RC is limited.

Regarding the primary electron donor, accumulating evidence is found that the accessory Chl of the D1-branch (Chl_{D1}) acts as primary electron donor (Groot et al., 2005; Holzwarth et al., 2006; Novoderezhkin et al., 2005), however still different opinions are found in the literature suggesting that "special pair" pigments may play this role (Novoderezhkin et al., 2005; Krausz et al., 2005). To answer these questions one must provide a working model of the RC, that is a theoretical model that is capable to describe the optical properties of the RC. At least three such models were proposed: a multimer model in which all pigments have the same site energies, and are excitonicaly coupled (creating delocalized states) (Durrant et al., 1995; Renger et al., 2002a; Barter et al., 2003), a monomer model in which all pigments are not excitonicaly coupled, apart form "special pair" pigments (P_{D1} & P_{D2}) and a pentamer model, which is a multimer model with decoupled pheophytin of the inactive D2 branch (Jankowiak et al., 1999).

Both antenna complexes were studied in great details by several groups (Groot et al., 1999; de Weerd et al., 2002; Groot et al., 1995; Alfonso et al., 1994; van Dorsson et al., 1987; Jankowiak et al., 2000; Hughes et al., 2006), suggesting existence of the several trap states (low energy states that can "trap" excitation energy) in each complex. In CP43 complex is it known that these trap states are most likely located on different layers of the membrane. There is evidence for the localization of the lowest excited state in PS2 on a peripheral pigment of the CP47 complex (Shen et al., 1994; de Weerd et al., 2002). However, apart from the latter precise location of remaining trap states in PS2 and their function is unknown. Another puzzle is why only some of these trap states show a triplet minus singlet signal (difference between absorption spectrum of complex with and without pigment(s) being in a triplet state), while others do not. One would expect due to the thermal distribution of energy the lowest energy pigment to have a dominant contribution to the triplet state, this is not the case in both the CP47 and the CP43 complex. Quenching of the triplet state by the β-carotene located next to the low energy pigment(s) was suggested as mechanism preventing stabilization of the triplet state. It is also not clear why energy relaxation after light excitation is about five times slower at low temperature in the CP47 than in the CP43 complex (50 ps. and 10 ps. respectively).

As it was mentioned above it is unknown in which way the excitation energy is transferred from the antenna to the RC in PS2. Several models were proposed, historically the earliest one was the so-called excited state radical pair equilibrium (ERPE) model (Schatz et al., 1987, 1988; Barter et al., 2001; Miloslavina et al., 2006; Holzwarth et al., 2006) that assumes the equilibration of excited states in the whole core complex to be fast compared to the primary electron transfer reaction in the RC. This model was used to explain several experiments (Schatz et al., 1987, 1988; Barter et al., 2001). This is the so-called trap limited model. However this model was not able to explain relatively slow excitation energy transfer from antenna to RC reported by several groups (Broess et al., 2006; Jennings et al., 2000; Pawlowicz et al., 2007) and fast electron transfer measured in the RC (Groot et al., 2005). In these cases the decay of excited states was infered to be limited by the transfer to the trap, it is the so-call transfer-to-the-trap limited model. Another model proposed by Andrizhiyevskaya et al. (2004) assumes that the decay of the excited states is neither transfer-to-the-trap nor trap limited, but excitation energy transfer and primary charge transfer occur on a similar time scale. The path on which excitation energy is transferred from antenna to RC is also not known. It is unclear if energy is transferred

simultaneously from stromal and lumenal side of both antenna or only from one layer of each complex.

Apart from all these problems one also has to keep in mind that it is not entirely sure if biochemical separation of the subcomplexes (RC,CP43,CP47) from PS2 does not alter the structure and consequently the spectroscopic properties of these complexes. This point has been raised ever since D1-D2-cyt$b$559 preparations became available (see e.g. Renger et al. (2005) and references therein).

This thesis is organized in the following way. First an overview of the theory used is given. In the next chapter the optical properties of the isolated RC are explained allowing to identify the localization of the primary electron donor and the localization of the triplet state. The following chapter is focused on the spectroscopic properties of the RC of PS2 core complexes using parameters (like site energies) obtained in the previous chapter for the isolated RC complex. The localization of the primary electron donor, the triplet state as well as the identities of the radical-pairs (e.g. $P^+_{D1}Pheo^-_{D1}$) in the RC of PS2 core complexes are determined. The next chapter deals with the identity and function of the trap states in the CP43 and the CP47 antenna complexes and the energy transfer paths from the antenna to the RC. The localization of the lowest energy state in the PS2 is confirmed, the identity of other trap states as well as their function are revealed. The excitation energy transfer in the whole PS2 and electron transfer in the RC is studied, allowing to find the *bottleneck* for the decay of excited state, i.e. answer to the question which of the proposed models (trap limited, transfer-to-the-trap limited or neither of both) is valid in PS2. In the end of this chapter a new mechanism for photoprotection in PS2 that arose from the calculations will be presented. Every chapter in this work, apart of the theory part, starts with an overview of the problems that are addressed, followed by the results and a discussion section. An overall summary is given in the end of this thesis.

Chapter 2

Theory of optical spectra and exciton energy transfer

In this chapter I want to the present theory used for the calculation of the optical spectra. In the beginning the Hamiltonian of the pigment-protein complex will be introduced, followed by the theory of the linear optical spectra. Next excitation energy transfer between pigments and pigment aggregates will be presented. Theory describing the time resolved pump-probe spectra will be introduced in the next part, followed by the theory of electron transfer in the RC. Several models of the energy transfer between different subunits of the PS2 will be introduced. In the end the parameters used for calculations of the optical spectra as well as genetic algorithm used for determination of the site-energies will be described.

2.1 Hamiltonian

The Chls of the pigment-protein complex (PPC) are described as two-level systems including their ground (S_0)- and excited (S_1)-state. The Hamiltonian of the PPC contains four parts

$$H = H_{\rm ex} + H_{\rm ex-vib} + H_{\rm vib} + H_{\rm ex-rad}\,. \tag{2.1}$$

$H_{\rm ex}$ is the excitonic Hamiltonian containing the low energy optical transition energies of the pigments and the excitonic coupling between them. The vibrational Hamiltonian $H_{\rm vib}$ describes the vibrational dynamics of the protein. The exciton-vibrational Hamiltonian $H_{\rm ex-vib}$ describes coupling between excitons and vibrations of the protein, while the exciton-radiational coupling Hamiltonian $H_{\rm ex-rad}$ describes coupling of the excitons to the external electromagnetic field.

2.1.1 Excitonic Hamiltonian $H_{\rm ex}$

The excitonic part $H_{\rm ex}$ contains the energies of the localized one- and two-exciton states $|m>$ and $|mn>$, respectively, and the excitonic couplings $V_{10,01}$ between different one- and two-exciton states

$$\begin{aligned} H_{\rm ex} &= E_m|m><m| + \sum_{m>n}(E_m + E_n + \delta^{(2{\rm exc})}_{mn})|mn><mn| \\ &+ \sum_{m,n} V_{10,01}(m,n)|m><n| + \sum_{m>n}\sum_{k} V_{10,01}(m,k)|mn><kn|\,. \end{aligned} \tag{2.2}$$

In $|m>$, the mth pigment is excited and all others are in the ground S_0-state, whereas in $|mn>$, in addition to the mth pigment, the nth pigment is excited. Any double excitation of a single pigment (Renger et al., 1997) is neglected, for simplicity. The energies of the two-exciton states contain the two-exciton shift $\delta^{(2{\rm exc})}_{mn}$

$$\delta^{(2{\rm exc})}_{mn} = V_{11,11}(m,n) - V_{11,00}(m,n) - V_{00,11}(m,n) \tag{2.3}$$

that results from the charge density coupling between the pigments. The two-exciton shifts $\delta^{(2{\rm exc})}_{mn}$, which are usually neglected, are included in the present treatment, because they have an influence on the non-linear spectra. The charge density couplings that enter the two-exciton shifts as well as the excitonic couplings $V_{10,01}(m,n)$ are obtained by a method developed previously (Madjet et al., 2006) (see below).

2.1.2 Vibrational Hamiltonian $H_{\rm vib}$

The vibrational dynamics of the protein is described by a set of harmonic oscillators

$$H_{\rm vib} = \sum_{\xi} \frac{\hbar\omega_\xi}{4} Q_\xi^2 + T_{nucl} \tag{2.4}$$

where T_{nucl} is a kinetic energy of the nuclei and $Q_\xi = q_\xi\sqrt{\frac{2\omega_\xi}{\hbar}}$, ω_ξ is the frequency of the ξth oscillator and q_ξ denotes the mass-weighted normal coordinates of the ξth mode.

2.1.3 Exciton-vibrational coupling Hamiltonian $H_{\rm ex-vib}$

The exciton-vibration coupling is described by

$$H_{\rm ex-vib} = \sum_{\mu\nu} V_{\mu\nu}|\mu><\nu| \tag{2.5}$$

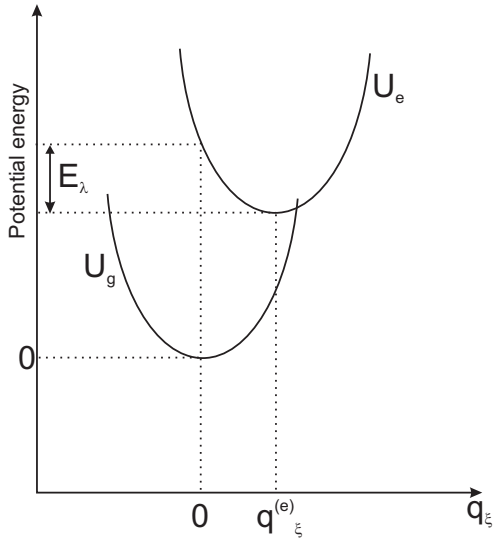

Figure 2.1: Potential energy surfaces of the ground (U_g) and excited (U_e) electronic state of a pigment in protein environment.

The operator $V_{\mu\nu}$ describes the coupling between one-exciton states $\mu = M$, $\nu = N$ and between two-exciton states $\mu = 2M$, $\nu = 2N$. It is expressed in the following way:

$$V_{MN} = \sum_{\xi} \sum_{m} c_m^{(M)} c_m^{(N)} \hbar\omega_\xi g_\xi^{(m)} Q_\xi \tag{2.6}$$

$$V_{2M2N} = \sum_{\xi} \sum_{m>n} c_{mn}^{(2M)} c_{mn}^{(2N)} \hbar\omega_\xi (g_\xi^{(m)} g_\xi^{(n)}) Q_\xi \tag{2.7}$$

where $c_m^{(M)}$ and $c_{mn}^{(2M)}$ are obtained from solutions of one- and two-exiton state eigenvalue problems. The dimensionless coupling constants $g_\xi^{(m)}$ read

$$g_\xi^{(m)} = \sqrt{\frac{\omega_\xi}{2\hbar}} \Delta q_\xi \tag{2.8}$$

where Δq_ξ is the difference of the minima of the potential energy surfaces (PES) for the electronic excited and ground state (Fig. 2.1).

The square of the coupling constants $g_\xi = g_\xi^{(m)}$, that are assumed to be the same for all sites m, enters the spectral density $J(\omega)$ of the exciton-vibrational coupling

$$J(\omega) = \sum_{\xi} g_\xi^2 \delta(\omega - \omega_\xi). \tag{2.9}$$

The spectral density is the key quantity for the optical spectra theory and will appear in all expressions for the optical spectra and energy transfer rate constants that will be discussed bellow.

2.1.4 Exciton-radiational coupling Hamiltonian $H_{\mathrm{ex-rad}}$

Coupling to the external field is described by $H_{\mathrm{ex-rad}}$ in the following way

$$H_{\mathrm{ex-rad}} = \sum_{\mu\nu} F_{\mu\nu}(t) |\mu><\nu| \tag{2.10}$$

with $F_{M0}(t)$ describing the radiative coupling of the ground state $|0>$ to the one-exciton state $|M>$ and $F_{2NM}(t)$ the coupling of the one-exciton state $|M>$ to the two-exciton state $|2N>$

$$F_{M0}(t) = -\sum_{s=pu,pr} E_{\Omega_s}(t)e^{-i\Omega_s t}\mu_M^{(s)} \tag{2.11}$$

$$F_{2NM}(t) = -\sum_{s=pu,pr} E_{\Omega_s}(t)e^{-i\Omega_s t}\mu_{M\to 2N}^{(s)} \tag{2.12}$$

The external field is described by the envelopes of $E_{\Omega_s}(t)$ of the pump (s=pu) and probe (s=pr) pulses with carrier frequencies Ω_s and their polarization vector $\vec{e_s}$. The dot products of $\vec{e_s}$ and the dipole moments of the excitonic transitions $\vec{\mu}_M$ and $\vec{\mu}_{M\to 2N}$ are denoted by $\mu_M^{(s)}$ and $\mu_{M\to 2N}^{(s)}$ as follows:

$$\mu_M^{(s)} = \vec{e_s}\vec{\mu}_M \equiv \vec{e}_s \sum_m c_m^{(M)}\vec{\mu}_m \tag{2.13}$$

$$\mu_{M\to 2N}^{(s)} = \vec{e_s}\vec{\mu}_{M\to 2N} \equiv \vec{e}_s \sum_{k>l} c_{kl}^{(2N)}(c_l^{(M)}\vec{\mu}_k + c_k^{(M)}\vec{\mu}_l) \tag{2.14}$$

where the local dipole moment $\vec{\mu}_m$ characterizes the $S_0 \to S_1$ transition of the pigment at site m, $\vec{\mu}_M$ is the dipole moment of the excitation of the one-exciton state $|M>$ and $\vec{\mu}_{M\to 2N}$ is the dipole moment of the optical transition from the one-exciton state $|M>$ to the two-exciton state $|2N>$.

2.1.5 Domains of strongly coupled pigments

If the excitonic coupling between the optical transitions of the pigments is larger than the static and dynamic disorder by the pigment-protein coupling, a delocalized excited state is formed. The localization of exciton states by static disorder in site energies is included in the calculations by a Monte Carlo method used to generate the disorder and to average the spectra obtained for the different sets of site energies. Dynamic localization is modeled implicitly by allowing delocalization only between those pigments, for which the excitonic coupling is comparable or stronger than the local dynamic disorder. A quantitative measure of the latter is the reorganization energy of the optical transition

$$E_\lambda = \int d\omega \hbar\omega J(\omega) = \hbar \sum_\xi \omega_\xi (g_\xi^{(m)})^2 \,, \tag{2.15}$$

that describes the energy that is released when the nuclei relax to a new equilibrium position after optical excitation of a pigment. The coupling constants g_ξ are related to the mutual shift in minimum position of the ground and excited state potential energy surface (eq. 2.8 and Fig. 2.1) If two pigments m and n are coupled by an excitonic coupling $V_{1001}(m,n)$ that is comparable or larger than the reorganization energy E_λ, they are included in the same domain d. One-exciton states

$$|M_d> = \sum_{m_d} c_{m_d}^{(M_d)}|m_d> \tag{2.16}$$

and two-exciton states

$$|2M_d> = \frac{1}{2}\sum_{m_d \neq n_d} c_{m_d n_d}^{(2M_d)}|m_d n_d> \tag{2.17}$$

are obtained for the pigments in one domain by diagonalization of the exciton Hamiltonian that contains in the diagonal the site energies and in the off-diagonal the excitonic couplings. After

this diagonalization, the exciton Hamiltonian $H_{\rm ex}$ in eq 2.2 becomes

$$\begin{aligned} H_{\rm ex} &= \sum_d \sum_{M_d} \mathcal{E}_{M_d} |M_d><M_d| + \sum_{2M_d} \mathcal{E}_{2M_d} |2M_d><2M_d| \\ &+ \sum_{a\neq b} \sum_{M_a,N_b} V_{M_a N_b} |M_a><N_b| \end{aligned} \tag{2.18}$$

with the energies of the delocalized one- and two-exciton states $\mathcal{E}_{M_d}$ and $\mathcal{E}_{2M_d}$, respectively, and the coupling $V_{M_a N_b}$ between delocalized one-exciton states $|M_a>$ and $|N_b>$ in different domains a and b, respectively,

$$V_{M_a N_b} = \sum_{m_a,n_b} c_{m_a}^{(M_a)} c_{n_b}^{(N_b)} V_{10,01}(m_a n_b)\,, \tag{2.19}$$

where $V_{1001}(m_a n_b)$ is the excitonic coupling between the optical transitions of pigment m_a in domain a and n_b in b. In the present limit of low pump intensities a population of two-exciton states can be neglected. Therefore, it is not necessary to take into account the coupling between two-exciton states in different domains.

2.2 Linear optical spectra

The linear optical spectra are obtained as a sum over the domain spectra. The absorption spectrum $\alpha(\omega)$ follows as

$$\alpha(\omega) = \sum_d \alpha_d(\omega) = \sum_d \langle \alpha_d^{(\rm hom)}(\omega)\rangle_{\rm dis} \tag{2.20}$$

where $\langle ...\rangle_{\rm dis}$ denotes an average over the disorder in site energies.

The disorder average is performed numerically by a Monte Carlo method. The homogeneous absorption of domain d is obtained as

$$\alpha_d^{(\rm hom)}(\omega) \propto \omega \sum_{M_d} |\mu_{M_d}|^2 D_{M_d}(\omega)\,, \tag{2.21}$$

where the transition dipole moment is given as

$$\vec{\mu}_{M_d} = \sum_{m_d} c_{m_d}^{(M_d)} \vec{\mu}_{m_d}\,. \tag{2.22}$$

The lineshape function $D_{M_d}(\omega)$ was obtained from a non-Markovian POP-lineshape theory within secular approximation and Markov approximation for the off-diagonal elements of the exciton-vibrational coupling:(Renger et al., 2002)

$$D_{M_d}(\omega) = \frac{1}{2\pi} \int_{-\infty}^{\infty} dt e^{i(\omega-\tilde{\omega}_{M_d 0})t}\; e^{G_{M_d}(t) - G_{M_d}(0)} e^{-|t|/\tau_{M_d}}\,. \tag{2.23}$$

The time-dependent function $G_{M_d}(t)$ describes the vibrational sideband of the exciton transition, the dephasing time τ_{M_d} that describes the life-time broadening due to exciton relaxation, and $\tilde{\omega}_{M_d 0}$ is the transition frequency that is shifted from the exciton transition frequency $\omega_{M_d 0}$ by the exciton-vibrational coupling (Renger et al., 2000, 2002). All of these quantities depend on the exciton coefficients $c_m^{(M)}$, the spectral density $J(\omega)$ as introduced in eq. 2.9, the correlation radius of protein vibrations R_c (Renger et al., 2001, 2002, 1998), and the mean number of vibrational quanta $n(\omega)$ that are excited at a given temperature (Bose-Einstein distribution function).

The time-dependent function $G_{M_d}(t)$ entering the line shape function in eq 2.23 is following.

$$G_{M_d}(t) = \gamma_{M_d M_d} G(t) \tag{2.24}$$

contains

$$G(t) = \int_0^\infty d\omega \{(1 + n(\omega))J(\omega)e^{-i\omega t} + n(\omega)J(\omega)e^{i\omega t}\}\,, \tag{2.25}$$

and the diagonal part of

$$\gamma_{M_d N_d} = \sum_{m_d, n_d} c_{m_d}^{(M_d)} c_{n_d}^{(N_d)} c_{m_d}^{(N_d)} c_{n_d}^{(M_d)} e^{-R_{m_d n_d}/R_c}\,. \tag{2.26}$$

The R_c in eq 2.26 is the correlation radius of protein vibrations (Renger et al., 2001, 2002, 1998) and $R_{m_d n_d}$ the center to center distance between pigments m_d and n_d. The

$$n(\omega) = \frac{1}{e^{\hbar\omega/kT} - 1} \tag{2.27}$$

in eq 2.25 denotes the mean number of vibrational quanta that are excited at a given temperature T. The dephasing time τ_{M_d} in eq 2.23 contains the life time broadening due to exciton relaxation between the state $|M_d>$ and the other delocalized states $|N_d>$ in the same domain d

$$\tau_{M_d} = \frac{1}{2} \sum_{N_d}^{N_d \neq M_d} k_{M_d \to N_d} \tag{2.28}$$

with the Redfield rate constant $k_{M_d \to N_d}$, given in eq 2.37 that contains the $\gamma_{M_d N_d}$ in eq 2.26 and the $n(\omega)$ in eq 2.27.

The frequency $\tilde{\omega}_{M_d 0}$ is the transition frequency between the ground state $|0>$ and the one-exciton state $|M_d>$ that contains a renormalization due to the diagonal and off-diagonal parts of the exciton-vibrational coupling (Renger et al., 2002, 2000),

$$\begin{aligned} \tilde{\omega}_{M_d 0} = \omega_{M_d 0} - \gamma_{M_d M_d} E_\lambda/\hbar + \textstyle\sum_{K_d \neq M_d} \gamma_{M_d K_d} \\ \times \wp \textstyle\int_{-\infty}^{\infty} d\omega \frac{\omega^2 \{(1+n(\omega))J(\omega) + n(-\omega)J(-\omega)\}}{\omega_{M_d K_d} - \omega}\,, \end{aligned} \tag{2.29}$$

where E_λ is the reorganization energy in eq 2.15, $\wp$ denotes the principal part of the integral and it holds $J(\omega) = 0$ for $\omega < 0$.

In the calculation of the linear dichroism (LD) and circular dichroism (CD) spectra the same disorder average as for linear absorption and the same lineshape function $D_{M_d}(\omega)$ in eq 2.23 are used but the $|\mu_{M_d}|^2$ in eq 2.21 is replaced in the calculation of CD by the rotational strength

$$r_{M_d} = \sum_{m_d > n_d} c_{m_d}^{(M_d)} c_{n_d}^{(M_d)} \vec{R}_{m_d n_d} \cdot \vec{\mu}_{m_d} \times \vec{\mu}_{n_d} \tag{2.30}$$

and in the case of LD by

$$|\mu_{M_d}|^2 (1 - 3\cos^2(\theta_{M_d}))\,. \tag{2.31}$$

Here, θ_{M_d} is the angle between the transition dipole moment $\vec{\mu}_{M_d}$ and the membrane normal.

Emission starts from an excited state that is assumed to be relaxed in the potential energy surfaces of the exciton states (Renger et al., 2002). The resulting homogeneous fluorescence signal $I_d^{(\mathrm{hom})}(\omega)$ reads (Renger et al., 2002)

$$I_d^{(\mathrm{hom})}(\omega) \propto \omega^3 \sum_{M_d} f(M_d) |\mu_{M_d}|^2 D'_{M_d}(\omega) \tag{2.32}$$

with the Boltzmann factor

$$f(M_d) = \frac{e^{-\hbar\omega_{M_d0}/kT}}{\sum_{N_d} e^{-\hbar\omega_{N_d0}/kT}} , \tag{2.33}$$

and the emission lineshape function

$$D'_{M_d}(\omega) = \frac{1}{2\pi}\int_{-\infty}^{\infty} dt e^{-i(\omega-\tilde{\omega}_{M_d0})t}\ e^{G_{M_d}(t)-G_{M_d}(0)} e^{-t/\tau_{M_d}} , \tag{2.34}$$

In the calculation of triplet minus singlet (T-S) spectra, the triplet absorption spectrum of the complex is calculated by neglecting the oscillator strength and excitonic couplings of the pigment, where the triplet state is localized. For the absorption spectra that involve a reduced (oxidized) pigment, in addition to neglecting the oscillator strength and excitonic couplings of that pigment, electrochromic shifts in site energies of the remaining pigments are taken into account in the following way. For the reduced (oxidized) pigment a negative (positive) elementary charge is evenly distributed over the atoms of the π-system of this pigment and the electrochromic shift ΔE of another pigment in the ground state is calculated as the interaction energy of the atomic partial charges δq_i of the reduced (oxidized) pigment and the vector $\Delta\vec{\mu}$ of the pigment in the ground state, $\Delta E = \frac{1}{4\pi\epsilon_{\text{eff}}}\sum_i \delta q_i \frac{\vec{r}_i}{r_i^3}\Delta\vec{\mu}$, where ϵ_{eff} is an effective dielectric constant and $\vec{r}_i$ is a vector between the centers of the pigment in the ground state and the reduced pigment. The vector $\Delta\vec{\mu} = \vec{\mu}_e - \vec{\mu}_g$ denotes the change in permanent dipole moments of the excited and ground state, which is known (Krawczyk et al., 1991) for chlorophylls to be oriented approximately in the direction of $N_B \rightarrow N_D$ and to have a magnitude of about 1D. However the best agreement with experimental difference spectra is achieved when the $\Delta\vec{\mu}$ vector is rotated in plane by 15 degrees with respect to the $N_B \rightarrow N_D$ direction towards N_C. The same orientation of the $\Delta\vec{\mu}$ vector for the two Pheos is taken.

2.3 Excitation by an ultrashort pump pulse

The creation of exciton population by an ultrashort pump pulse is described in second order perturbation theory in the exciton-radiational coupling and within rotating wave approximation. A Gaussian-shaped pulse envelope

$$E_\Omega(t) = \frac{E_0}{\sqrt{2\pi}\tau_p} e^{-t^2/(2\tau_p^2)} , \tag{2.35}$$

is assumed, where the full width at half maximum (fwhm) of $E_\Omega(t)$ is $2\tau_p\sqrt{2\ln 2}$. Neglecting exciton relaxation, i.e., the off-diagonal part of the exciton-vibrational coupling, during the action of the short pump-pulse, the exciton population $P^{(d)}_{M_d}(0)$ created by such a pulse is obtained as (Adolphs et al., 2006)

$$P^{(d)}_{M_d}(0) = \frac{E_0^2|\vec{\mu}_{M_d}|^2}{3\hbar^2}\int_{-\infty}^{\infty} d\tau e^{-i(\Omega-\omega'_{M_d0})\tau} e^{G_{M_d}(\tau)-G_{M_d}(0)} e^{-\tau^2/(4\tau_p^2)} , \tag{2.36}$$

where $\hbar\omega'_{M_d0} = \hbar\omega_{M_d0} - \gamma_{M_dM_d}E_\lambda$,with the E_λ in eq 2.15, is the energy difference between the minima of the PES of exciton state $|M_d>$ and the ground state $|0>$. Eq. 2.36 includes the diagonal part of the exciton-vibrational coupling ,i.e., the mutual shift of exciton potential energy surfaces, without approximation.

2.4 Excitation energy transfer

2.4.1 Intra domain exciton relaxation

Exciton relaxation between different exciton states $|M_d>$ and $|N_d>$ in the same domain d is described by the Redfield rate constant (e.g. ref Renger et al. (2001))

$$\begin{aligned} k_{M_d \to N_d} &= 2\pi \gamma_{M_d N_d} \omega^2_{M_d N_d} \\ &\times \{J(\omega_{M_d N_d})(1 + n(\omega_{M_d N_d})) + J(\omega_{N_d M_d}) n(\omega_{N_d M_d})\} , \end{aligned} \tag{2.37}$$

with $\gamma_{M_d N_d}$ given in eq. 2.26

2.4.2 Inter domain exciton transfer

Exciton transfer between excited states in different domains a and b is described by the rate constant $k_{M_a \to N_b}$ obtained using generalized Förster theory as (Fetisova et al., 1996; Sumi, 1999; Mukai et al., 1999; Scholes et al., 2000; Jang et al., 2004; Müh et al., 2007)

$$k_{M_a \to N_b} = 2\pi \frac{|V_{M_a N_b}|^2}{\hbar^2} \int_{-\infty}^{\infty} d\omega D'_{M_a}(\omega) D_{N_b}(\omega) , \tag{2.38}$$

with the inter–domain exciton coupling $V_{M_a N_b}$ in eq 2.19. The functions $D'_{M_a}(\omega)$ and $D_{N_b}(\omega)$ are the normalized fluorescence and absorption lineshape functions of exciton states $|M_a>$ and $|N_b>$, respectively. The POP lineshape functions in eqs 2.23 and 2.34 are used.

2.4.3 Master equation

The populations of exciton states are related by the following master equations

$$\begin{aligned} \tfrac{d}{dt} P^{(a)}_{M_a}(t) = -\textstyle\sum_{d,N_d} \left(k_{M_a \to N_d} P^{(a)}_{M_a}(t) + k_{N_d \to M_a} P^{(d)}_{N_d}(t) \right) , \\ a = 1...N_{\rm dom}, M_a = 1...N^{(a)}_{\rm pig} , \end{aligned} \tag{2.39}$$

where $N_{\rm dom}$ is the number of domains and $N^{(a)}_{pig}$ is the number of pigments in domain a. For the rate constants $k_{M_a \to N_d}$, the Redfield expression in eq 2.37 is used, if $a = d$, and the generalized Förster rate constant in eq 2.38, if $a \neq d$. In matrix form eq 2.39 reads $\frac{d}{dt}\vec{P}(t) = -A\vec{P}(t)$, where the exciton populations are the elements of $\vec{P}(t)$ and the kinetic matrix A contains in the diagonal the elements $A_{M_a M_a} = \sum_{d,N_d} k_{M_a \to N_d}$ and in the off-diagonal $A_{M_a N_d} = -k_{N_d \to M_a}$. The standard solution for $\vec{P}(t)$ is given as

$$\vec{P}(t) = \sum_i d_i \vec{c}_i e^{-\lambda_i t} , \tag{2.40}$$

where the λ_i and $\vec{c}_i$ are the eigenvalues and (right) eigenvectors of the kinetic matrix A, respectively. The constants d_i are obtained from the initial condition $\vec{P}(0) = \sum_i d_i \vec{c}_i$, where the element $P^{(a)}_{M_a}(0)$ of $\vec{P}(0)$ is the initial population of the exciton state $|M_a>$ in domain a created by the short pulse (eq 2.36). In the case of PS-II core complexes, in addition to the exciton states, radical pair states are included that are coupled to the exciton states as described further below.

2.5 Time resolved pump-probe spectra

In pump-probe spectroscopy, the pigment-protein complex is excited by a short pump pulse and the excitation energy transfer/relaxation is tested by a delayed probe pulse. It is assumed that the delay τ_d between the probe pulse and the pump pulse is large enough so that any vibrational coherences or coherences between different exciton levels have decayed. A delta function-shaped probe pulse $E_0^{(\mathrm{pr})}\vec{e}_{\mathrm{pr}}\delta(\tau_d)$ is used with polarization $\vec{e}_{\mathrm{pr}}$. This delta-pulse is an idealization of a short experimental probe pulse with white spectrum. The pump-probe signal $\Delta\alpha(\tau_{\mathrm{d}})$ is the difference between the absorption measured by the probe pulse at a delay time τ_d after the pump pulse and the absorption measured by the probe pulse alone. If the probe pulse is dispersed in a monochromator after the sample, in addition to the dependence on the delay time, also the frequency dependence of $\Delta\alpha(\tau_{\mathrm{d}}) = \int d\omega \Delta\alpha_{\mathrm{disp}}(\tau_{\mathrm{d}},\omega)$ can be measured. The dispersed pump-probe signal $\Delta\alpha_{\mathrm{disp}}(\tau_{\mathrm{d}},\omega)$, in the present approximation, has three contributions:

$$\Delta\alpha_{\mathrm{disp}}(\tau_{\mathrm{d}},\omega) \propto \mathrm{GB}(\omega) + \mathrm{SE}(\omega,\tau_{\mathrm{d}}) + \mathrm{ESA}(\omega,\tau_{\mathrm{d}})\,, \tag{2.41}$$

time-independent ground state bleaching $\mathrm{GB}(\omega)$, and time-dependent stimulated emission $\mathrm{SE}(\omega,\tau_{\mathrm{d}})$ and excited state absorption $\mathrm{ESA}(\omega,\tau_{\mathrm{d}})$. Using a POP-lineshape theory, the following expressions are obtained (Renger et al., 2002)

$$\mathrm{GB}(\omega) = -\left\langle \sum_d \sum_{M_d} (\mu_{M_d}^{(\mathrm{pr})})^2 D_{M_d}(\omega) \sum_{K_d} P_{K_d}^{(0)} \right\rangle_{(\mathrm{dis+orient})} \tag{2.42}$$

with $\mu_{M_d}^{(\mathrm{pr})} = \vec{\mu}_{M_d}\vec{e}_{\mathrm{pr}}$, the $P_{K_d}^{(0)}$ in eq 2.36, and the absorption lineshape function $D_{M_d}(\omega)$ in eq 2.23,

$$\mathrm{SE}(\omega) = -\left\langle \sum_d \sum_{M_d} (\mu_{M_d}^{(\mathrm{pr})})^2 D'_{M_d}(\omega) P_{M_d}(\tau_{\mathrm{d}}) \right\rangle_{(\mathrm{dis+orient})} \tag{2.43}$$

with the fluorescence lineshape function $D'_{M_d}(\omega)$ in eq 2.34 and the time-dependent exciton populations $P_{M_d}(\tau_{\mathrm{d}})$ obtained from the solution of the master equation described above (eq 2.39), and

$$\mathrm{ESA}(\omega) = -\left\langle \sum_d \sum_{M_d,2N_d} (\mu_{M_d\to 2N_d}^{(\mathrm{pr})})^2 D'_{M_d\to 2N_d}(\omega) P_{M_d}(\tau_{\mathrm{d}}) \right\rangle_{(\mathrm{dis+orient})} \tag{2.44}$$

where $\mu_{M_d\to 2N_d}^{(\mathrm{pr})}$ is the scalar product between the probe pulse polarization $\vec{e}_{\mathrm{pr}}$ and the transition dipole moment $\vec{\mu}_{M_d\to 2N_d}$. The ESA lineshape function $D'_{M_d\to 2N_d}(\omega)$ is given as

$$D'_{M_d\to 2N_d}(\omega) = \frac{1}{2\pi}\int_{-\infty}^{\infty} dt e^{i(\omega-\tilde{\omega}_{2N_dM_d})t}\; e^{G_{N_dM_d}(t)-G_{2N_dM_d}(0)} e^{-|t|/\tau_{2N_dM_d}} \tag{2.45}$$

The function $G_{N_dM_d}(t)$ is given as

$$G_{N_dM_d}(t) = (\gamma_{2N_d2N_d} + \gamma_{M_dM_d} - 2\gamma_{2N_d2N_dM_dM_d})G(t) \tag{2.46}$$

with the $G(t)$ in eq 2.25 and the diagonal part of

$$\begin{aligned}\gamma_{2N_d2K_d} = \textstyle\sum_{m_d>n_d}\sum_{k_d>l_d}(c_{m_dn_d}^{(2N_d)})^2(c_{k_dl_d}^{(2K_d)})^2 \\ \times(e^{-R_{m_dk_d}/R_c} + e^{-R_{m_dl_d}/R_c} + e^{-R_{n_dk_d}/R_c} + e^{-R_{n_dl_d}/R_c})\end{aligned} \tag{2.47}$$

and

$$\gamma_{2N_d 2N_d M_d M_d} = \sum_{m_d > n_d} \sum_{k_d} (c_{m_d n_d}^{(2N_d)})^2 (c_{k_d}^{(M_d)})^2 \times (e^{-R_{m_d k_d}/R_c} + e^{-R_{n_d k_d}/R_c}) \tag{2.48}$$

The transition frequency $\tilde{\omega}_{2N_d M_d} = \tilde{\omega}_{2N_d 0} - \tilde{\omega}_{M_d 0}$ contains the $\tilde{\omega}_{M_d 0}$ in eq 2.35 and the frequency

$$\tilde{\omega}_{2N_d 0} = \omega_{2N_d 0} - \frac{E_\lambda}{\hbar} \gamma_{2N_d 2N_d} \,. \tag{2.49}$$

The inverse dephasing time $(\tau_{2N_d M_d})^{-1}$ in eq 2.45 is given as

$$(\tau_{2N_d M_d})^{-1} = \tau_{2N}^{-1} + \tau_{M_d}^{-1} \tag{2.50}$$

with the one exciton dephasing time constant $\tau_{M_d}^{-1}$ in eq 2.34 and $\tau_{2N_d}^{-1} = \sum_{2K_d} k_{2N_d \to 2K_d}$, that contains the Redfield rate constant for exciton relaxation between the two-exciton states $2N_d$ and $2K_d$.

$$\begin{aligned} k_{2N_d \to 2K_d} &= 2\pi \gamma_{2N_d 2K_d} \omega_{2N_d 2K_d}^2 \\ &\times \{ J(\omega_{2N_d 2K_d})(1 + n(\omega_{2N_d 2K_d})) + J(\omega_{2K_d 2N_d}) n(\omega_{2K_d 2N_d}) \} \,. \end{aligned} \tag{2.51}$$

The $\langle ... \rangle_{\text{dis+orient}}$ in eqs 2.42-2.44 denotes an average over disorder in site energies and over the orientation of the complex with respect to the external pump and probe field polarizations. As in the experiments (de Weerd et al., 2002a), a magic angle (54.7°) is assumed between the polarizations of the pump- and the probe pulse, $\vec{e}_{\text{pu}}$ and $\vec{e}_{\text{pr}}$, respectively.

2.5.1 Life time density map of time-dependent emission

In order to illustrate the time and frequency dependence of exciton relaxation, life time density (LFD) maps of the time-dependent emission are calculated. The time-dependent emission $I(\omega, t)$ is obtained as

$$I(\omega, t) \propto \omega^3 \left\langle \sum_{d, M_d} |\mu_{M_d}|^2 D'_{M_d}(\omega) P_{M_d}^{(d)}(t) \right\rangle_{\text{(dis+orient)}} \tag{2.52}$$

with the fluorescence lineshape function $D'_{M_d}(\omega)$ in eq 2.34 and the exciton state population $P_{M_d}^{(d)}(t)$, resulting from the solution of eq 2.39. Inspired by the Müller-Holzwarth LFD maps (e.g. ref Müller et al. (2003)), the emission $I(\omega, t)$ is expressed as

$$I(\omega, t) = \omega^3 \int_0^\infty d\tau A(\omega, \tau) e^{-t/\tau} \tag{2.53}$$

where $A(\omega, \tau)$ is the LFD map. By introducing eq 2.40 in eq 2.52 and comparison with eq 2.53 the LFD map $A(\omega, \tau)$ is obtained as

$$A(\omega, \tau) = \left\langle \sum_i \sum_{d, M_d} |\mu_{M_d}|^2 D'_{M_d}(\omega) d_i c_i^{(M_d, d)} \delta(\tau - \lambda_i^{-1}) \right\rangle_{\text{(dis+orient)}} \tag{2.54}$$

We note that the present calculation of the LFD map avoids an inverse Laplace transform that is needed, if the map is obtained directly from experimental data.

2.6 Electron transfer in the RC

Primary electron transfer in the RC is included phenomenologically by including three radical pair states RP1, RP2, and RP3 and assigning respective forward and backward rate constants for electron transfer. The following molecular identities are assumed for these states (Holzwarth et al., 2006; Groot et al., 2005; Raszewski et al., 2005): RP1=$\mathrm{Chl}^+_{\mathrm{D1}}$ $\mathrm{Pheo}^-_{\mathrm{D1}}$, RP2=$\mathrm{P}^+_{\mathrm{D1}}$ $\mathrm{Pheo}^-_{\mathrm{D1}}$, and RP3=$\mathrm{P}^+_{\mathrm{D1}}$ $\mathrm{Q}^-_{\mathrm{A}}$, where P_{D1} is the "special pair" Chl of the D1-branch. The first radical pair state RP1 is created by electron transfer from the exciton states $|M>$ of the RC pigments with a rate constant

$$k_{M\to \mathrm{RP1}} = |c^{(M)}_{\mathrm{Chl_{D1}}}|^2 k_{\mathrm{intr}}\,, \tag{2.55}$$

where $|c^{(M)}_{\mathrm{Chl_{D1}}}|^2$ is the probability to find the primary electron donor $\mathrm{Chl_{D1}}$ excited in exciton state $|M>$ and k_{intr} is the intrinsic rate constant for the reaction

$$\mathrm{Chl^*_{D1}Pheo_{D1}} \overset{k_{\mathrm{intr}}}{\to} \mathrm{Chl^+_{D1}Pheo^-_{D1}}\,. \tag{2.56}$$

The forward and the back reaction are approximately related by

$$k_{M\to \mathrm{RP1}}/k_{\mathrm{RP1}\to M} \approx e^{\Delta G^{(0)}_{\mathrm{intr}}/kT} \tag{2.57}$$

where $\Delta G^{(0)}_{\mathrm{intr}}$ equals the difference in standard free energy of the intrinsic electron transfer reaction in eq 2.56. The rate constants $k_{\mathrm{RP1}\to\mathrm{RP2}}$ and $k_{\mathrm{RP2}\to\mathrm{RP1}}$ are related by $k_{\mathrm{RP1}\to\mathrm{RP2}}/k_{\mathrm{RP2}\to\mathrm{RP1}} = \exp\{\Delta G_{\mathrm{RP1/RP2}}/kT\}$. The free energy difference between RP2 and RP3 is assumed to be so large that a back reaction RP3 $\to$ RP2 can be neglected, i.e., irreversible trapping at RP3 is assumed. For closed RCs (reduced $\mathrm{Q_A}$) a double reduction of $\mathrm{Q_A}$ can be neglected on the relevant time scale considered here, i.e., $k_{\mathrm{RP2}\to\mathrm{RP3}} = 0$ in this case.

2.7 Compartment models

2.7.1 Fast relaxation in domains

If fast intra-domain exciton relaxation is assumed, the exciton transfer between two domains starts from a (quasi) equilibrated excited state manifold of the donor domain, and the inter-domain transfer rate constant $k_{a\to b}$ becomes

$$k_{a\to b} = \sum_{M_a,N_b} f(M_a) k_{M_a\to N_b}\,, \tag{2.58}$$

with the rate constant $k_{M_a\to N_b}$ in eq 2.38 and the Boltzmann factor $f(M_a)$ in eq 2.33.

The primary electron transfer rate constant in this limit is given as

$$k_{\mathrm{RC}\to\mathrm{RP1}} = \sum_{M_a}^{a=\mathrm{RC}} f(M_a)|c^{(M_a)}_{\mathrm{Chl_{D1}}}|^2 k_{\mathrm{intr}} \tag{2.59}$$

where M_a counts the exciton states of the domain of the primary electron donor. This domain is formed by the six strongly coupled RC pigments.

2.7.2 Fast relaxation in larger compartments

For further simplification, different domains are included into a compartment I and fast equilibration of excitation energy is assumed in the whole compartment. The rate constant for excitation energy transfer between compartments I and J is then obtained as

$$k_{I\to J} = \sum_{a,b}^{a\epsilon I, b\epsilon J} \sum_{M_a,N_b} f(I,M_a) k_{M_a\to N_b} \tag{2.60}$$

where a and b count the domains in compartments I and J and $f(I, M_a)$ is the Boltzmann factor

$$f(I, M_a) = \frac{e^{-\mathcal{E}_{M_a}/kT}}{\sum_{c,K_c}^{c\epsilon I} e^{-\mathcal{E}_{K_c}/kT}} \,. \tag{2.61}$$

The primary electron transfer between the compartment I that contains the RC and RP1 is then obtained as

$$k_{I\to \mathrm{RP1}}^{(\mathrm{RC}\epsilon I)} = \sum_{M_a}^{a=\mathrm{RC}} f(I, M_a) |c_{\mathrm{Chl_{D1}}}^{(M_a)}|^2 k_{\mathrm{intr}} \,. \tag{2.62}$$

Compartments of different sizes are used below to find the bottleneck for the decay of excited states in PS-II core complexes.

2.8 Parameters

The parameters of the theory are (i) the excitonic and charge density couplings between the pigments, (ii) the spectral density of the pigment-protein coupling, and (iii) the site energies of the pigments.

2.8.1 Excitonic and charge density couplings

The recent 3.0 Å structure of PS-II (Loll et al., 2005) to calculate the excitonic couplings between the reaction center pigments by the *ab initio* TrEsp method, developed previously (Madjet et al., 2006), that combines the accuracy of the *ab initio* transition density cube method (Krüger et al., 1998) with the simplicity of the semi empirical transition monopole method (Chang, 1977) is used.

The excitonic couplings V_{1001} are obtained by the TrEsp method (Madjet et al., 2006) as

$$V_{1001}(m, n) = \sum_{I,J} \frac{q_I(1,0) q_J(1,0)}{|\mathbf{R}_I^{(m)} - \mathbf{R}_J^{(n)}|} \tag{2.63}$$

The TrEsp charges $q_I(1,0)$ of the $S_0 \to S_1$ transition were determined such as to fit the electrostatic potential of the transition density obtained with TDDFT using a B3LYP exchange correlation functional and a 6-31G* basis set, as explained in detail in ref (Madjet et al., 2006). The charges were rescaled to yield an effective dipole moment of 4.4 D for Chl$a$ and 3.5 D for Pheo that takes into account screening and local field effects of the Coulomb coupling in the dielectric of the protein in an effective way.

The charge density couplings V_{aabb} in eq 2.3

$$V_{aabb}(m, n) = \frac{1}{\epsilon_{\mathrm{eff}}} \sum_{I,J} \frac{q_I(a,a) q_J(b,b)}{|\mathbf{R}_I^{(m)} - \mathbf{R}_J^{(n)}|} \,, \tag{2.64}$$

are calculated with the ground and excited state partial charges $q_I(0,0)$ and $q_I(1,1)$. These charges were obtained from a fit of the electrostatic potential of the ground and excited state charge densities, respectively, using the same *ab initio* method as for the transition density.

The coupling between P_{D1} and P_{D2} was drastically reduced compared to the coupling obtained from structural data with lower resolution and the transition monopole charges of Chang (Chang, 1977). Judging from the structural data, considerable wavefunction overlap can be expected between the two "special pair" chlorophylls P_{D1} and P_{D2}. This overlap results in a Dexter type exchange coupling, in addition to Förster type Coulomb coupling obtained by the TrEsp method. To estimate the exchange contribution we have refitted the eleven D1D2-cyt$b$559

spectra, studied previously (Raszewski et al., 2005), taking the "special pair" coupling as well as the site energies as fit parameters. The coupling was allowed to vary between 60 cm^{-1} and 240 cm^{-1}. We obtained the same optimal site energies as previously (Raszewski et al., 2005) and an optimal "special pair" coupling of 140-170 cm^{-1}. In parallel, we performed quantum chemical calculations of the excited state energies and transition dipole moments of the "special pair" monomers and the whole dimer (Madjet *et al.*, manuscript in preparation). The short range coupling was extracted by comparing the monomer and dimer results, using an effective two-state Hamiltonian. The obtained short range coupling was quantitatively too small. We have translated the "special pair" chlorophylls in the error range set by the crystallographic resolution (Biesiadka, 2007) and obtained agreement with the above fitted coupling value. The excitonic couplings used in the calculations are given in the Appendix (coupling for RC are given in Table 7.1, while the ones used for the CP43 and CP47 are given in Tables 7.2 and 7.3 respectively).

2.8.2 Spectral density

The spectral density of the pigment-protein coupling in the B777-complex, consisting of a single bacteriochlorophyll *a* molecule coupled to an α-helix, was extracted recently (Renger et al., 2002) from fluorescence line narrowing spectra measured (Creemers el al., 1999) at 1.7 K. Here, the same normalized functional form $J_0(\omega)$ is assumed ($\int_0^\infty J_0(\omega)\, d\omega = 1$),

$$J_0(\omega) = \frac{1}{s_1 + s_2} \sum_{i=1,2} \frac{s_i}{7!\, 2\omega_i^4}\, \omega^3\, e^{-(\omega/\omega_i)^{1/2}} \tag{2.65}$$

with the extracted parameters $s_1 = 0.8$, $s_2 = 0.5$, $\hbar\omega_1 = 0.069$ meV and $\hbar\omega_2 = 0.24$ meV. The spectral density $J(\omega)$ is described by (Müh et al., 2007; Raszewski et al., 2005; Adolphs et al., 2006; Renger et al., 2007)

$$J(\omega) = S J_0(\omega)\,. \tag{2.66}$$

A Huang-Rhys factor $S = 0.65$ is used for the RC pigments, that was estimated from the temperature dependence of the absorption spectrum of D1-D2-cyt$b$559 complexes (Raszewski et al., 2005). The Huang-Rhys factor of the pigments in the core antenna subunits will be estimated from the temperature dependence of the absorption spectra of CP43-complexes.

2.8.3 Site energies

The site energies of the pigments in the D1/D2 complexes as well as in CP43 and CP47 core antennae are determined from a fit of linear absorption, linear dichroism, circular dichroism, and fluorescence spectra (see sec. 2.9). In the case of D1/D2 complexes and CP47, these four spectra are used in the fit. For CP43, the circular dichroism spectrum is excluded, because the experimental spectrum is non-conservative and therefore cannot be described by the present exciton theory.

The rate constants for excitation energy transfer are determined by the site energies, the excitonic couplings, the spectral density and the correlation radius of protein vibrations R_c. For the latter a value of 5Å is assumed, as determined from calculation of transient absorption spectra and comparison with experimental data on D1-D2-cyt$b$559 complexes (Renger et al., 2002b) and on complexes of the water soluble chlorophyll binding protein (WSCP) (Renger et al., 2007).

2.9 Genetic algorithm

The value of every site energy of the chlorines in PS2 may vary from circa 650 nm to 690 nm with continuous distribution. Therefore the total number of all combinations is infinite. One has to put some restrains to the number of possible site energies, in this case it was reasonable to vary the site energies within the 655-690 nm interval with 1 nm step, which results in 35 possible site energy values for every chlorine. Unfortunately the total number of all combination (e.g. for the D1/D2 complex it is 35^8 which is $\approx 2.2 * 10^{12}$) is too large to calculate optical spectra for all possible combinations. One had to develop some kind of algorithm that is able to determine these site energies in a reasonable time. A genetic algorithm was developed, which bases on the evolutionary phenomenon of adopting to the environmental conditions. In this case the environment is just the set of experimental data that has to be simulated and evolution is performed in the set of site energies due to mutation processes.

I will describe the whole process of developing the genetic algorithm for better understanding and clarity. The idea was to create several (in this case 20) sets of n values of site energies that correspond to the n pigments present in complex, for D1/D2 n=8 and for CP43 and CP47 n=13 and 16 respectively. The values of these site energies were chosen by random from the 655-690 nm interval. These initial sets of the site energies was called "Initial Parents" (IP). After that for every member of IP absorption (OD), fluorescence (Flu), circular (CD) and linear (LD) dichroism spectra were calculated and compared with experimental data. The quality of the agreement between experimental and simulated spectra is described by the scoring function S:

$$S = \sum_{j=1,4} \sum_{i=1,n} w_j [(f_j^{(exp)}(\omega_i) - f_j^{(sim)}(\omega_i))^2 + (f_j'^{(exp)}(\omega_i) - f_j'^{(sim)}(\omega_i))^2] \tag{2.67}$$

where j $1 \ldots 4$ denotes OD, CD, LD and Flu, n is the number of experimental points, $f_j(\omega_i)$ is the value of the function f_j and $f'(\omega_i)$ is the value of it's first derivative. Introduction of the first derivative was necessary to avoid (especially in case of CD) flattening of the simulated spectrum. Such a situation could occur when the CD signal shows negative contribution in the same wavelength where OD, LD and Flu shows positive contributions. Therefore it was necessary to strengthen the CD contribution. The weighting factors w_j were introduced for this purpose.

The scoring function was calculated for every IP and the two (10% of initial number of IP) sets with the highest scoring were kept for the next cycle of the genetic algorithm, while the remaining ones were abandoned. These two sets became "Parents" for the next generation of "Children". Children were created in the following way: every parent was cloned 9 times (to keep population level constant in time). After cloning procedure, one or two point mutations were applied on every clone. The point mutation is a process that for randomly chosen pigment, changes its site energy in a random way to a new value from the 655-690 nm interval. The number of point mutations (one or two) was also determined by random. The next step was to calculate simultaneously OD, LD, CD and Flu for every set as well as their scoring functions, and to create a new ranking. The two best sets were promoted to be "Parents" (under condition that their S was better than previous "Parents"', if not, then old "Parents" became new "Parents). This whole procedure was repeated till the moment there was no change on the first two places of the ranking for some number ($\approx$ 100) of cycles. To avoid a situation where the ranking is getting worse, two best sets from the previous cycle were kept and compared with the current ones, in case of improvement they were abandoned otherwise they were kept.

Further on two major changes were introduces to the algorithm. The first one was including a "Crossing over" procedure, which allows more dramatic changes than point mutations. "Crossing over" gives good results if it is applied on the sets from the middle of the ranking. When it was applied on the sets from the top or bottom of the ranking, in most cases no improvement was

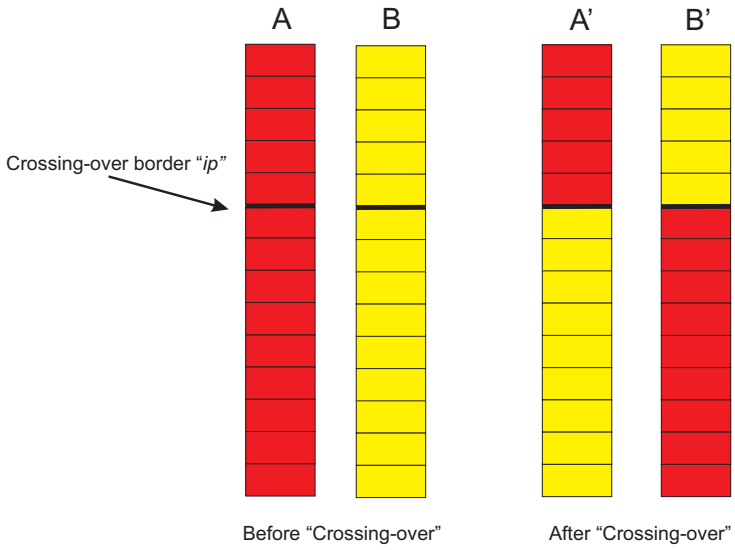

Figure 2.2: Crossing-over.

visible. It is so, because top sets are already good and there is a very slim chance of improving them by a drastic change, while bad ones have in general small chance of improvement. For best results two (again 10%) sets with average scoring were taken and their site energies were "crossed over" in the following way (see Fig. 2.2):

1. A pigment number i_p is randomly chosen and serves as a border for the crossing over operation.

2. The site energies of all pigments i with $i < i_p$ of the first set are exchanged with respective site energies of the second set.

This operation allowed to shorten the calculation time by approximately 20% for all complexes.

The second change in the genetic algorithm was the inclusion of a "Fine tuning" procedure, where point mutation were allowed only to vary site energies in a very small range (usually $\pm$ 2 nm from their original values). It was applied in the very end of the evolution process, where radical point mutation are very likely to do more harm than good. This procedure proved to be very useful in case of D1/D2 complexes, however in case of both antenna systems it did not improve the fit results.

The whole procedure of obtaining site energies was repeated for 100 times. The resulting 100 sets of optimal site energies were further investigated. Approximately 20% of the best sets had more or less the same score and resulted in similar site energy values, indicating a global rather than a local minimum.

Chapter 3

Optical spectra of isolated Photosystem II reaction centers

In this chapter a detailed calculation of optical properties of reaction center (D1-D2-cyt$b$559) complexes based on the structural analysis of photosystem II of *T. elongatus* is presented. The calculations of absorption, linear dichroism, circular dichroism, fluorescence spectra, all at 5 K, and the temperature dependence of the absorption spectrum are used to extract the local optical transition energies of the reaction center pigments, the so-called site energies, from experimental data. The site energies are verified by calculations and comparison with seven additional independent experiments. Exciton relaxation and primary electron transfer in the reaction center are studied using the site energies. The calculations are used to interpret transient optical data. Evidence is provided for the accessory chlorophyll of the D1-branch as being the primary electron donor and the location of the triplet state at low temperatures.

This chapter is organized in the following way. First an overview of the problems addressed in this chapter is given. Next, the calculation of the stationary spectra of the D1/D2 subunits and comparison with experimental data are used to determine site energies of the pigments in this subunit. These site energies are tested afterwards in the calculation of various independent spectra. These parameters are later used to study exciton relaxation and primary electron transfer, which provides evidence for $\mathrm{Chl_{D1}}$ being the primary electron donor as well as a host for the triplet state at low temperatures.

3.1 Overview

As in the bacterial reaction center (bRC), electron transfer in PS-II is known (Shkuropatov et al., 1997, 1999) to proceed only along one of the two branches, that are related by a pseudo-twofold rotation symmetry. However, an important difference between these two types of RCs is that only the PS-II RC can create a high enough redox potential for the splitting of water and the evolution of oxygen that forms the basis for our life. Neither the reasons nor the consequences of the high redox potential of PS-II RC are well understood. One reason for the higher redox potential is likely to be the somewhat smaller overlap of the two "special pair" chlorophyll wavefunctions that leads to a more localized cation state in PS-II than in bRC.

A consequence of the high redox potential is that the PS-II RC cannot use carotenoids for photoprotection, i.e. the quenching of chlorophyll triplet states, because the carotenoids would be oxidized if they were in close enough vicinity of the RC chlorophylls for Dexter type triplet transfer. An alternative quenching mechanism for the triplet states concerns the quenching by the singly reduced quinone Q_A (van Mieghem et al., 1995; Noguchi, 2002). This quenching is more efficient in PS-II than in bRC because in the latter the triplet state is localized at the special pair whereas in the former it is likely to be localized at the accessory chlorophyll of the D1-branch (van Mieghem et al., 1991), Chl_{D2}, which is closer to Q_A.

Due to the large excitonic coupling between the two special pair bacteriochlorophylls in bRC, the excitation energy relaxes to the low–energy special pair band and electron transfer starts from the special pair. In addition, it was found (van Brederode et al., 1997, 1999a) that direct excitation of the accessory bacteriochlorophyll can lead to primary charge separation from there. The latter observation triggered a discussion on the primary donor in PS-II (van Brederode et al., 1999; Dekker et al., 2000; Prokhorenko et al., 2000; Diner et al., 2001, 2002; Barter et al., 2003), since in PS-II the excitonic coupling in the "special pair" is much weaker than in the bRC and, therefore, the lowest excited state in the PS-II RC is not necessarily localized at the "special pair". In fact, fluorescence line narrowing spectra at 5 K (Peterman et al., 1998) contain signatures of a carbonyl stretch vibration at 1669 cm^{-1} which was assigned by static and time–resolved infrared spectroscopy to Chl_{D2} (Noguchi et al., 1993, 1998, 2001). In the light of the latter finding and the structural similarity between the two types of RCs it may be expected that the detour of electron transfer starting at the accessory bacteriochlorophyll in bRC becomes the main primary electron transfer event in PS-II.

An interesting prediction of a previous multimer model (Merry et al., 1996) is the existence of two low energy exciton states which are localized on the two different branches of the RC. This model was used to explain the relatively slow relaxation times that were measured in transient anisotropy experiments (Merry et al., 1996) at room temperature. Consistent with this idea the decrease of the quantum yield of fluorescence between 4 K and 70 K (Groot et al., 1994) was explained by assuming that trap states localized on the electron transfer inactive branch are responsible for fluorescence and that those states are thermally activated and quenched by charge transfer upon raising the temperature (Groot et al., 1994). The present calculations do not support the latter idea. Instead, they are consistent with the suggestion (Peterman et al., 1998) that a certain fraction of the RCs is unable to perform charge separation and fluoresces. With respect to the anisotropy decay (Merry et al., 1996), the calculations suggest that it is due to excitation energy transfer between $Pheo_{D2}$ and Chl_{D2}.

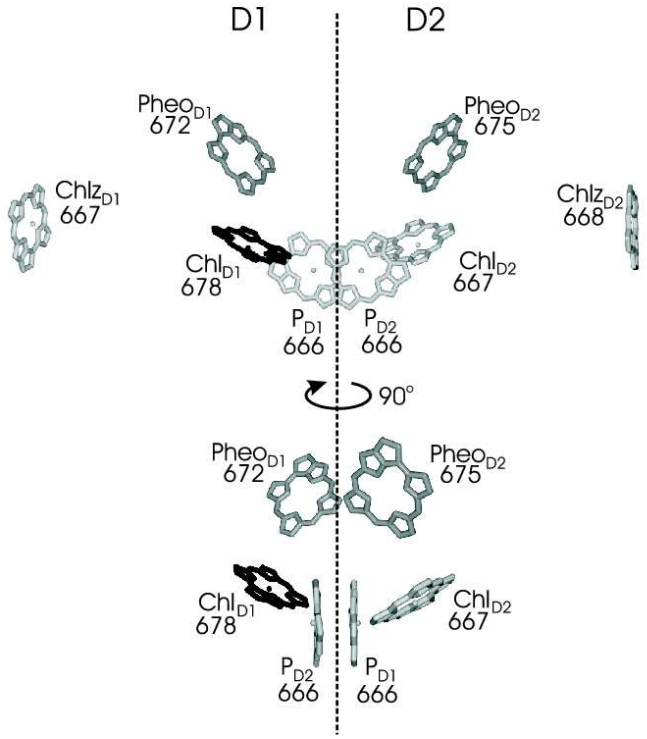

Figure 3.1: Arrangement of pigments in the PS-II RC. Numbers are the wavelengths in nm corresponding to the site energies of the pigments.

3.2 Results

3.2.1 Obtaining site energies of the D1/D2 complexes

The genetic algorithm was used to determine the values of the site energies of the 6 chlorophylls and 2 pheophytins in D1/D2 subunit of PS2. For the fit the experimental data (OD, CD, LD and Fluorescence at 6K) measured by Germano et al. (2001, 2000) were used. Several (∼20%) of the obtained sets of optimal site energies contain more or less the same values (difference ∼1-2 nm), they all share the same unique property, i.e. the accessory chlorophyll of the D_1-branch (Chl_{D1}) has the lowest site energy (∼678 nm). The values of the optimal site energies are given in Fig. 3.1. The calculations were performed using the inhomogeneous width (Fwhm) of 180 cm^{-1} and Huang-Rhys factor S=0.65, results are shown in Fig. 3.2. The Huang-Rhys factor was determined by calculations of OD the temperature dependence measured by Germano et al. (2001) at 6K, Konermann et al. (1996) at 10K, 77K, 150K and 277K (Fig. 3.7). It is clear that all of the calculated spectra show a very good agreement with experimental data (Fig. 3.2).

3.2.2 Calculation of independent spectra

Cryogenic temperatures The site energies obtained from genetic algorithm were verified by calculation of several optical spectra of D1/D2 complexes and comparison with experimental data. We calculated all spectra that were available:

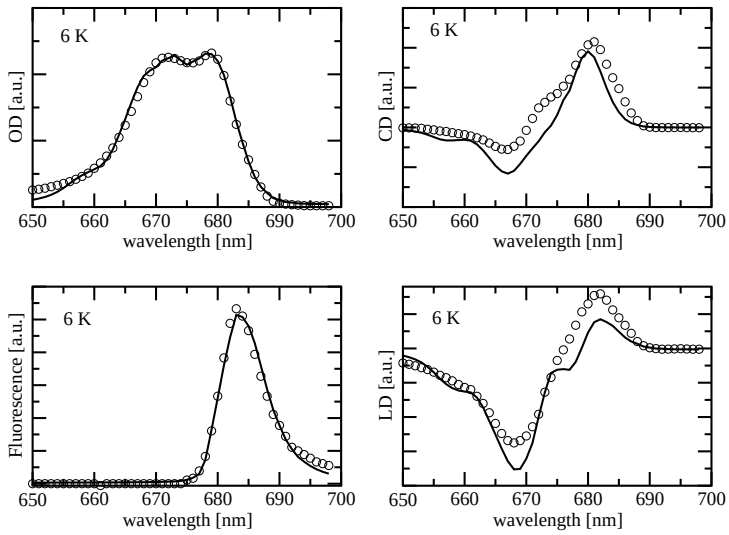

Figure 3.2: Absorption (OD), circular dichroism (CD), fluorescence and linear dichroism (LD) spectra of D1-D2 complexes at 6 K. Solid lines show calculations obtained for the optimized site energies given in Fig. 3.1. Circles are the experimental data by Germano et al. (2001, 2000).

1. Triplet minus singlet (T-S) spectra at 10K (Germano et al., 2001) to verify site energies of P_{D1} and Chl_{D1}.

2. OD, CD and LD for chemically modified Pheophytin to verify site energies of $Pheo_{D1}$ and $Pheo_{D2}$ (Germano et al., 2001)

3. Absorption of so-called RC5 complexes (D1-D2 complexes that consist only 5 chlorophylls) to verify position of $Chlz_{D1}$ as $Chlz_{D2}$ (Vacha et al., 1995)

4. Difference spectra $Pheo^{-}_{D1}-Pheo_{D1}$ that involve reduced $Pheo_{D1}$ (Vacha et al., 2002) and $P^{+}_{D1}Pheo^{-}_{D1}-P_{D1}Pheo_{D1}$ where in addition P_{D1} is oxidized (van Kan et al., 1990) were calculated as well as T-S spectra at 77K and at room temperature (Durrant et al., 1990), to verify the site energies of $Pheo_{D1}$ and P_{D1}

T-S spectra at 6K were measured by Germano et al. (2001). The T-S spectrum is presented in Fig. 3.3, it is clear that triplet state localized on the Chl_{D1} gives excellent agreement with experiment, while triplet state localized on the P_{D1} does not explain the experiment.

Recently Germano and co-workers replaced the pheophytin of the in-active D_2 branch with chemically modified pheophytin and measured OD, CD and LD of such D1/D2 complex. This modified pheophytin absorbs in the solution about 13 nm to the blue of the native one. Since this shift can be different in protein environment it was treated as parameter during the calculations. Reasonably good fits of OD, CD and LD were obtained for ∼23 nm shift, results are presented in Fig. 3.4. The calculated absorption difference spectrum (Fig. 3.4A solid line) is in a very good agreement with experimental data in both spectra main bleaching is appearing at 679 nm and positive peak at ∼672 nm. The same holds for LD (Fig. 3.4C solid line) the main peak in the experiment and in the calculation occurs at 680 nm. Whereas the experimental bleaching at 667 nm is well represented by the calculated one. The small experimental bleaching at about 655 nm is almost absent in the theory. In the case of CD (Fig. 3.4D solid line) all experimental bands are reproduced by theory, however the height of band at 670 nm is too strong in the theory and the experimental shoulder at 682 nm occurs at 680 nm in the theory. Finally a similar exchange experiment was done for $Pheo_{D1}$, however in this case it was impossible to

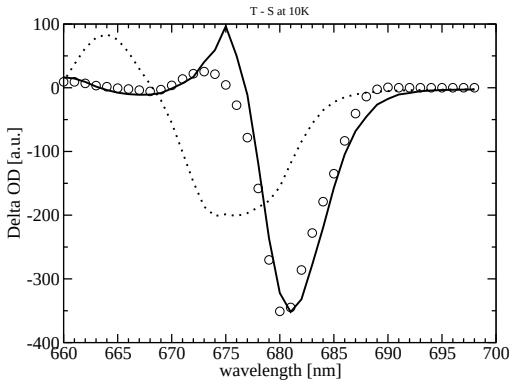

Figure 3.3: Triplet minus singlet spectra at 10K. Circles are experimental data by Germano et al. (2001). Solid line is calculation assuming triplet on Chl_{D1}, dashed line is calculation assuming triplet on P_{D1}.

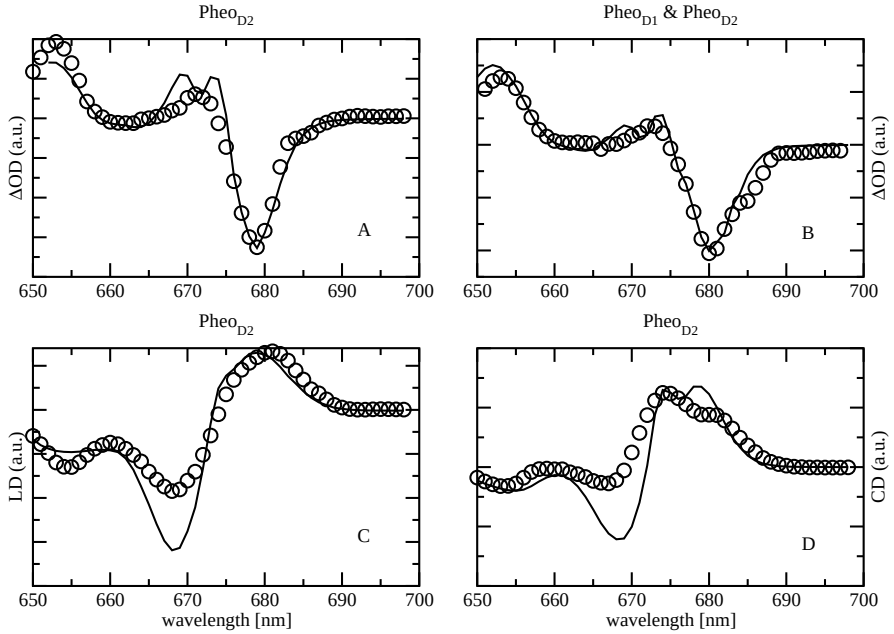

Figure 3.4: A): Absorption difference (ΔOD) for exchanged $Pheo_{D2}$, B): Absorption difference (ΔOD) for exchanged $Pheo_{D2}$ and $Pheo_{D1}$ C): Linear dichroism (LD) for exchanged $Pheo_{D2}$, D): Circular dichroism (CD) for exchanged $Pheo_{D2}$. All at 6K. Solid lines are calculations, circles are experimental data by Germano et al. (2001).

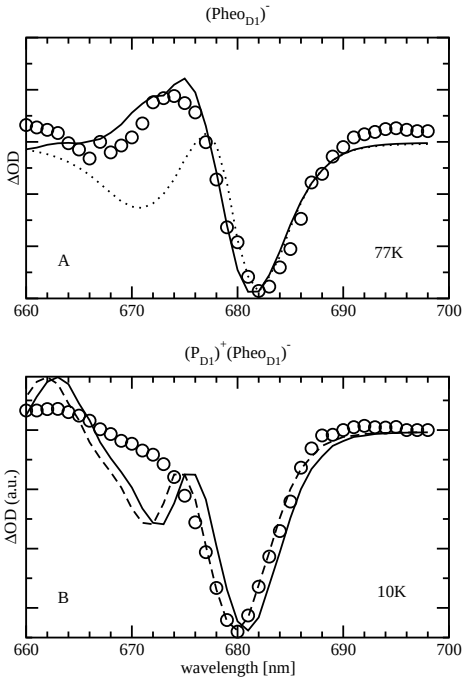

Figure 3.5: A): Absorption difference $\mathrm{Pheo_{D1}}^-$ at 77K, circles are experimental data by Vacha et al. (2002) solid line is calculation including electrochromic shift, while dotted line is calculation excluding electrochromic shift. B): Absorption difference $\mathrm{P^+_{D1}Pheo^-_{D1}}-\mathrm{P_{D1}Pheo_{D1}}$at 10K. Circles are experiment by van Kan et al. (1990), solid line is calculation, dashed line is calculation with site energies lowered by 1 nm (see text).

exchange only $\mathrm{Pheo_{D1}}$ but both had to be exchanged (Germano et al., 2001, 2000). The result of the calculation is shown in Fig. 3.4B (solid line). Excellent agreement between theory and experiment is obtained. In Fig. 3.5A the absorption spectrum for reduced $\mathrm{Pheo_{D1}}$ is compared with experimental data measured by Vacha et al. (2002) at 77K. The dotted line shows the calculation without electrochromic shift of the site energies, such calculation describes main bleaching at ∼680 nm but does not describe positive band at 675 nm that is present in the experiment. Including electrochromic shifts of site energies with effective dielectric constant ϵ_{eff}=1.5, gives excellent agreement between experimental and calculated spectra.

The next spectrum that was calculated was absorption difference for oxidized $\mathrm{P_{D1}}$ and reduced $\mathrm{Pheo_{D1}}$ at 10K. Experimental data were collected by van van Kan et al. (1990). Assuming ϵ_{eff}=1.5 like in case of $\mathrm{Pheo^-_{D1}}-\mathrm{Pheo_{D1}}$ spectrum gave solid curve in Fig. 3.5B. In theory and experiment main bleaching appears at ∼680 nm, however the experimental high energy shoulder at ∼672 nm appears in the theory as a separated peak.

In Fig.3.6 theoretical absorption spectra of D1/D2 complexes that lack one of the two Chlz (RC5) are compared with measured data by Vacha et al. (1995) at 77K. Only one case ($\mathrm{Chlz_{D1}}$ is absent) is shown for clarity in figure. In any case (either $\mathrm{Chlz_{D1}}$ or $\mathrm{Chlz_{D2}}$ is absent) the calculations match the experiment. For better visibility both theoretical and experimental (simply substracting experimental RC6 from RC5) difference spectra of RC5-RC6 were calculated. The experimental curve (squares in Fig. 3.6) has a main bleaching at 667 nm that is present in the theoretical curve but additionally to that there is also a very small secondary bleaching at ∼687

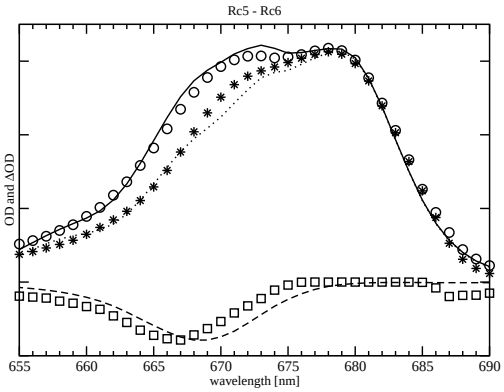

Figure 3.6: Absorption and absorption difference of RC6 and RC5 complexes (see text) at 77K. Circles (RC6) and stars (RC5) are experimental values by Vacha et al. (1995), solid and dotted lines are calculations. Dashed line and squares are theoretical and experimental difference spectra, RC5-RC6.

nm that is not present in the theory.

Temperature dependence The temperature dependence of the absorption spectrum is shown in Fig. 3.7. Experimental data were collected at 6K by Germano et al. (2001) and 10K, 77K, 150K, 277K by Konermann et al. (1996). The present model of site energies (see Fig. 3.1) nicely explains the temperature dependence of the OD spectrum, assuming Hung-Rhys factor S=0.65. The overall quality of the fit can by improved by shifting the $\mathrm{Chl_{D1}}$ site energy to the blue with respect to its value at 5K by 0.5 nm. for 77K, 1 nm for 150K and 3 nm for 277K. This feature will be discussed later in detail.

The triplet minus singlet spectrum was the second experiment for which the temperature dependence was calculated. Experimental data were collected by Germano et al. (2001) at 10K, and by Durrant et al. (1990) at 77K and room temperature. Results of calculations and corresponding experiments are presented in Fig. 3.8. It is absolutely clear that in 10K theoretical curve with the triplet state localized on the $\mathrm{Chl_{D1}}$ fully resembles experimental one, while placing the triplet state on the $\mathrm{P_{D1}}$ does not. At higher temperatures it is impossible to explain the T-S spectrum by placing the triplet state just on the $\mathrm{Chl_{D1}}$ (see Fig. 3.8 B&C). It is however possible that at higher temperatures the triplet state is not fully localized on the $\mathrm{Chl_{D1}}$ but rather delocalized over $\mathrm{Chl_{D1}}$ and $\mathrm{P_{D1}}$. The relative population of the two triplet states localized on $\mathrm{Chl_{D1}}$ and on $\mathrm{P_{D1}}$ follows thermal (Boltzmann) distribution. Therefore estimating this relative population at one temperature should determine this ratio at any other temperature. Really good fit for 77K was obtained if it is assumed that the relative population of the two triplet states $^3\mathrm{Chl_{D1}}$and $^3\mathrm{P^3_{D1}}$is 75:25. Such mixing ratio corresponds to an energy gap between $^3\mathrm{Chl_{D1}}$and $^3\mathrm{P^3_{D1}}$of 10 meV. At room temperature this energy gap results in a relative population of 57:43. In Fig. 3.8 the results of the calculations are shown. They match perfectly well the experimental data.

3.2.3 Delocalization of excited states

Fig. 3.9 compares the density of exciton states $d_{\mathrm{M}}(\omega)$ of the six core pigments with exciton states pigment distribution $d_{\mathrm{m}}(\omega)$. The two lowest exciton states M=1 and 2 are almost completely

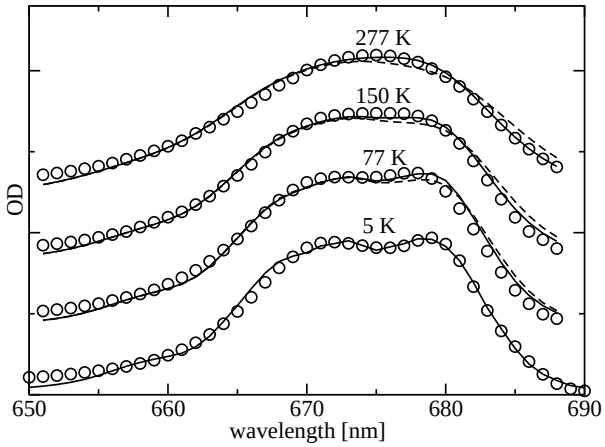

Figure 3.7: Temperature dependence of absorption spectra of D1-D2 complexes. Circles correspond to the experimental data by Germano et al. (2001) and Konermann et al. (1996), solid lines are the spectra calculated taking into account a temperature dependence of the site energy of Chl_{D2} (678 nm at 5K, 677.5 nm at 77 K, 677 nm at 150 K, and 675 nm at 277 K), dashed lines are calculations with constant site energy of Chl_{D1} (678 nm). The spectra at different temperatures have been shifted vertically by adding a constant for better visibility.

dominated by contributions from Chl_{D1} and $Pheo_{D2}$, respectively, as seen in Fig. 3.9 (*top*). The "special pair" pigments (P_{D1} and P_{D2}) contribute equally to the exciton states M=3 and 6. $Pheo_{D1}$ dominates exciton state M=4 and Chl_{D2} exciton state M=5.

3.2.4 Calculation of primary electron transfer

In Fig. 3.10 decay of exciton population due to primary electron transfer is calculated for 7K and for room temperature, assuming that the primary electron donor is either P_{D1} (*top*) or Chl_{D1} (*bottom*). For the calculation at room temperature in both cases the decay rates are in the same order of magnitude. At cryogenic temperature the decay rate obtained for Chl_{D1} being primary electron donor increases, while, if it is assumed to be P_{D1} being primary electron donor, this rate dramatically decreases. At low temperature the decay becomes multiexponential. For these calculations a temperature independent intrinsic charge separation constant $k_{\rm int} = (2\text{ps})^{-1}$ was assumed.

3.3 Discussion

3.3.1 Character of excited states in D1/D2 complex

The largest site energies are obtained for P_{D1} and P_{D2} and the lowest one for Chl_{D2}. As a consequence of this difference in site energies which is larger than the coupling in the "special pair", the lowest exciton state is not dominated by the special pair as in bRC but by Chl_{D2} (upper part of Fig.3.9). This result is in agreement with fluorescence line narrowing (Peterman et al., 1998) and infrared spectroscopic studies by Noguchi et al. (2001). Similarly, because of its second lowest site energy, $Pheo_{D2}$ dominates the second lowest exciton state.
The strong coupling between P_{D1} and P_{D2} gives rise to two exciton states at 675 and 660 nm which are delocalized over the two pigments, as seen in the middle part of Fig. 3.9. In this respect the P_{D1}/P_{D2} dimer is still a "special pair" as its counterpart in bRc. The high-energy exciton state of the "special pair" carries only very little oscillator strength, as can be judged

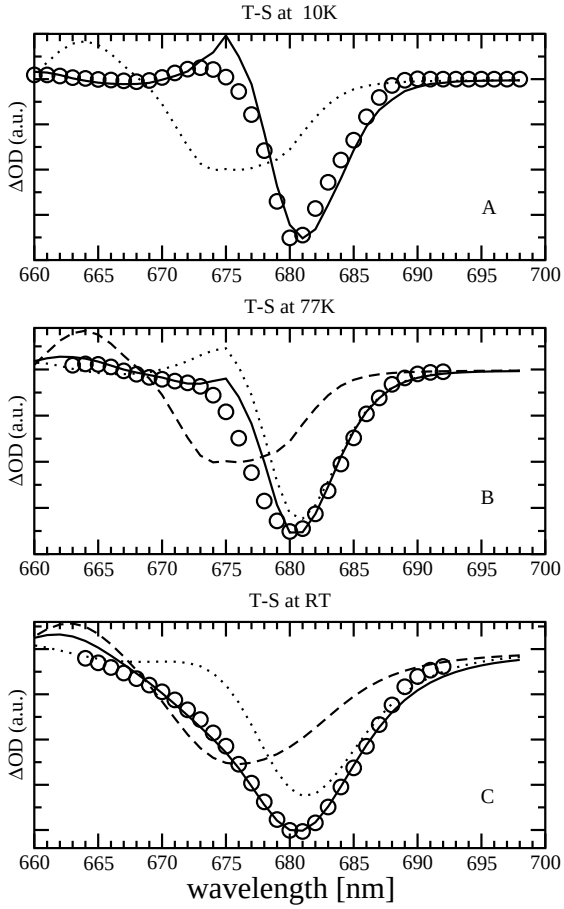

Figure 3.8: A): T-S spectra at 10K. Circles are experimental data by Germano et al. (2001), solid line is calculation assuming triplet state on Chl_{D1}, dotted line is calculation assuming triplet state on P_{D1}. B): T-S spectra at 77K. Circles are experimental data by Durrant et al. (1990). Dotted line is calculation assuming triplet on Chl_{D1}, dashed line is calculation assuming triplet on P_{D1}. Solid line is mixture of both assuming thermal distribution of the triplet state between Chl_{D1} and P_{D1}. C): T-S spectra at room temperature. Circles are experimental data by Durrant et al. (1990). Dotted line is calculation assuming triplet state on Chl_{D1}, dashed line is calculation assuming triplet on P_{D1}. Solid line is mixture of both assuming thermal distribution of the triplet state between Chl_{D1} and P_{D1}.

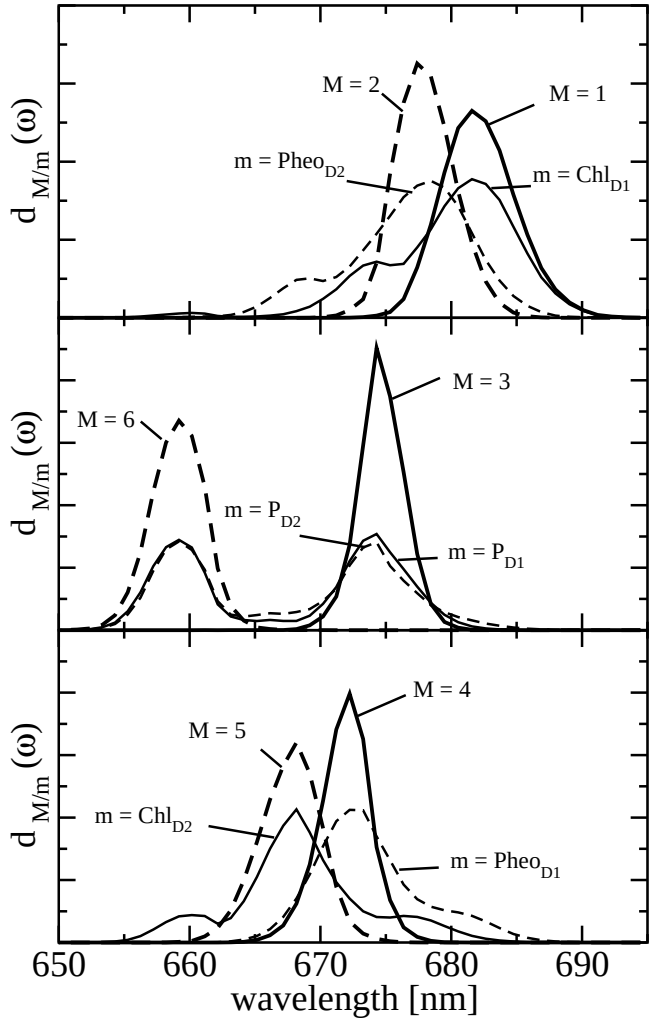

Figure 3.9: Density of exciton states $d_{\mathrm{M}}(\omega)$, and exciton states pigment distribution $d_{\mathrm{m}}(\omega)$ of the six core pigments.

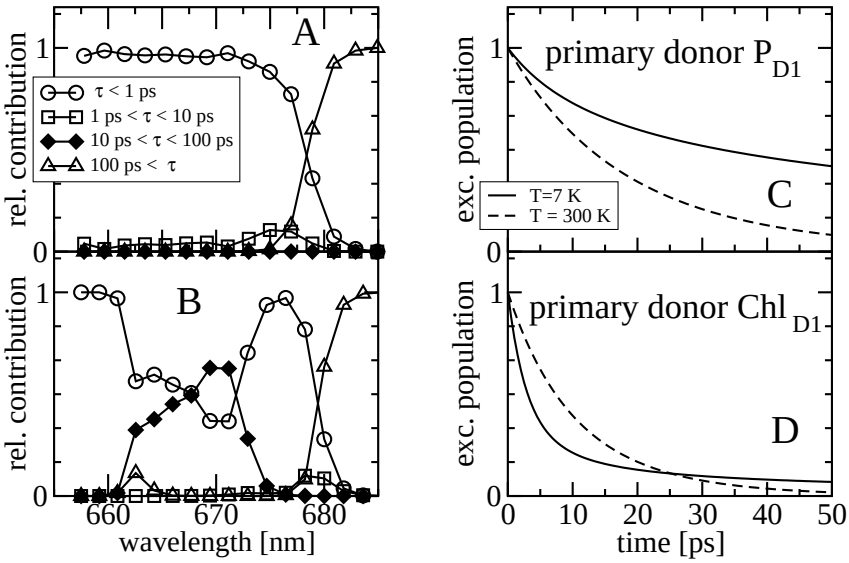

Figure 3.10: Left part: Calculation of disorder averaged exciton lifetimes at 6 K, A: for the 6 strongly coupled core pigments, B: including also the two peripheral chlorophylls $\mathrm{Chlz_{D1}}$, $\mathrm{Chlz_{D2}}$. Right part: Calculation of exciton population decay at 7 K (solid lines) and at room temperature (dashed lines) due to primary electron transfer, C: assuming primary donor is $\mathrm{P_{D1}}$, D: assuming primary donor is $\mathrm{Chl_{D1}}$.

from the absorption spectrum in the upper right part of Fig. 3.2.
Although the remaining exciton states are dominated by single pigments, there is still delocalization as it becomes obvious in Fig. 3.9 by the additional peaks in the exciton states pigment distributions $d_m(\omega)$. The density of exciton states

$$d_M(\omega) = \langle \sum_M \delta(\omega - \omega_M) \rangle_{\mathrm{dis}} \tag{3.1}$$

is compared in Fig. 3.9 with the exciton states pigment distribution

$$d_m(\omega) = \langle \sum_M |c_m^{(M)}|^2 \delta(\omega - \omega_M) \rangle_{\mathrm{dis}} \,, \tag{3.2}$$

where $\hbar\omega_M$ is the energy of the Mth exciton state, $|c_m^{(M)}|^2$ is the probability that pigment m is excited in the Mth exciton state. For example from the $d_{\mathrm{Pheo_{D1}}}(\omega)$ in the lower part of Fig. 3.9 it is seen that $\mathrm{Pheo_{D1}}$ contributes mainly to an exciton state at 672 nm (M=4) but that it also participates in the lowest exciton state (M=1). Overall, the delocalization of excited states of the core pigments in the present model is lower than in the previous multimer model of equal site energies (Durrant et al., 1995; Renger et al., 2002a) and larger than in a model that assumes delocalization only in the special pair (Konermann et al., 1996).
The excited states of the peripheral chlorophylls are localized and carry the oscillator strength of monomeric chlorophyll. The stronger coupling between the six core pigments redistributes their oscillator strength to the red side of the spectrum, as found earlier by Durrant et al. (1995) and Renger et al. (2002a). Therefore, there is a large contribution from Chlz in the blue part of the absorption spectrum of D1-D2 RC-complexes.
The temperature dependence of the site energy of $\mathrm{Chl_{D2}}$ inferred from the calculation of the temperature dependence of absorption and T-S spectra may be due to a partial charge transfer character of the excited state of $\mathrm{Chl_{D2}}$. In bacterial reaction centers a 30 nm blue shift of

the low–energy absorption band was observed by Huber et al. (1998) between 15 K and room temperature. This shift was explained recently by Renger et al. (2004) by a dynamic localization of a mixed excited/charge transfer state.

From unconventional Stark spectra measured by Frese et al. (2003) such a charge transfer character of a state in the red side of the spectrum was suggested. Further support for this view is obtained from calculation of absorption difference spectra of PS-II core complexes. In those calculations the same site energies as in D1-D2 complexes can be assumed except for Chl_{D2} which has a 3 nm red-shifted site energy in PS-II core complexes. Since charge transfer interactions depend on wavefunction overlaps of different pigments, small conformational changes of the protein, as they may occur in different preparations, can have a visible effect on the optical spectra. The small negative bleaching between 685 nm and 690 nm in the experimental difference spectrum of the preparations with 5 and 6 chlorophylls (Fig. 3.6) might have the same origin. Alternatively, it was suggested by Konermann et al. (1996) that an additional non-stochiometrically bound chlorophyll absorbs at this wavelength.

Besides the site energies, an important parameter determined from the temperature dependence of the absorption spectrum in Fig. 3.7 is the Huang Rhys factor S=0.65. This value is in agreement with the S=0.7 determined from hole burning studies (Groot et al., 1996) for the lowest state and the $S = 0.7$ determined for $Pheo_{D1}$ by Tang et al. (1990) and the $S < 1$ determined for higher energy exciton states by Jankowiak et al. (1989). Larger S-values (S=1.6... 1.9) for a low-energy exciton state have been obtained from fluorescence line narrowing (Peterman et al., 1998) and site selective triplet minus singlet absorption spectra measured by Jankowiak et al. (1989) and Kwa et al. (1994).

In calculations, for simplicity, the same S-factor was assumed for all pigments of the same subunit. A more detailed description should include the mixing with charge transfer states and will lead to a larger S-factor of the states with partial charge transfer character (Renger et al., 2004).

3.3.2 Verification of site energies of D1/D2 complex pigments

Position at which pigments manifest their presence in spectra is due to excitonic coupling shifted with respect to their site energies. Such situation is clearly visible in the difference spectra in Figs. 3.3 and 3.4 A, B. The three low–energy pigments, Chl_{D1}, $Pheo_{D1}$ and $Pheo_{D2}$, show a negative bleaching at about 680 nm, instead of 678nm or 672/675nm. Excitonic coupling is also responsible for the positive peak occurring between 670 nm and 678 nm in the 10 K T-S spectrum and in the difference spectra with modified pheophytins.

In the case of reduced $Pheo_{D1}$ (site energy of 672nm) in Figs. 3.5 A and B, position of negative bleaching ∼681nm. is a consequence of mixture of excitonic and electrochromic effects. By reducing $Pheo_{D1}$ the change in excitonic coupling to Chl_{D1} leads to a blue shift of the low-energy exciton band, that is dominated by Chl_{D1}, causing the main bleaching at 681 nm in the difference spectrum. The bleaching of an exciton state at 671 nm (dotted line in Fig. 3.5 A), that is dominated by $Pheo_{D1}$, is compensated by electrochromic effects in the difference spectrum with reduced $Pheo_{D1}$ in Fig. 3.5 A. So although one would expect in this experiment to see clear effect of reducing $Pheo_{D1}$ on absorption spectrum, what is seen instead is contribution of Chl_{D1}. Worth noting is, that the contribution of $Pheo_{D1}$ in the lowest exciton state (and hence its excitonic coupling with Chl_{D2}) is seen also in the lower part of Fig. 3.9. In the spectrum with reduced $Pheo_{D1}$ and oxidized P_{D1} in Fig. 3.5 B this bleaching appears in the theoretical spectrum as a separate peak and in the experimental spectrum as a shoulder.

The value of $\epsilon_{\text{eff}} = 2$ used in the calculation of electrochromic shifts in site energies is smaller than the $\epsilon_{\text{eff}} = 4.5 - 4.7$ for the electron transfer active L-branch of bRC but similar to the $\epsilon_{\text{eff}} = 1.5 - 1.6$ for the electron transfer inactive M-branch of bRC reported by Steffen et al.

(1994).

The localization of the triplet at Chl_{D2} at low temperatures in Fig. 3.3 agrees with an earlier prediction of van Mieghem et al. (1991) who inferred from EPR measurements that the triplet is localized on a pigment with a chlorine plane that is tilted by 30 degrees with respect to the membrane. The verification and specification of this earlier proposal (van Mieghem et al., 1991) by calculations that are based on parameters extracted from independent experiments is one of main results of this thesis. The calculations in Fig. 3.3 proof, both, the site energy of Chl_{D2} and the localization of the triplet state at this pigment at low temperatures.

The thermally activated hopping of the triplet between Chl_{D1} and P_{D1} at higher temperatures in Fig. 3.8 is in agreement with FTIR measurements by Noguchi et al. (1993), EPR measurements by Kamowski et al. (1996) and T-S spectra on mutants by Diner et al. (2001). For the energy difference of the two triplet states of D1/D2 complex, $^3Chl_{D1}$ and $^3P_{D1}$, values of 8 meV and 13 meV were inferred from the temperature dependence of the spectra by Noguchi et al. (1993) and Kamowski et al. (1996). The present value of 10 meV is in between those two earlier values. The contribution due to the triplet state at P_{D1}, provides evidence for the site energy of the "special pair" pigments P_{D1} and P_{D2} which give rise to an exciton state around 675 nm (compare Fig. 3.9) that is bleached upon triplet formation at P_{D1} and leads to the high energy shoulder in the spectrum in Fig. 3.8.

The experimental and calculated difference spectra, RC-5 - RC-6 in Fig. 3.6 show a main bleaching around 667 nm, which agrees with the site energies assigned for the two Chlz. Since the excited states of the Chlz are localized, the bleaching occurs at the position of their site energy. There is support for the present assignment of nearly equal site energies for the two Chlz from time-dependent measurements as will be discussed in detail later.

Finally, there is one experiment (Jankowiak et al., 1999) where $Pheo_{D2}$ was reported to be reduced and a main bleaching in the difference spectrum was measured at 668 nm, which cannot be described by the present set of parameters. The interpretation (Jankowiak et al., 1999) of the 668 nm bleach as site energy of $Pheo_{D2}$ is in contrast with the present assignment of 675 nm, which can explain the exchange experiments by Germano et al. (2001, 2000) that find a main bleaching at 680 nm as shown in Fig. 3.4 A, B and discussed above. Based on their interpretation of the 668 nm bleach, it was suggested (Jankowiak et al., 1999) that $Pheo_{D2}$ is effectively decoupled from the other reaction center pigments. On the basis of the recent structural data (Biesiadka et al., 2004; Ferreira et al., 2003), neither the excitonic couplings, nor the present determination of site energies support this so–called pentamer model (Jankowiak et al., 1999).

3.3.3 Functional implications

Using the parameters determined and verified from optical spectra, excitation energy transfer was calculated in Fig. 3.10. The left part of Fig. 3.10 shows that exciton relaxation among the six core pigments occurs on a subpicosecond time scale in agreement with pump-probe experiments (Durrant et al., 1992). In the right part of Fig. 3.10 it is seen that $Chlz_{D1}$ and $Chlz_{D2}$ transfer their excitation energy on a 10-100 ps time scale to the core pigments. The latter result is in agreement with pump–probe experiments by (Vacha et al., 1995) who find a 50 % decrease of a slow component around 670 nm when they compare the kinetics in RC-5 and RC-6 preparations after 665 nm excitation. It is likely that the remaining 50 % of the slow component in RC-5 preparations is due to the second Chlz and, therefore, that both Chlz absorb around 670 nm, in agreement with the present and our earlier (Renger et al., 2002a) calculations.

The life times in the 100 fs - 1 ps range obtained at room temperature at low energies around 680 nm (inset of upper left part in Fig. 3.10) agree with relaxation times found in transient anisotropy measurements (Merry et al., 1996) at room temperature. From the anisotropy studies

(Merry et al., 1996) an angle of 70 ±10 degrees was obtained for the two low energy exciton states that are responsible for the decay of the anisotropy. As shown in the upper part of Fig. 3.9 the two lowest exciton states in the present model are dominated by Chl_{D2} and $Pheo_{D2}$. The angle between their optical transition dipole moments is 68 degrees. We conclude that the experimental anisotropy decay reflects excitation energy transfer between Chl_{D2} and $Pheo_{D2}$.

In the calculation of primary electron transfer, assuming a constant intrinsic rate constant k_{intr}, a very different temperature dependence of the primary electron transfer is found when the primary donor is assigned either to Chl_{D2} or to P_{D1}. The first case is associated with an acceleration of electron transfer, because at low temperatures only the lowest exciton state is populated and this state is dominated by Chl_{D2}. Because of the minor contribution of P_{D1} in the lowest exciton state (as seen in the middle part of Fig. 3.9), electron transfer slows down considerably with decreasing temperature if P_{D1} is assumed to be the primary donor. There are contrasting experimental evidences concerning either an increase (Groot et al., 1997) or a decrease (Greenfield et al., 1997, 1999) of the primary electron transfer rate with temperature.

A rather direct way of detecting primary charge transfer was chosen by (Greenfield et al., 1997, 1999) who detected the time-dependent rise of the pheophytin anion band and simultaneously the bleach of the Qx band of pheophytin. In their studies (Greenfield et al., 1997, 1999) the fast phase of electron transfer was found to increase between $(8\mathrm{ps})^{-1}$ at 277 K and $(5\mathrm{ps})^{-1}$ at 7 K. This increase of the rate is in agreement with the present calculations, if the primary electron donor is identified as Chl_{D2}. If P_{D1} is the donor the calculated decrease of the rate with decreasing temperature is much more dramatic than in the alternative set of experimental data (Groot et al., 1997). Based on the above results we infer that Chl_{D1} is likely to be the primary donor in PS-II.
We note, that the multiexponential decay that is calculated for low temperatures is due to the disorder that can give rise to a lowest energy exciton state that is localized on a pigment different from the primary donor, an effect discussed earlier by (Prokhorenko et al., 2000). However, this effect disappears at higher temperatures when more states than the lowest exciton state contribute, although multiexponential decay is also measured at room temperature (Greenfield et al., 1997). We, therefore, conclude that additional sources for dispersive kinetics are present in the experiment, as, for example, a distribution of intrinsic charge transfer rate constants.

This point is related to the question: Which is the fluorescent state in D1D2-complexes at low temperatures ? In the calculation of fluorescence in Fig. 3.2 we implicitly assumed that there exists a certain fraction of complexes which are not capable of performing charge transfer and fluoresce but have an identical excitonic structure as those complexes which transfer electrons. In the following the internal consistency of this assumption is discussed.

In electron transfer active complexes, the quantum yield of the fluorescence is limited by the competition of fluorescence and charge transfer, both occurring from an equilibrated excited state manifold. The relative yield $\langle k_{\mathrm{flu}}/(k_{\mathrm{flu}}+k_{\mathrm{cs}})\rangle_{\mathrm{dis}}$, calculated from the present parameters, the k_{et} and a $k_{\mathrm{flu}} = (4\mathrm{ns})^{-1}$ (Groot et al., 1996), varies between 0.02 at 4 K and 0.008 at 60 K. These values have to be compared with the ratio $\eta_{\mathrm{D1D2}}/\eta_{\mathrm{Chl}}$ of fluorescence quantum yields of D1D2-complexes and of chlorophyll *a* in solution, that varies between $0.07/0.3 = 0.23$ at 4 K and $0.06/0.3 = 0.20$ at 60 K (Groot et al., 1994). The one order of magnitude difference between the calculated and measured yields shows that in the present model the trap fluorescence is too weak to explain the experiment. However, part of the decrease of the experimental yield with increasing temperature might be due to decreasing trap fluorescence.

The spectrum, obtained for the trap fluorescence by weighting the homogeneous fluorescence of every complex by the factor $k_{\mathrm{flu}}/(k_{\mathrm{flu}}+k_{\mathrm{cs}})$ and averaging over disorder, is similar in shape to the fluorescence spectrum calculated in Fig. 3.2 but red–shifted by 2-3 nm. In addition, in the present model, the trap fluorescence is dominated by $Pheo_{D2}$. However, site selection

experiments show, that the fluorescence at low temperatures is mainly due to chlorophyll and not due to pheophytin (Kwa et al., 1994; Peterman et al., 1998; Konermann et al., 1997). In summary, the present model is consistent with a fluorescence occurring from an exciton state with the main contributions from Chl_{D2} and disagrees with a model that assumes major contributions to the fluorescence from trap states. It is inferred, therefore, that Chl_{D2} plays a double role, it acts as the primary electron donor in one fraction and fluoresces in another fraction of complexes in the sample.

What could be the functional relevance of Chl_{D2} to be the location of the triplet state and the primary electron donor ? As discussed in the introduction it was suggested (van Mieghem et al., 1995; Noguchi, 2002) that triplets at Chl_{D2} can be efficiently quenched by singly reduced Q_A. Since these triplet states which are formed by charge recombination can react with triplet oxygen to form the physiologically dangerous singlet oxygen, the proposed quenching mechanism (Noguchi, 2002), and thereby the location of the triplet state, are of importance for protecting the photosystem under light stress.

If Chl_{D2} is the primary electron donor, electron transfer is favored energetically only along one branch for the following reasons: The neighboring P_{D1} has the lowest oxidation potential since the cation is known to be stabilized there, and so in a simple picture it has the highest HOMO level of the core pigments. Therefore, it is likely that the highest LUMO level also belongs to P_{D1} and, hence, P_{D1} could transfer an excited electron energetically downhill along both branches. For the same reasons, the Chl_{D2} can transfer the electron downhill only to the $Pheo_{D1}$. The unidirectionality of electron transfer in PS-II might have the advantage to limit the photophysical damage to one branch.

Chapter 4

Optical spectra of reaction centers in Photosystem II core complexes

In this chapter absorbance difference spectra associated with the light-induced formation of functional states in photosystem II core complexes from *Thermosynechococcus elongatus* and *Synechocystis* sp. PCC 6803 (e.g. ^{3}P-^{1}P, $P^+_{D1}Pheo^-_{D1}-P_{D1}Pheo_{D1}$, $P^+_{D1}Q^-_A-P_{D1}Q_A$) are described. In addition, effects of site-directed mutations of D1-His198, the axial ligand of the "special pair" chlorophyll P_{D1}, and D1-Thr179, an amino acid residue nearest to the accessory chlorophyll Chl_{D1}, on the spectral properties of reaction center are analyzed. Using pigment transition energies (site energies) determined in the previous chapter from independent experiments on D1-D2-cyt*b*559 complexes, good agreement between calculated and experimental spectra is obtained. The only difference in site energies of the reaction center pigments in D1-D2-cyt*b*559 and photosystem II core complexes concerns Chl_{D1}. Compared to isolated reaction centers, the site energy of Chl_{D1} is red shifted by 4 nm and less inhomogeneously distributed in core complexes. The site energies cause primary electron transfer at cryogenic temperatures to be initiated by an excited state that is strongly localized on Chl_{D1} rather than from a delocalized state as assumed in the previously described multimer model. This result is consistent with earlier experimental data on "special pair" mutants and with calculations on D1-D2-cyt*b*559 complexes, presented in the last chapter. The calculations show that at 5 K the lowest excited state of the reaction center is lower by about 10 nm than the low-energy exciton state of the two "special pair" chlorophylls P_{D1} and P_{D2} which form an excitonic dimer. The experimental temperature dependence of the wild type difference spectra can only be understood in the present model if temperature dependent site energies are assumed for Chl_{D1} and P_{D1}, reducing the above energy gap from 10 to 6 nm upon increasing the temperature from 5 to 300 K. At physiological temperature there are considerable contributions from all pigments to the equilibrated excited state P^*. The contribution of Chl_{D1} is twice that of P_{D1} at ambient temperature, making it likely that the primary charge separation will be initiated by Chl_{D1} under these conditions. The calculations of absorption difference spectra provide independent evidence that after primary electron transfer the hole stabilizes at P_{D1}, and that the physiologically dangerous charge recombination triplets, which may form under light stress, equilibrate between Chl_{D1} and P_{D1}.

This chapter is organized in the following way. First an overview of the problems addressed in this chapter is given. Next calculations of difference spectra of wild type and mutant core complexes, that identify the functional states are presented. The temperature dependence of the wild type difference spectra is discussed. At the end a discussion of (i) the necessary revision of the multimer model, (ii) an identification of functional states at physiological temperatures, and (iii) functional implications of our exciton model is provided.

4.1 Overview

The following scheme of primary reactions was established for PS-II by various spectroscopic techniques (recent reviews are given in Refs. (Renger et al., 2005; Diner et al., 2002)). Optical excitation of the reaction center, either directly or via excitation energy transfer from the core antennae CP43 and CP47 generates a state commonly referred to as P^* which donates an electron to the pheophytin of the electron transfer active D1-branch, $Pheo_{D1}$ and a state $P^+Pheo^-_{D1}$ is formed. The electron is transferred further to the plastoquinone Q_A and the hole via a tyrosine, Tyr_Z, to the manganese cluster, where the water splitting reaction takes place. Under light stress, a triplet state $^3P_{680}$ may be generated in the reaction center by charge recombination of $^3[Pheo^-_{D1}\ P^+_{680}]$. Although the overall reaction scheme is clear, the molecular identities of some of the functional states and the mechanistic and kinetic details are not.

It is still not entirely clear whether electron transfer at physiological temperatures starts at the accessory chlorophyll of the D1-branch Chl_{D1} or at the "special pair" chlorophyll P_{D1} or both. On the one hand there are recent reports by Groot et al. (2005) and Holzwarth et al. (2006) who inferred independently from femtosecond IR studies and pump-probe experiments in the visible spectral region, respectively, that the primary electron transfer at physiological temperatures occurs between Chl_{D1} and $Pheo_{D1}$. However, the reported timescale for the pheophytin reduction differs by a factor of four to five. Whereas Groot *et al.* report a 600-800 fs time constant, that of Holzwarth *et al.* is 3 ps.

In contrast, Novoderezhkin et al. (2005), based on a fit of linear and time-resolved non-linear optical spectra, using an exciton model including charge transfer (CT) states, concluded that the primary charge separated state is an intra "special pair" CT state that either is directly optically excited or populated within 100 fs by exciton relaxation from the core pigments. This idea seems to be in line with studies of Krausz et al. (2005) who detected a long wavelength excited state capable of charge separation. One difference between the two CT states is that the one of Novoderezhkin *et al.* is broadened inhomogeneously whereas the one of Krausz was shown to be homogeneously broadened (Krausz et al., 2005). In more recent work, Novoderezhkin et al. (2007) concluded that two parallel electron transfer pathways exist, one starting from an intra dimer CT state of the "special pair" and one at Chl_{D1}, where the relative importance of the two pathways is determined by the specific realization of disorder in site energies.

A key idea about the identity of the primary electron donor in PS-II came from van Brederode and van Grondelle *et al.* (van Brederode et al., 1997, 1999,a), who found that in bacterial reaction centers there is ultrafast electron transfer from the excited state of the accessory bacteriochlorophyll (B_A) of the L-branch. Electron transfer from B^*_A is an order of magnitude faster than electron transfer from the low energy exciton state of the special pair. However, in bacterial reaction centers the slow pathway is dominant because of the large energy gap between the low energy special pair exciton state and the remaining excited states that gives rise to an equilibrated excited state population that is localized at the special pair. The fact that the excited states of the PS-II reaction center are much closer in energy, as seen, e.g. from the absorption spectrum, led van Brederode and van Grondelle *et al.* to suggest (van Brederode et al., 1999a) that the fast side pathway in bacterial reaction centers might be the dominant one in PS-II.

Very much related to the question of the identity of the primary electron donor is the extent to which P^* is a delocalized excited state of the core pigments, as assumed in the multimer model, or an excited state, that is localized on a particular pigment, the primary electron donor. In the original multimer model proposed by Durrant et al. (1995) all of the pigments, in the absence of excitonic couplings, had the same mean transition energy (site energy). In such a model, all of the exciton states are delocalized over a number of core pigments, where the extent of delocalization and the energy and population of a particular exciton state depend on the particular realization of static disorder, caused by slow conformational motion of the protein.

As the coupling between the two "special pair" chlorophylls is the largest in all multimer models (Durrant et al., 1995; Leegwater et al., 1997; Prokhorenko et al., 2000; Renger et al., 2002; Barter et al., 2003), the lowest exciton state contains a considerable contribution from the "special pair" chlorophylls.

In contrast to these traditional multimer models, we suggested an exciton model (see sec. 3.2, and Raszewski et al. (2005)) with blue shifted site energies of the "special pair" pigments and a red shifted site energy of Chl_{D2}, that results in a high degree of localization of the lowest exciton state on the latter, a second lowest exciton state with a large contribution from the pheophytin $Pheo_{D2}$ of the inactive D2-branch and where only the third lowest exciton state is the low-energy exciton state of the "special pair". This model explains 11 independent optical spectra of the D1-D2-cyt*b*559 complexes, including difference spectra with chemically modified, oxidized and reduced pigments and pigments in the triplet state (Raszewski et al., 2005) (see sec.3.2). In a recent work of Novoderezhkin et al. (2007) similar site energies were inferred.

The D1-D2-cyt*b*559 complexes unfortunately contain neither the manganese cluster nor the primary quinone electron acceptor Q_A. Consequently, it is not possible to investigate with this material the whole sequence of primary and secondary electron transfer reactions. In addition, because of the rather harsh isolation procedure of the D1-D2-cyt*b*559 complexes, it cannot be excluded that the transition energies of the reaction center pigments might be different from those in core complexes. This point has been raised ever since D1-D2-cyt*b*559 preparations became available (see e.g. Renger et al. (2005) and references therein). In this chapter evidence is provided that the D1-D2-cyt*b*559 complexes represent a valid model system for the reaction center pigments in PS-II core complexes, as concerns the transition energies of the pigments. The only modification with respect to proposed site energies of D1-D2-cyt*b*559 complexes concerns Chl_{D1}, the site energy of which is red shifted in core complexes and less inhomogeneously distributed.

A major difficulty in interpreting optical experiments on PS-II core complexes is that the bands of the reaction center pigments strongly overlap each other as well as the bands of the pigments in the core antenna subunits, CP43 and CP47. Therefore it is difficult in such a complex to excite particular states of the reaction center. An alternative is to measure optical difference spectra of core complexes in which particular reaction center pigments have been converted into a different electronic state. The optical difference spectrum reveals only those pigments that are coupled to the pigment that has undergone a change in electronic state. As the couplings between the reaction center pigments and the pigments in the CP43 and CP47 subunits are weak, the difference spectra provide direct information about the reaction center pigments of PS-II core complexes without interference from the antenna pigments. The combination of optical difference spectroscopy with site-directed mutagenesis, in which amino acid residues in the local environment of certain chlorophylls are replaced, provides valuable information regarding the transition energies of these pigments located at the sites of mutation.

Studies of the lowest excited state P^* and of the state P^+_{680} at low temperatures, from triplet minus singlet (T-S) and P^+_{680}- P_{680} difference spectra on wild type and mutants of the axial ligands of the "special pair" chlorophylls of *Synechocystis* sp. PCC 6803 provided evidence that electron transfer starts at Chl_{D1} and that the hole stabilizes at P_{D1} at low temperatures (Diner et al., 2001). In addition, recent experiments on mutants with changes in the local environment of Chl_{D1} have provided direct evidence that the charge recombination triplet is localized on Chl_{D1} at low temperatures (Schlodder et al., 2008).

In this chapter an independent verification of the molecular identities of the states P^*, P^+_{680}, and $^3P_{680}$ from exciton calculations of wild type difference spectra at low temperature and comparison with experimental data is presented. It is demonstrated that the exciton model presented previously in sec. 3.2 for D1-D2-cyt*b*559 complexes (Raszewski et al., 2005), explains these wild type spectra as well as the difference spectra measured on mutant core complexes.

An important question is: Do the experimental and theoretical studies at cryogenic temperatures reflect the same primary reactions that occur in the living cell, i.e., at physiological temperatures ? There is a remarkable change of several difference spectra with increasing temperature (Hillmann et al., 1995). At low-temperature multiple bands are visible in the P^+_{680}-P_{680} difference spectrum, whereas at room temperature just a single bleaching band at 680 nm appears, the origin of the spectroscopic term P^+_{680}. This strong overlap of different bands at physiological temperatures is a major obstacle in identifying functional states.

It is shown in this chapter that the identity of the functional states does not change significantly as function of temperature. The temperature dependence of the dielectric constant and of the site energies of Chl_{D1} and P_{D1} are responsible for the temperature dependence of the difference spectra involving P^+_{680}. This change in site energies, however, does not alter the exciton model, in that the lowest excited state is still localized at Chl_{D1}. In the case of the T-S spectrum, at higher temperatures more than one triplet state contributes.

4.2 Results

4.2.1 Difference absorption spectra

Three calculated optical difference spectra are compared in Fig. 4.1 with experimental spectra measured by Hillmann et al. (1995) on core complexes of *Thermosynechococcus elongatus*, the same PS-II core complex for which the three dimensional structure was recently determined (Loll et al., 2005). The site energy of the accessory chlorophyll of the D1-branch, Chl_{D1}, was red-shifted by 4 nm from 678 nm in D1-D2-cyt*b*559 complexes (see sec.3.2) (Raszewski et al., 2005) to 682 nm in PS-II core complexes.

In the calculation of the difference spectrum (P^+_{680} $Pheo^-$ - P_{680} Pheo) in the upper part of Fig. 4.1 it was assumed that the electron is localized at the pheophytin of the D1-branch, $Pheo_{D1}$, and the hole resides at the "special pair" chlorophyll of the same branch, P_{D1}. The first assumption is justified by the fact that electron transfer occurs only along the D1-branch (Shkuropatov et al., 1997, 1999) and the second one, suggested earlier from difference spectra measured on mutant core complexes (Diner et al., 2001), was verified by considering different possibilities of hole stabilization as discussed in detail further below. The experimental and calculated spectra show two bleachings, one around 675 nm and one around 685 nm. When the electrochromic shifts are neglected, only a single bleaching around 675 nm is obtained, whereas the one at 685 nm vanishes. The strongest electrochromic shift of 5.6 nm to the blue was calculated for the accessory chlorophyll of the D1-branch, Chl_{D1}.

The two bleachings are also seen in the experimental and calculated (P^+_{680} Q^-_A - $P_{680}Q_A$) spectrum in the middle part of Fig. 4.1. In the calculated spectrum, the low energy bleaching also vanishes if no electrochromic shifts are included. However, the amplitude of the low energy bleaching is smaller than the bleaching of the high energy one, whereas in the P^+_{680} $Pheo^-$ - P_{680} Pheo spectrum discussed above the low energy bleaching is stronger. The site energy of Chl_{D1} shifts most appreciably in the P^+_{680} Q^-_A spectrum, by 3.3 nm to the blue. This shift is only about half of that calculated for P^+_{680} $Pheo^-$. The best agreement between the experimental and calculated spectra is obtained by assuming that the hole is localized at P_{D1}, as suggested earlier (Diner et al., 2001). The spectra for alternative placement of the cation in the state P^+_{680} including P^+_{D2}, $(P_{D1}P_{D2})^+$, and Chl^+_{D1} are shown in Fig. 4.2 and give less satisfying agreement with the experimental data.

The experimental and calculated T-S spectra in the lower part of Fig. 4.1 show a main bleaching around 684 nm. We note that the position of this bleaching is red shifted by about 3 nm with respect to the one reported for D1-D2-cyt*b*559 complexes (Germano et al., 2001). The experimental spectra were measured for two different states of Q_A, singly (squares) and

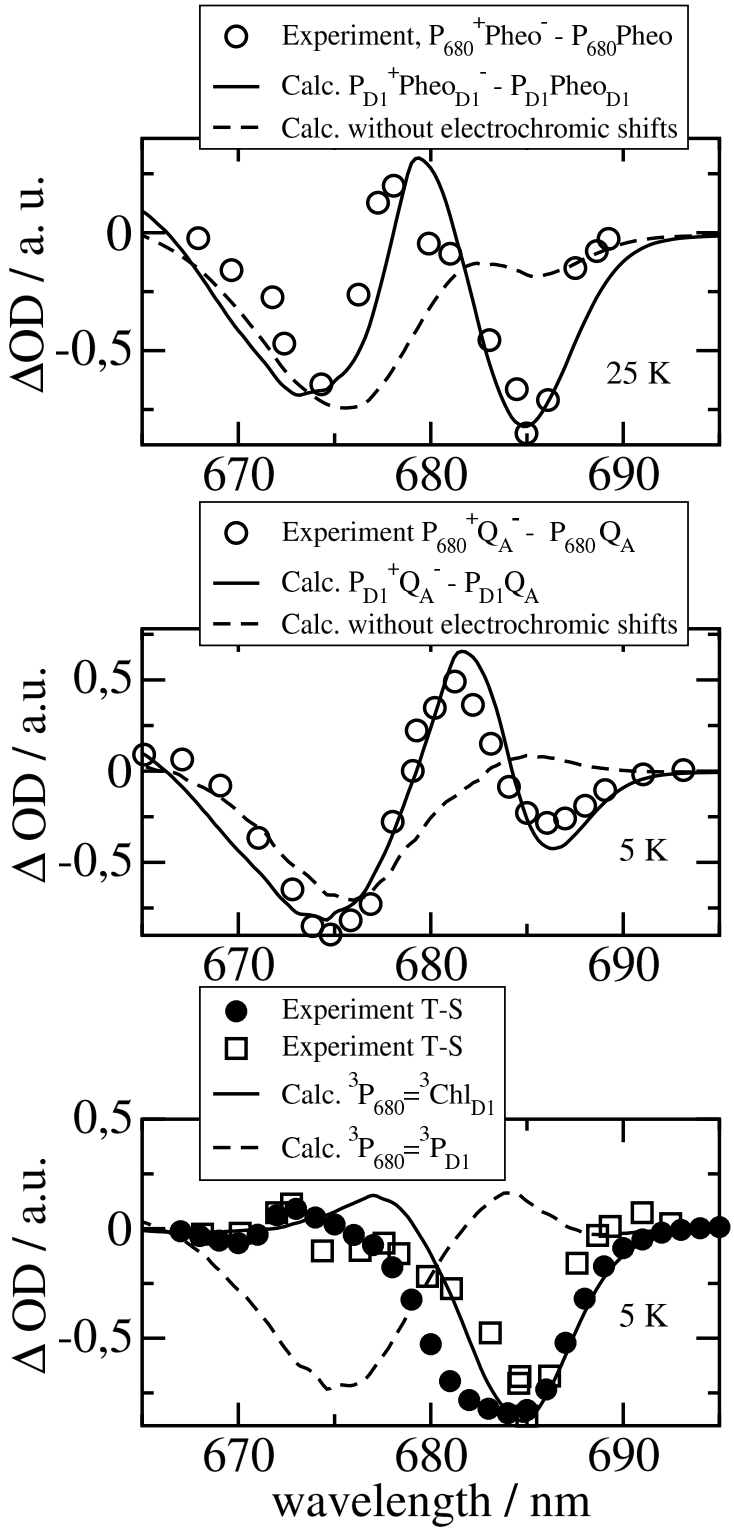

Figure 4.1: Experiments (Hillmann et al., 1995) and calculations of optical difference spectra of PS-II core complexes from *Thermosynechococcus elongatus*. The calculations were performed using the site energies determined previously 3.2 (Raszewski et al., 2005), except for Chl_{D1} which was shifted by 4 nm to the red. The wavelengths in nm assigned to each pigment are P_{D1}: 666 nm, P_{D2}: 666 nm, Chl_{D1}: 682 nm, Chl_{D2}: 667 nm, $Pheo_{D1}$: 672 nm, $Pheo_{D2}$: 675 nm. The two experimental T-S spectra were obtained for singly (open squares) and doubly (filled circles) reduced Q_A. In the latter case it is also possible that Q_A has dissociated from the core complex.

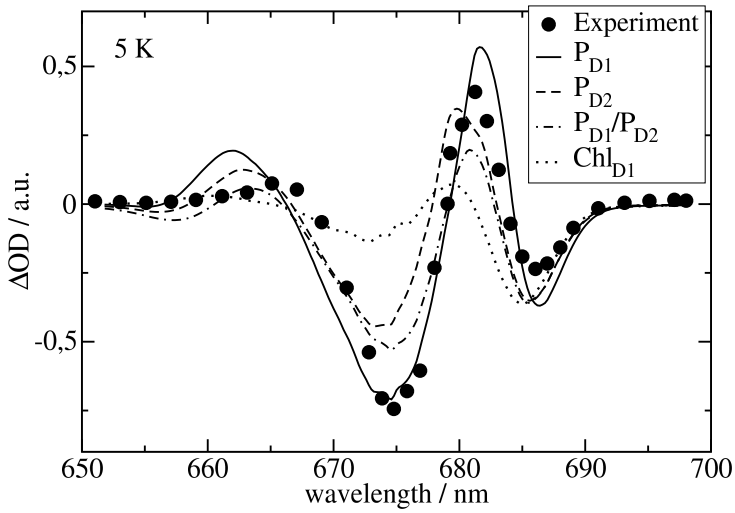

Figure 4.2: Calculation of P^+_{680} Q^-_A - $P_{680}Q_A$ difference spectrum using different assumptions for the localization of the cation in the P^+_{680} state, in comparison with experimental data (Hillmann et al., 1995). For $P^+_{680} = (P_{D1}P_{D2})^+$, 0.5 elementary positive charges were put on both "special pair" chlorophylls for the calculation of electrochromic shifts. For better comparison with experimental data, the calculated spectra were scaled such that their low energy bleaching gets equal in magnitude.

doubly (filled circles) reduced, giving rise to two different widths of the main bleaching. The reason for the difference is unclear and indicates larger conformational disorder of the protein for doubly reduced Q_A. In the calculations, the triplet state was assumed to be localized at Chl_{D1}, in agreement with recent mutant spectra (Schlodder et al., 2008), discussed below. An alternative assignment of the triplet state as $^3P_{D1}$ yields a main bleaching at 675 nm (dashed curve) in strong contradiction with the experimental data. T-S spectra calculated assigning the triplet state to any other pigment in the reaction center are shown in Fig. 4.4 and also do not fit the experimental data of Fig. 4.1.

The density of exciton states $d_M(\omega)$ (eq 3.1) is compared in Fig. 4.3 with the exciton states pigment distribution $d_m(\omega)$ (eq 3.2). The very similar shape of $d_{M=1}(\omega)$ and $d_{m=\mathrm{Chl_{D1}}}(\omega)$ shows that the lowest exciton state $M = 1$ around 685 nm is dominated by Chl_{D1}. The next higher exciton state $M = 2$ has large contributions from $Pheo_{D2}$ and minor contributions from other pigments (Chl_{D2}, P_{D1}, P_{D2}). As seen in the middle part of Fig. 4.3 the "special pair" chlorophylls P_{D1} and P_{D2} form two delocalized exciton states $M = 3$ around 675 nm and $M = 6$ around 658 nm.

One might get the impression that it is easy to detect the "special pair" exciton states. However, Fig. 4.3 just considers the distribution of different pigments over the exciton states but not the oscillator strengths of the latter which determines the probability of an optical transition. According to this calculations, about 80 percent of the oscillator strength of the "special pair" is in the lower dimer state at 675 nm. Further, when interpreting optical difference spectra where a pigment was converted to a different electronic state one also has to take into account that this pigment does not participate in the delocalization of exciton states anymore.

This effect is seen in the T-S spectra in Fig. 4.4. The positions of the main bleachings obtained by assuming the triplet to be localized on P_{D1}, P_{D2}, and Chl_{D1} agree with the peak positions of the corresponding $d_m(\omega)$ in Fig. 4.3. However, the relative intensities of the minor peaks are different. Moreover the high energy exciton transition of the special pair seen in $d_{P_{D1}}(\omega)$ and $d_{P_{D2}}(\omega)$ at about 658 nm is not seen as a bleaching in the $^3P_{D1}$-P_{D1} and $^3P_{D2}$-P_{D2} spectra. Instead a positive band appears around 662 nm. This band is due to the monomer

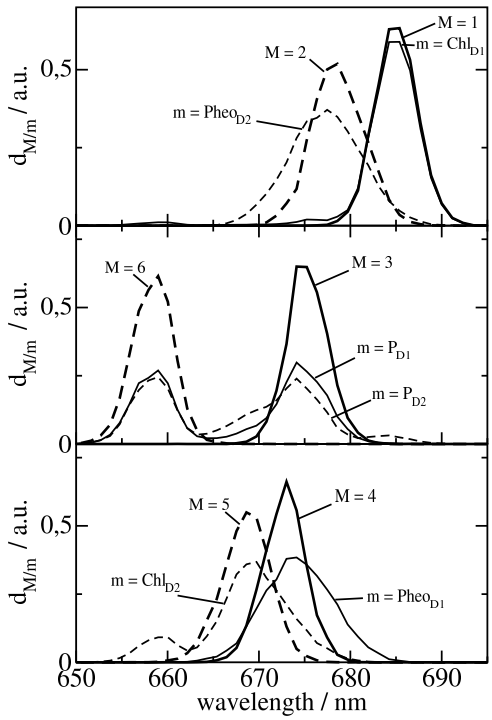

Figure 4.3: Density of exciton states $d_M(\omega)$ (Eq. 3.1) and exciton states pigment distribution (Eq. 3.2) for the 6 strongly coupled reaction center pigments.

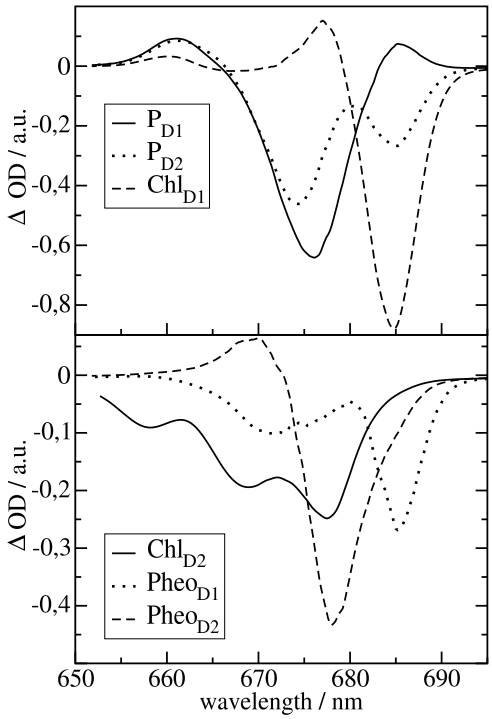

Figure 4.4: T-S spectra at 5 K calculated assuming the triplet state to be localized on the respective reaction center pigments.

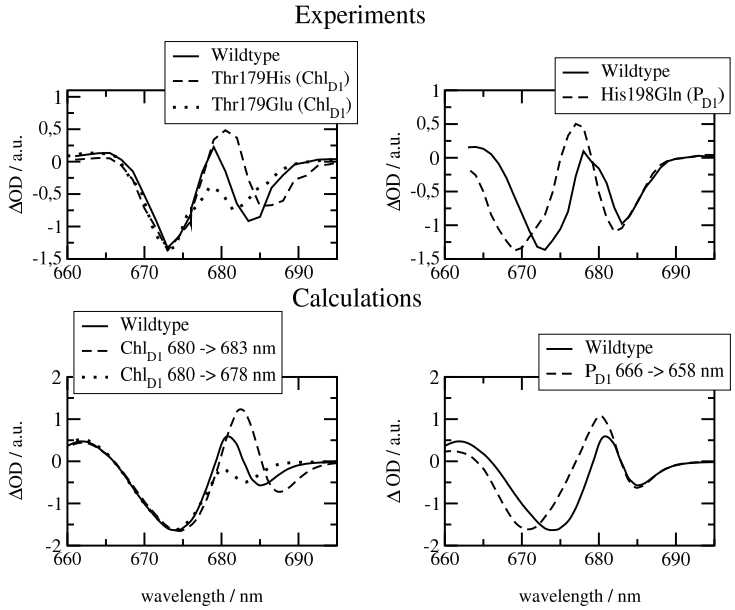

Figure 4.5: Experiments (upper part) and calculations (lower part) of wild type and mutant P^+_{680} Q^-_A - $P_{680}Q_A$ spectra of *Synechocystis* sp. PCC 6803 at 80 K.

absorption band of the special pair pigment that remains in its singlet state, while the other pigment is in the triplet state. As the monomer band is broader (due to the missing resonance energy transfer narrowing) and more intense than the low energy exciton band of the special pair, the latter is completely covered. Another interesting result is that the $^3P_{D1}$-P_{D1} and $^3P_{D2}$-P_{D2} spectra differ at long wavelengths. Obviously there is a mixing between the excited states of the special pair chlorophyll P_{D2} and Chl_{D1} that redistributes oscillator strength. In that sense, although qualitatively true, it is too simple to speak about the exciton states of the special pair.

In the case of Chl_{D2} and the two pheophytins (lower part of Fig. 4.4), the positions of the main bleachings in the T-S spectra are shifted with respect to the peaks of the respective $d_m(\omega)$ in Fig. 4.3. Obviously the change in excitonic couplings that occurs when one pigment goes to the triplet state becomes even more important in this case. For example, the function $d_{\mathrm{Pheo_{D2}}}(\omega)$ shows that $Pheo_{D2}$ contributes strongest to an exciton state at 675 nm, whereas the main bleaching of the $^3Pheo_{D2}$-$Pheo_{D2}$ spectrum occurs at almost 679 nm. The excitonic coupling obviously redistributes oscillator strength between $Pheo_{D2}$ and Chl_{D2} in the singlet spectrum that is moved back in the triplet spectrum. The $^3Pheo_{D2}$-$Pheo_{D2}$ closely resembles the difference spectrum measured by Germano et al. (2001) for exchange of $Pheo_{D2}$ by a chemically modified pheophytin (see chapter 3.2), the absorbance of which is blue shifted. Due to the strong blue shift this pigment is effectively decoupled from the other pigments and the absorbance difference (except for the strongly blue shifted monomer absorption of the exchanged pheophytin) becomes very similar to the T-S spectrum calculated here.

4.2.2 Difference spectra of wild type and mutants of *Synechocystis* sp. PCC 6803

The P^+_{680} Q^-_A - $P_{680}Q_A$ spectra of wild type and mutants of *Synechocystis* sp. PCC 6803 are shown in Fig. 4.5. The axial ligand D1-His198 of the "special pair" chlorophyll P_{D1} was replaced by a glutamine in the D1-His198Gln mutant, whereas the D1-Thr179, which overlies the accessory chlorophyll Chl_{D1}, was replaced with a His or a Glu in the D1-Thr179 mutants. It has been proposed (Loll et al., 2005) that a water molecule, hydrogen bonded to D1-Thr179,

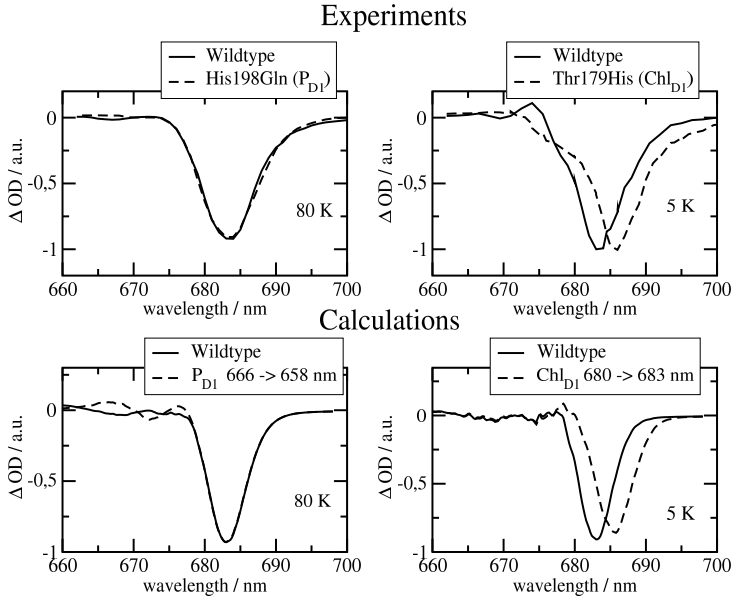

Figure 4.6: Experiments (upper part) and calculations (lower part) of wild type and mutant T-S spectra of *Synechocystis* sp. PCC 6803.

is the axial ligand of Chl_{D1}. The experimental spectra are shown in the upper part and the calculations in the lower part of this figure. The site energy of Chl_{D1} was shifted from 682 in *T. elongatus* to 680 nm to describe the spectral position of the low-energy bleaching in the wild type of *Synechocystis* sp. PCC 6803.

The shift of the low energy bleaching of the Chl_{D1} mutant, where Thr179 was replaced by His on the left half of Fig. 4.5 can be explained by shifting the site energy of Chl_{D1} by 3 nm to the red in the calculation of the mutant spectrum. The blue shift that is measured of the same band when Thr179 is replaced by Glu can be reproduced by assuming a 2 nm blue shift of the site energy of Chl_{D1} in the calculation. These mutations and site energy shifts do not effect the high energy absorbance band around 673 nm.

However the latter is shifted by the mutation of the axial ligand of P_{D1} as shown in the right half in Fig. 4.5. Upon changing His198 to Gln, a blue shift of the high energy bleaching results, a shift that is explained by assuming an 8 nm blue shift of the site energy of P_{D1} in the calculations. An important experimental and theoretical result here is that a local change at Chl_{D1} changes only the low energy bleaching in the spectrum and a local change at P_{D1} influences mainly the high–energy bleaching.

The T-S spectra of the same mutants and wild types are compared in Fig. 4.6 with the calculations. In agreement with experiment, a local change at P_{D1} does not influence the spectrum, whereas a red shift of the experimental and calculated bleaching occurs for the Chl_{D1} D1-Thr179His mutant. The same 3 nm red shift of the site energy of Chl_{D1} was assumed as in the calculations of the $P_{680}^{+}\ Q_A^{-}$ - $P_{680}Q_A$ spectrum of this mutant in Fig. 4.5.

The temperature dependence of the experimental T-S spectrum of wild type *Synechocystis* sp. PCC 6803 (Diner et al., 2001) is compared in Fig. 4.7 with the calculations. The site energy of Chl_{D1} was varied with temperature in accordance with previous analysis of D1-D2-cyt$b$559 reaction centers (chapter 3.2) (Raszewski et al., 2005), and the analysis of core complexes of *T. elongatus* below. As in the previous analysis of the D1/D2 complexes, it was assumed that there is a thermal equilibrium of the triplet state occupation at $^3Chl_{D1}$ and $^3P_{D1}$. From the fit of the spectra in Fig. 4.7 infers a free energy difference between the two triplet states of 11 meV, a

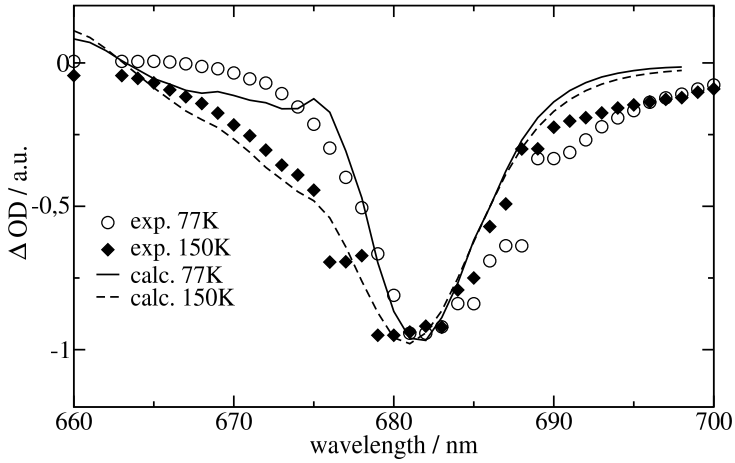

Figure 4.7: Experiments (Diner et al., 2001) and calculations of the temperature dependence of T-S spectra of *Synechocystis* sp. PCC 6803. The site energy of Chl_{D1} was assumed to change with temperature, corresponding to wavelengths of 680 nm at 77 K and 678 nm at 150 K.

value that is very close to the 10 meV determined for D1-D2-cyt$b$559 complexes (see chapter 3.2) (Raszewski et al., 2005) and in between the 8 meV (Noguchi et al., 1993) and the 13 meV (Kamowski et al., 1996) determined from FTIR and EPR studies, respectively, on D1D2-cyt$b$559 complexes.

4.2.3 Calculation of $Q_A^- - Q_A$ difference spectra

dffsf Several experiments in which $Q_A$was reduced were performed by Krausz *et al.* (*private communication*) and Schlodder et al. (2008). These were $Q_A^- - Q_A$ difference spectra of spinach, pea, BBY fragments and *Synechococus*, among with its mutations of Chl_{D1} coordinating amino acid threonine 179 into histidine and glutamic acid.

$Q_A^- - Q_A$ difference spectra of different species. Parameters used for calculations of $Q_A^- - Q_A$ difference spectra of different species do not differ from those used for the calculations of the spectra discussed above (sec. 3.2). The results of the calculations are compared with experimental data in Fig. 4.8. It is seen that the calculated spectra are in excellent agreement with the experimental data. Both the experimental bleaching at ∼685 nm and the peak at ∼683 nm are obtained in the calculation as well as the secondary bleaching at ∼675 nm (∼680 nm in case of *Synechococus*). The shape of the difference spectrum is explained in the following way: the bleaching at ∼685 nm is caused like in the $P_{D1}^+ Q_A^- - P_{D1} Q_A$ difference spectrum by electrochromic shift of the site energy of the Chl_{D1} by ∼1–2 nm to the blue. The site energy of $Pheo_{D1}$ red-shifts by ∼1–2 nm, which results in a shoulder on the blue slope of the peak at ∼683 nm (best visible in Fig. 4.8 *A* & *D*). This red-shift of $Pheo_{D1}$ is one of the reasons of the bleaching at ∼675 nm (∼680 for *Synechococus*). It has to be mentioned that the site energies of P_{D1} and P_{D2} blue shift by ∼1–2 nm and this shift co-creates a bleaching at ∼675 nm together with $Pheo_{D1}$. The positive contribution due to the blue shift of the site energies of the P_{D1} and P_{D2} in the difference spectrum covers practically the negative contribution that is due to the red shift of the site energy of $Pheo_{D1}$.

$Q_A^- - Q_A$difference spectra of Thr179His *Synechocystis* **mutant.** Recently Schlodder et al. (2008) measured the $Q_A^- - Q_A$spectrum of a *Synechocystis* mutant together with the WT $Q_A^- - Q_A$spectrum for comparison. The mutated Chl_{D1}-coordinating amino acid was turned

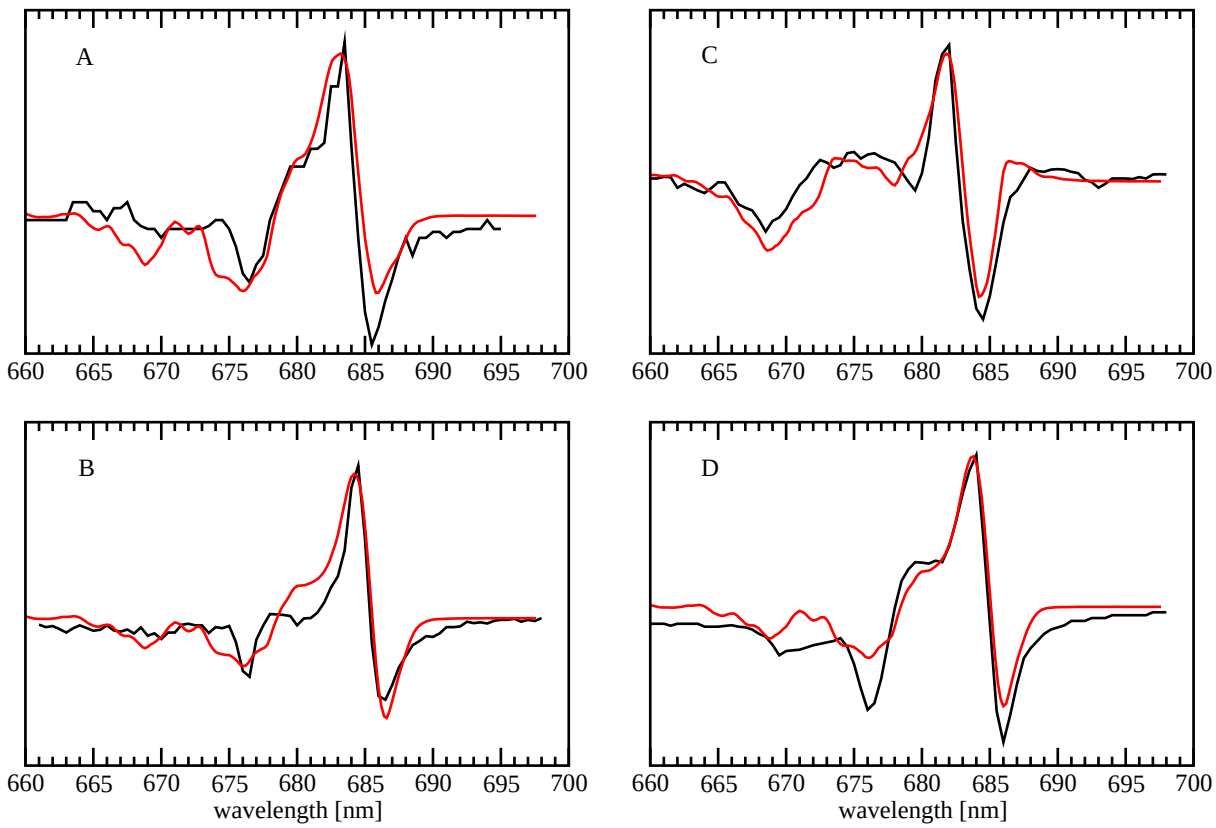

Figure 4.8: Calculation of $Q_A^- - Q_A$ spectra from different species at 1.7K A:) Difference spectra of spinach, experimental curve is black while calculated curve with parameters: Chl_{D1} at 681.5 nm, $D_{inh} = 180cm^{-1}$, $D_{inh}(Chl_{D1}) = 72cm^{-1}$ is red. B:) Difference spectra of BBY fragments, experimental curve is black while calculated curve with parameters: Chl_{D1} at 682 nm, $D_{inh} = 180cm^{-1}$, $D_{inh}(Chl_{D1}) = 54cm^{-1}$ is red. C:) Difference spectra of *Synechococus*, experimental curve is black while calculated curve with parameters: Chl_{D1} at 679.5 nm $D_{inh} = 200cm^{-1}$, $D_{inh}(Chl_{D1}) = 60cm^{-1}$ is red. D:) Difference spectra of pea, experimental curve is black while calculated curve with parameters: Chl_{D1} at 681 nm $D_{inh} = 180cm^{-1}$, $D_{inh}(Chl_{D1}) = 54cm^{-1}$ is red. All experimental data were collected by Krausz (*private communication*). D_{inh} is the width (Fwhm) of the inhomogeneous distribution function of the site energies.

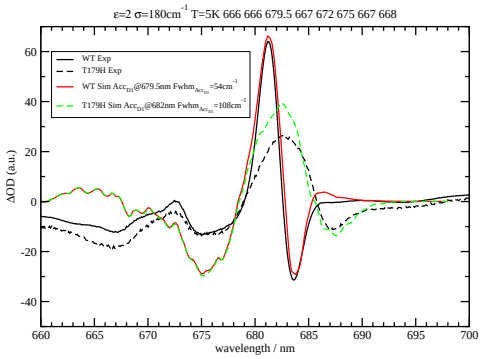

Figure 4.9: Calculation of $Q_A^- - Q_A$spectra of Thr179His *Synechocystis* mutant at 5K. Black lines are experimental data by Schlodder *et al.*, solid for WT and dashed for mutant. Red solid line is calculation of WT, while green dashed line is calculation of mutant spectrum.

from threonine into histidine at position 179 of the D1 polypeptide chain. The calculation of the WT $Q_A^- - Q_A$spectrum was performed using standard parameters (see 3.2), only the site energy of Chl_{D1} was shifted to 682 nm and its inhomogeneous distribution function was narrowed to 54 cm^{-1}. The calculated WT spectrum is compared in Fig. 4.9 with the experimental data, yielding excellent agreement. Both bleachings (∼677 and ∼684 nm) and the peak (∼681 nm) appear at the correct positions in the calculated curve. The calculated heights of the main bleaching (∼684 nm) and of the peak are very similar to the experimental heights, the calculated height of the secondary bleaching (∼677 nm) is a bit too large.

To calculate the mutant spectrum, site energy values determined previously for the same mutation were taken (see sec. 4.2.2). A width of 108 cm^{-1} was assumed for the inhomogeneous distribution function. A spectrum that resembles the experimental one closely is shown in Fig. 4.9. The experimental $Q_A^- - Q_A$spectrum of the mutant shows a clear movement of the main bleaching from ∼684 to ∼688 nm combined with a lowering of the bleaching amplitude when compared to $Q_A^- - Q_A$spectrum of the WT. The peak that appears at ∼681 nm in the WT changes its position by 1 nm to the red. All of these features are reproduced by the calculated $Q_A^- - Q_A$spectrum of the mutant. The secondary bleaching that appears at ∼677 nm in the experiment is also present at the same position in the calculation.

$Q_A^- - Q_A$difference spectra of Thr179Glu *Synechocystis* mutant. An analogous experiment to the one described above, but with histidine mutated into glutamic acid, was performed by Schlodder et al. (2008). The results of the experiment and calculations are presented in Fig. 4.10. Mutation of Chl_{D1}-coordinating threonine into glutamic acid effects the $Q_A^- - Q_A$spectrum in the following way. The main beaching at ∼684 nm disappears, while the positive peak at ∼681 nm is moved to ∼680 nm and looses intensity (Fig. 4.10).

Similarly to the $P_{D1}^+ Q_A^- - P_{D1} Q_A$difference spectrum of the Thr179Glu mutant (sec: 4.2.2) the site energy of Chl_{D1} had to be blue shifted in the calculation in order to describe the experimental data. A blue shift of the Chl_{D1} site energy by only 0.5 nm, and a change of the inhomogeneous width to 90cm^{-1} leads to excellent agreement between calculated and experimental spectra. All experimental features of the $Q_A^- - Q_A$mutant spectrum are reproduced by the calculation. The bleaching at ∼684 nm disappears, the peak at ∼681 nm moves to ∼680 nm and decreases its intensity, while other feature of the spectrum do not change.

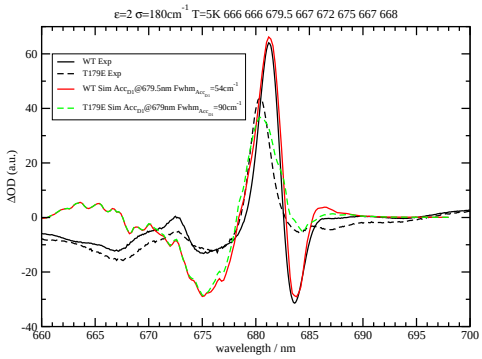

Figure 4.10: Calculation of $Q_A^- - Q_A$spectra of Thr179Glu *Synechocystis* mutant at 5K. Black lines are experimental data by Schlöder *et al.*, solid for WT and dashed for mutant. Red solid line is calculation of WT, while green dashed line is calculation of mutant spectrum.

4.2.4 Calculation of $D^+Q_A^-$ - DQ_A absorption difference spectra.

It is unknown where exactly positive charge is located when a $Q_A^- - Q_A$difference spectrum is recorded. There are several possibilities, it can be located on one of the carotenoids of the D1 or D2-side or on one of the Chlz.

All of these possibilities were taken into consideration.The calculated spectra shown in Fig. 4.11 contain the contributions due to Q_A formation: (a) the blue shift of the Q_Y band of Chl_{D1} and (b) the red shift of the Q_Y band of $Pheo_{D1}$, which is hidden under the first larger contribution. The $D^+Q_A^-$ - DQ_A absorption difference spectra are dominated by the contribution due to the positive charge. Interestingly, band shifts in opposite direction are calculated when placing the positive charge on the D1 or on the D2 side. The position of the positive charge relative to the plane of Chl_{D1} determines the direction of the electrochromic shift: Car_{D1}^+ and $Chlz_{D1}{}^+$ induce a blue shift and Car_{D2}^+ and $Chlz_{D2}{}^+$ a red shift of the Q_Y band of Chl_{D1}. There is a 11 cm^{-1} blue shift of the site energy of Chl_{D1} by $Q_A{}^-$. This blue shift is overcompensated by a 17 cm^{-1} red shift caused by Car_{D1}^+ or $Chlz_{D1}{}^+$. In contrast, Car_{D2}^+ and $Chlz_{D2}{}^+$ lead to a blue shift of the site energy of Chl_{D1} by 6 and 5 cm^{-1}, respectively, increasing the blue shift of this site energy, caused by $Q_A{}^-$.

4.2.5 Temperature dependence of difference absorption spectra

Finally the temperature dependence of the P_{680}^+ Q_A^- - $P_{680}Q_A$ and P_{680}^+ $Pheo^-$ - $P_{680}Pheo$ difference spectra of *T. elongatus* is examined.

The calculated spectra are compared in Fig. 4.12 with the experimental data (Hillmann et al., 1995). A temperature dependence was assumed for the site energy of Chl_{D1} and P_{D1} and for the dielectric constant ϵ_{eff} used in the calculation of electrochromic shifts. The site energy shift of Chl_{D1} with temperature is as described in the previous calculations on D1-D2-cyt*b*559 reaction center spectra (chapter 3.2) (Raszewski et al., 2005), whereas the site energy shift of P_{D1} is new. Due to these temperature dependencies and the increase in homogeneous broadening with increasing temperature, the double peak at low temperatures is transformed into a single negative peak at 680 nm at physiological temperature.

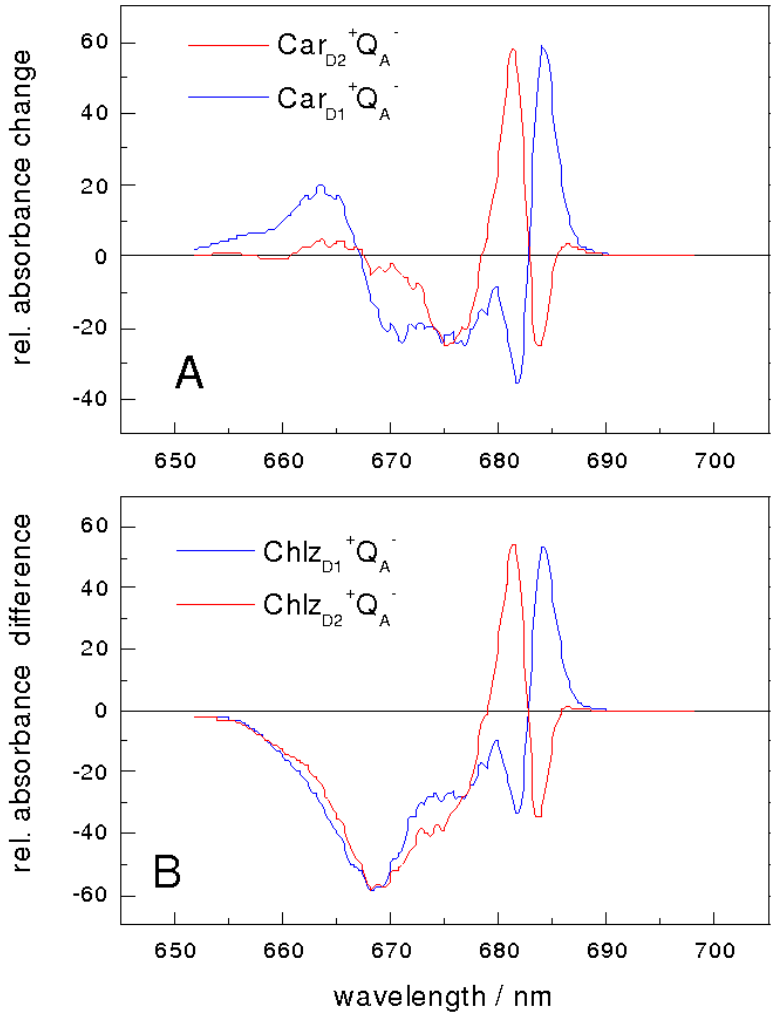

Figure 4.11: Calculation of absorption difference spectra due to the reduction of Q_A and the oxidation of a secondary donor (either Car or Chl). The calculated ($Car_{D1}{}^{+}Q_A{}^{-}$- $Car_{D1}Q_A$) and ($Car_{D2}{}^{+}Q_A{}^{-}$- $Car_{D2}Q_A$) absorbance difference spectra are shown in panel A , whereas panel B shows calculations of the ($Chl_{zD1}{}^{+}Q_A{}^{-}$-$Chl_{zD1}Q_A$) and ($Chl_{zD2}{}^{+}Q_A{}^{-}$- $Chl_{zD2}Q_A$) absorbance difference spectra.

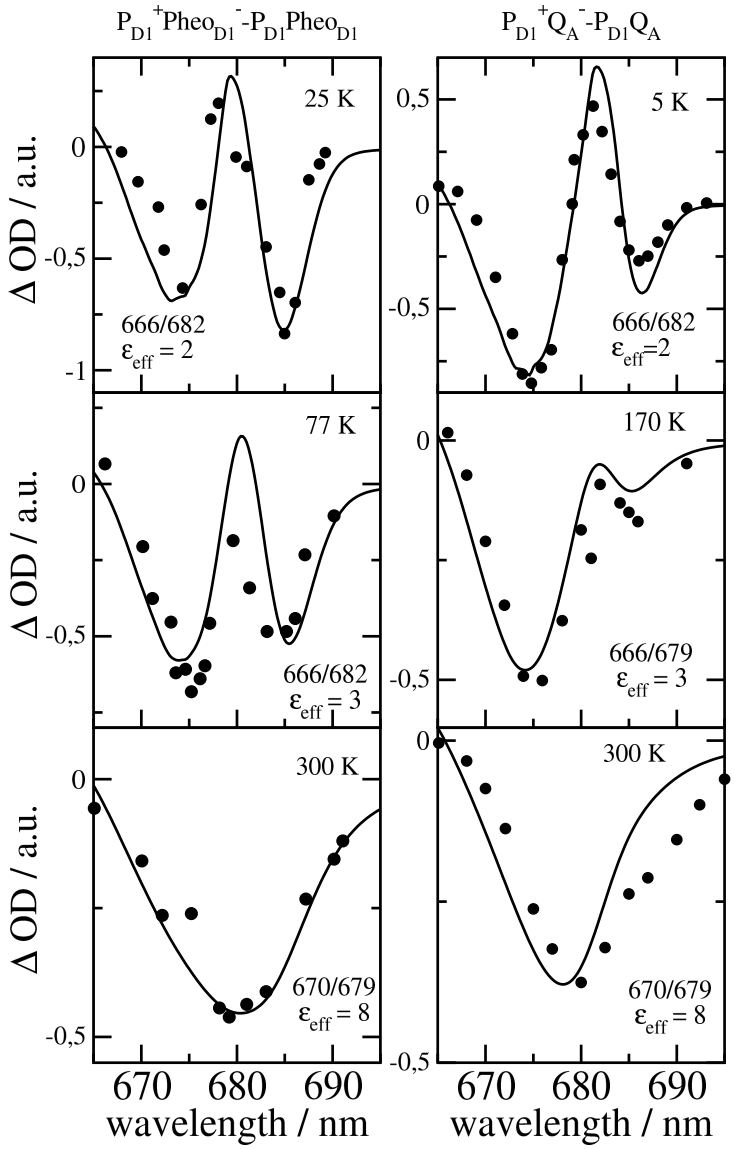

Figure 4.12: Temperature dependence of the P^+_{680} $Pheo^-$ - P_{680}Pheo (left half) and the P^+_{680} Q^-_A - $P_{680}Q_A$ (right half) spectra of *T. elongatus*. The calculations (solid lines) are compared with experimental data (Hillmann et al., 1995). The temperature dependent wavelengths corresponding to the site energies of P_{D1} and Chl_{D1} (P_{D1}/Chl_{D1}) and the dielectric constants (ϵ_{eff}) are shown as well at each temperature.

4.3 Discussion

4.3.1 Revision of the multimer model

The calculation of optical difference spectra of WT and mutant core complexes shows that the exciton Hamiltonian that we proposed previously for D1-D2-cyt$b$559 complexes (Raszewski et al., 2005) also applies to the reaction center pigments of PS-II core complexes. The only difference in the excited state energies between these two preparations involves $\mathrm{Chl_{D1}}$. Its site energy is even more red shifted in core complexes and its inhomogeneous width is smaller than that of the other pigments. A consequence of the red shift is an even stronger localization of the lowest excited state of the reaction center on $\mathrm{Chl_{D1}}$ as seen by the almost identical functions $\mathrm{d}_{m=\mathrm{Chl_{D1}}}$ and $\mathrm{d}_{M=1}$ in Fig. 4.3. At low temperatures there is about a 10 nm gap between this lowest excited state and the lowest energy exciton state of the "special pair". The experiments and calculations on the various mutants in Figs. 4.5 and 4.6 provide a direct proof of this assignment. The fact that in the exciton theory just one site energy (that of the pigment with the mutated protein environment) had to be shifted in order to explain the mutant spectra, shows that the mutation was indeed local and did not lead to a large conformational change of the protein.

A close inspection of the experimental $\mathrm{P^+_{680}\ Q^-_A}$ - $\mathrm{P_{680}Q_A}$ wildtype and His198Gln mutant spectra in the upper right panel of Fig. 4.5 shows that changing the environment of $\mathrm{P_{D1}}$ leads, besides the dominating shift of the 673 nm band, to a slight shift of the long wavelength band at 683 nm. At first glance, the latter could be caused by a changed contribution of $\mathrm{P_{D1}}$ in the lowest exciton state, i.e., by the excitonic coupling between $\mathrm{Chl_{D1}}$ and $\mathrm{P_{D1}}$. However, in this case, one would expect also a shift of the 673 nm band, if the environment of $\mathrm{Chl_{D1}}$ is changed, a shift that is neither seen in the experiment nor in the calculations in the upper and lower left panel of Fig. 4.5, respectively. The absent shift and the fact that the calculations of the His198Gln mutant spectra in the lower right panel of Fig. 4.5 do not reproduce the slight shift at long wavelengths seen in the experiment (upper right part) is an evidence that the site energy of $\mathrm{Chl_{D1}}$ is slightly red shifted in the His198Gln mutant. This result is in line with the fact that the site energy of $\mathrm{Chl_{D1}}$ is found to react more sensitive to different preparations than those of the other pigments.

Whereas a replacement of Thr179 by His leads to a red shift of the site energy of $\mathrm{Chl_{D1}}$, a replacement by Glu results in a blue shift. The reason for the red shift might be the stronger dispersive interaction (Heinz et al., 2001; Bayliss, 1950; Longuet-Higgens et al., 1957) between the strongly polarizable π electrons of His and $\mathrm{Chl_{D1}}$ and the blue shift might be caused by the charge density coupling (Eccles et al., 1983; Adolphs et al., 2006; Müh et al., 2007; Adolphs et al., 2007) between the ground and excited state of $\mathrm{Chl_{D1}}$ and the negative charge on Glu, assuming a standard protonation state of this residue.

Interestingly, a replacement of His by Gln in the $\mathrm{P_{D1}}$ mutant leads to a site energy shift of 8 nm to the blue whereas replacing Thr by His in the $\mathrm{Chl_{D1}}$ mutant just results in a 3 nm red shift. The reason for the different magnitudes might be in the strong distance dependence of the dispersive interaction and the fact that the His at $\mathrm{P_{D1}}$ is an axial ligand, whereas in the case of $\mathrm{Chl_{D1}}$ the His might still be connected via a water molecule, i.e. further away than the one at $\mathrm{P_{D1}}$.

The evidence for the excited state structure of the reaction center pigments provided by the experiments and the present exciton theory is so strong, that a revision of the multimer model of PS-II is necessary. The two essential changes are (i) the lowest excited state of the reaction center is localized at $\mathrm{Chl_{D1}}$ and (ii) the low-energy exciton state of the "special pair" absorbs at 6-10 nm shorter wavelengths (higher energies).

Except for the exciton model presented here (Raszewski et al., 2005), and the recent model of Novoderezhkin (Novoderezhkin et al., 2007), in all previous exciton models, mostly of the

multimer type, i.e. assuming the same (mean) site energies of all pigments, there are considerable contributions from the excited states of the "special pair" chlorophylls P_{D1} and P_{D2} in the lowest exciton state. Even in the multimer calculations of Prokhorenko and Holzwarth (Prokhorenko et al., 2000), who correctly predicted the primary electron donor at low temperatures from calculations and comparison with their photon echo data, the lowest excited state is clearly dominated by P_{D1} and P_{D2}, an assignment that is in contrast with the present studies. In an earlier paper of Novoderezhkin et al. (2005), different site energies were proposed for the reaction center pigments, based on fits of linear as well as non-linear optical spectra. However, still the lowest excited state had large contributions from the "special pair" and therefore could not explain the experiments described here. These results demonstrate how difficult it is to find an exciton model of PS-II that has predictive power. On the one hand, non-linear spectra contain more information about the system, but on the other hand, it is more difficult to describe these spectra as more parameters are needed than for the description of linear spectra. In that respect, mutant experiments are ideally suited to check an exciton Hamiltonian, since no new parameters are involved and just one site energy has to be shifted, if the mutation indeed is local.

The assignment of the site energies (chapter 3.2) (Raszewski et al., 2005) on the D1-D2-cyt$b$559 complexes was verified by calculations of a large number of additional spectra and comparison with experimental data. In the case of core complexes, one has had to rely on a few difference spectra, namely $P^+_{D1}Pheo^-_{D1}-P_{D1}Pheo_{D1}$, $P^+_{D1}Q^-_A-P_{D1}Q_A$, T-S and $D^+Q^-_A$ - DQ_A difference spectra, where D represents the carotenoid on the D2-side of the reaction center or the peripheral Chlz on this side as discussed previously (Fig. 4.11)

Comparing the $Q^-_A-Q_A$absorbance difference spectra of PS II (Steward et al., 2000) and bacterial reaction centers (Vermeglio et al., 1977) it is remarkable that in PS II the blue shift of the accessory chlorophyll Chl_{D1} is the predominant feature, whereas in bacterial reaction centers the red shift of $Pheo_A$ is the predominant feature. The reason for the former effect is twofold: (1) The site energy of PheoD1 is in the central range of site energies determined for the RC pigments in PS II (Raszewski et al., 2005). The different electrochromic shifts of the RC pigments largely overlap in this spectral region. Nevertheless, PheoD1 experiences the largest red shift (47 cm^{-1}) by Q_A of all RC pigments and therefore contributes to the positive band around 680 nm in the difference spectra in Figs. 4.9,4.10 (black lines) (2) Chl_{D1} has the lowest site energy in the RC and in addition a much smaller inhomogeneous width than the other RC pigments. Both factors lead to a dominant contribution of this pigment in the difference spectra at long wavelengths, despite the fact that its electrochromic blue shift is smaller in magnitude by a factor of 4 than the red shift of $Pheo_{D1}$. An alternative interpretation of the wildtype difference spectra in Figs. 4.9,4.10 was presented by Krausz and coworkers(Årsköld et al., 2003). The long wavelength signal was interpreted in terms of an electrochromic blue shift of $Pheo_{D1}$, that in this case is calculated to shift to the red. To explain the blue shift, a protein induced 90 degree rotation of the $\Delta\mu$ vector, representing the difference in permanent dipole moments between the excited and the ground state of $Pheo_{D1}$, compared to the orientation of this vector determined for pheophytin a in solution (see the Ref. given in Årsköld et al. (2003)) was proposed. To check the two possibilities to explain the spectrum, discussed above, mutant experiments described above were performed where the local environment of Chl_{D1} was changed. In fact, the calculations of the mutant spectra were even performed before the experiment. In the calculations just the site energy of Chl_{D1} was shifted by an amount determined independently on other difference spectra on the same mutant, as described before. The experiment perfectly confirmed the predictions of the calculations, concerning the band positions, but resulted in a somewhat larger broadening of the bands. This result led to the assumption of a larger inhomogeneous distribution of the site energy of Chl_{D1} in the mutant, which resulted in quantitative agreement between calculated spectra and the experimental data as seen in Figs. 4.9,4.10. These calculations demonstrate the predictive power of exciton model presented here and provide compelling evidence for the present

interpretation. Calculation shown for the $Q_A^- - Q_A$ of different species provide clear evidence that this exciton model works for various different species.

One will have to await a structural study with higher resolution in order to calculate the excitonic coupling in the "special pair" with greater precision. The present value of 150 cm^{-1}, inferred from refitting the D1-D2-cyt$b$559 spectra, can only be understood by including a Dexter type exchange contribution, which however depends critically on the detailed atom positions. Applying a point dipole approximation also leads to a large excitonic coupling, but such an approximation is not valid for the present small interpigment distance, as our present TrEsp calculation shows (see Table 7.1 in Appendix). At present, there is no direct experimental evidence for the value of the excitonic coupling in the "special pair". The high energy exciton component has a rather small oscillator strength and therefore is not easy to detect. An inspection of the calculated $P_{680}^+ Q_A^-$ - $P_{680}Q_A$ spectra in the lower part of Fig. 4.5 reveals a small positive band around 662 nm. A similar band is found in the experiment on the wild type complexes in the upper part of this figure at 665 nm and may reflect the electrochromically shifted monomer band of P_{D2} that becomes visible upon oxidation of P_{D1}. A direct extraction of the excitonic coupling from the relative positions of the monomer and exciton bands will still be difficult, since in a dimer of closely packed chlorophylls like P_{D1} and P_{D2}, in addition to the excitonic coupling, the shift of the monomer and exciton energies by the charge density coupling and by mixing with charge transfer states has to be taken into account.

A higher resolution structural study might also help to identify the charge transfer states and their influence on the excited state properties. From non-conventional Stark spectra it was suggested that the low energy exciton state is mixed with a charge transfer state (Frese et al., 2003). Experimental evidence was provided that at cryogenic temperatures charge separation occurs upon long wavelength excitation that could also reflect a low lying CT state (Krausz et al., 2005). In the present calculations indirect evidence regarding CT states is found from the fact that two site energies (Chl_{D1} and P_{D1}) change with temperature. This change could reflect a temperature dependent dephasing of the quantum mechanic mixing of an exciton and a CT state (Renger et al., 2004).

4.3.2 Identification of functional states at physiological temperatures

The previous section have provided independent evidence that at low temperatures the lowest excited state is localized at Chl_{D1} (Fig. 4.3), that the hole stabilizes at P_{D1} (Fig. 4.2) and that the triplet localizes at Chl_{D1} (bottom panel of Fig. 4.1 and Fig. 4.4). These identities agree with those inferred earlier from mutant spectra (Diner et al., 2001) measured at 5K. In the previous chapter 3.2, I presented evidence that, if P_{D1} were the primary electron donor at low temperatures there would be a much stronger temperature dependence of the primary electron transfer rate than has been detected in D1-D2-cyt$b$559 reaction centers (Greenfield et al., 1997, 1999; Groot et al., 1997). As in core complexes, the site energy of Chl_{D1} is even more red shifted, the mechanism of primary charge separation at low temperature is the same: The excitation energy is funneled to Chl_{D1} forming the state P^*=Chl_{D1}^* and charge separation leads to the primary radical pair Chl_{D1}^+ $Pheo_{D1}^-$, before the hole gets stabilized at P_{D1}, where the state P_{680}^+=P_{D1}^+ is formed.

The situation is more complicated at physiological temperatures. The calculations of the temperature dependence of the difference spectra in Fig. 4.12 suggest that the same identity of the state P_{680}^+=P_{D1}^+ can be assumed at higher temperatures. This finding is in agreement with pulsed EPR studies by Zech et al. (1997) which determined a distance of 27.4 ± 0.3 Å between the negative charge on Q_A^- and the positive charge on P_{680}^+. From this distance it cannot be concluded whether the cation resides on P_{D1} or P_{D2}. However, a cation localization on Chl_{D1} or Chl_{D2} can be excluded as well as a distribution of the cation state over all 4 Chls.

In order to describe the temperature dependence of the spectra in Fig. 4.12 it was necessary to assume (i) an increase of the dielectric constant ϵ_{eff} from 2-3 to 8 as the temperature is increased from below to above 170 K and (ii) a shift of the site energies of P_{D1} and Chl_{D1} around this temperature.

The internal dielectric constant of proteins reflects on the one hand the possible degree of orientation of its polar side chains and its amide backbone dipoles in response to an electric field. In addition to this orientational polarization there is the polarization of electron clouds often termed ϵ_∞ since it remains the only contribution if the frequency of the field is very high. ϵ_∞ is given by the square of the refractive index. For typical organic solvents $\epsilon_\infty \approx 2$. The orientational polarization of a polar solvent is influenced by the temperature. Below the glass transition temperature around 200 K (Nienhaus et al., 1991) the orientational degrees of freedom are frozen out causing a sudden drop of the dielectric constant around this temperature (Yu, 1993). In a protein such a transition is also expected (Parak et al., 1982; Smith et al., 1990; Nienhaus et al., 1991; Rasmussen et al., 1992; McMohon et al., 1998; Kriegl et al., 2003; Fenimore et al., 2004), explaining the low value of 2-3 for ϵ_{eff} at low temperatures inferred in the present study.

From measurements and calculations on a charge recombination reaction in bacterial reaction centers, occurring in the 100 ns time range, information about conformational protein dynamics at different temperatures was obtained (McMohon et al., 1998; Kriegl et al., 2003). Below the glass transition temperature, the restricted conformational motion led to a wide distribution of electron transfer rates that became much narrower above this temperature. Below 100 K no change of the distribution was found, indicating that the conformational dynamics of the protein does not change further below 100 K. In the present calculations a slight increase of ϵ_{eff} from 2 at 25 K to 3 at 77 K is found. This increase could reflect a thermal activated barrier crossing in the rugged landscape of the protein, as detected by monitoring spectral diffusion in hole burning (Zollfrank et al., 1991) and photon echo (Leeson et al., 1995) experiments at cryogenic temperatures. On the other hand, using $\epsilon_{\text{eff}} = 2$ in the calculation of the 77 K spectrum in Fig. 4.12 still describes the experiment qualitatively. Therefore, the evidence for an increase of ϵ_{eff} below 100 K is much weaker than for the $\epsilon_{\text{eff}} = 8$ at 300 K. Without the latter, the room temperature spectra could not even be qualitatively described.

Whereas the free rotation of polar solvent molecules results in large values for the dielectric constant at ambient temperatures like $\epsilon = 80$ for liquid water, in a protein, the polar side chains and the amide backbone cannot rotate freely but are constrained by intermolecular forces. These constraints and the smaller density of polar groups lead to a much smaller high-temperature dielectric constant of proteins. The value $\epsilon_{\text{eff}} = 8$ obtained from our calculation of the room temperature spectra is practically identical with the $\epsilon_{\text{eff}} = 7$ inferred (Dashdorj et al., 2004) from electrochromic shift calculations of chlorophylls around the secondary electron acceptor in photosystem I at room temperature. The same $\epsilon_{\text{eff}} = 8$ as in the present study was determined from the electric field strength measured inside an α-helix in water at 273 K (Lockhart et al., 1992).

The inferred temperature dependence of the site energies of Chl_{D1} and P_{D1} in Fig. 4.12 might reflect a mixing of exciton states with charge transfer states, as noted above. It was more straightforward to allow for a temperature dependence of the site energy than to explicitly include the CT states into the calculation of optical spectra. At present, there is no theory that can include all three aspects: a dynamic localization of excited states (Renger et al., 2004), and lifetime broadening and vibrational sidebands of exciton transitions (Renger et al., 2002). Due to the strong coupling of a CT state to the vibrations, a temperature dependent localization of the mixed excitonic/CT state can be expected (Renger et al., 2004).

One important difference between low and high temperatures is that the state P^* at high temperatures will be formed not only by the lowest exciton state localized at Chl_{D1}, but the

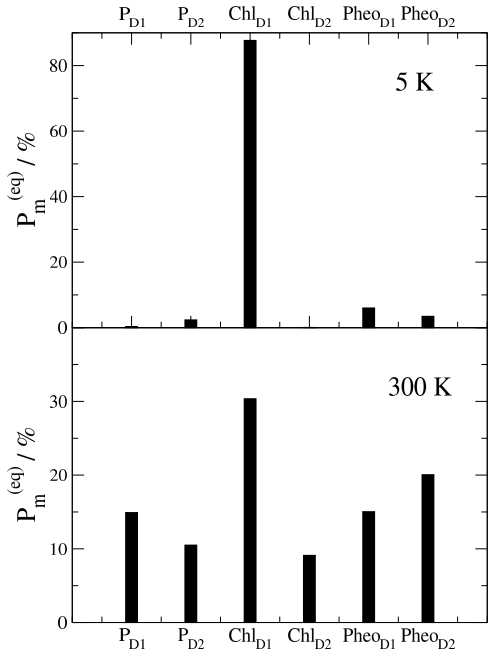

Figure 4.13: Thermal population of local excited states $P_m^{(\mathrm{eq})}$ (Eq. 4.2) at T= 5K (upper part) and T=300 K (lower part).

thermal energy kT is sufficient to substantially populate higher exciton states, in particular the low energy exciton state of the "special pair" and in principle electron transfer could start from both pigments, $\mathrm{Chl_{D1}}$ and $\mathrm{P_{D1}}$. To quantify the contributions from the different pigments to $\mathrm{P^*}$ one assumes, that exciton relaxation between the six core pigments is fast compared to primary electron transfer and therefore that the electron transfer rate constant can be described as

$$k_{\mathrm{ET}} = P_m^{(\mathrm{eq})} k_{m^* n \to m^+ n^-} \tag{4.1}$$

where $k_{m^* n \to m^+ n^-}$ is the intrinsic rate constant for creation of the primary radical pair $m^+ n^-$ and $P_m^{(\mathrm{eq})}$ is the (quasi) equilibrium population of the local excited state of pigment m.

$$P_m^{(\mathrm{eq})} = \langle \sum_M f(M) |c_m^{(M)}|^2 \rangle_{\mathrm{dis}}. \tag{4.2}$$

Here the Boltzmann factor $f(M) = \exp\{-\hbar\omega_M/kT\}/\sum_N \exp\{-\hbar\omega_N/kT\}$ describes the thermal population of the Mth exciton state, $|c_m^{(M)}|^2$ is the quantum mechanical probability to find pigment m excited in the Mth exciton state, and $\langle \cdots \rangle_{\mathrm{dis}}$ denotes an average over static disorder in site energies.

In Fig. 4.13 the thermal populations $P_m^{(\mathrm{eq})}$ defined above are shown for two different temperatures. At 5 K practically only $\mathrm{Chl_{D1}}$ contributes in the thermal population of exciton states that represents the state $\mathrm{P^*}$. At physiological temperature there is still a 30 % contribution by $\mathrm{Chl_{D1}}$, however also the remaining pigments contribute significantly. The contribution by $\mathrm{P_{D1}}$ is about 15 % and the smallest contributions of 8 % is due to $\mathrm{Chl_{D2}}$.

It is still an open question why in the bacterial reaction center the electron transfer starting at the accessory bacteriochlorophyll is one order of magnitude faster than the one starting at the special pair (van Brederode et al., 1997, 1999). However, from the nearly perfect overlay of $\mathrm{Chl_{D1}/Pheo_{D1}}$ in PS-II reaction centers and in the homologous bacterial reaction centers, as shown in Fig. 4.14, it is likely that the electron transfer coupling matrix elements in the two

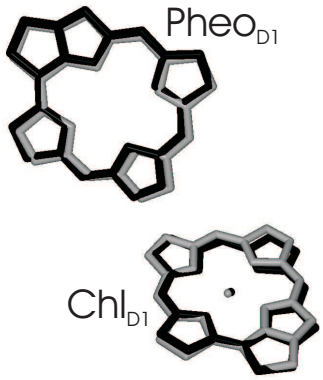

Figure 4.14: Overlay of accessory (bacterio-) chlorophylls and pheophytins of the electron transfer active branch of PS-II (grey) and the bacterial reaction center (black). The overlay was determined from a minimization of the mean square deviation in positions of equivalent atoms of the two molecules using the program VMD (W. Humphrey, A. Dalke, K. Schulten *J. Molec. Graphics* **1996** *14.1* 33.).

reaction centers are similar. Therefore it seems not unlikely, despite uncertainties of other factors like the driving force of the process, that also in PS-II subpicosecond electron transfer can occur starting at Chl_{D1}. At room temperature the excited state is most localized on Chl_{D1}, which strongly suggests that this electron transfer pathway dominates in PS-II. From calculations of the temperature dependent fluorescence decay of PS-II core complexes and comparison with experimental data (Miloslavina et al., 2006) additional evidence for the presence of ultrafast primary electron transfer is obtained as discussed in the next chapter 5 (Raszewski et al., 2008).

Considering that the electron hole stabilizes at P_{D1}, it is likely that this pigment has the highest HOMO level of the reaction center pigments. Furthermore, from the blue shifted transition energy of P_{D1}, it follows that the LUMO of P_{D1} is higher than that of Chl_{D1}. Therefore, an excited electron at Chl_{D1} is transferred energetically downhill only to $Pheo_{D1}$, which has a lower LUMO due to chemical differences. As the accessory chlorophyll in the D2 branch, Chl_{D2}, contributes mostly to an exciton state around 668 nm, even at room temperature this excited state is only weakly populated. This asymmetry in the excited state energies of the two accessory chlorophylls might be one of the factors that leads to unidirectional electron transfer in PS-II.

4.3.3 Functional implications

The particular challenge in the evolution of photosystems was to find a way to use water as a proton and electron source. The reduction potential of the $O_2/2H_2O$ couple at pH 6 is approximately 880 mV *vs* NHE, larger than the reduction potentials measured for chlorophyll in most solvents. A confluence of factors was therefore necessary to allow the "special pair" chlorophylls and also the accessory chlorophylls to be substantially more oxidizing than the potential required for water oxidation. One of these is the dielectric environment (Ishikita et al., 2006). Another factor is the degree of delocalization of the cationic state. Whereas the hole is localized on one of the two "special pair" halfs in PS-II (Rogby et al., 1994), most likely on P_{D1} according to mutant experiments at low temperatures (Diner et al., 2001) and the present calculations, it is more delocalized (Müh et al., 1985) over both special pair pigments in the bacterial reaction center, which does not have as severe constraints as in PS-II on the reduction

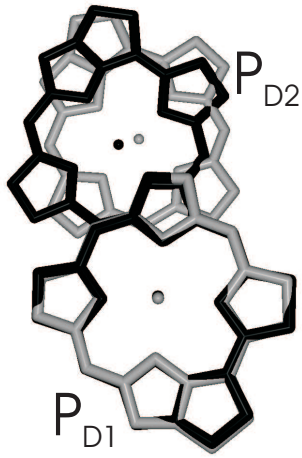

Figure 4.15: Overlay of the special pair (bacterio)chlorophylls of PS-II (grey) and the bacterial reaction center (black). The overlay was determined from a minimization of the mean square deviation in positions of equivalent atoms of the two molecules using the same program as in Fig. 4.14.

potential of the primary donor.

It is interesting to note that although the overall arrangement of pigments is very similar in the two reaction centers, an important difference is the mutual orientation of the two "special pair" chlorophylls, as seen in Fig. 4.15. Whereas there is a remarkable overlay of two rings in the bacterial reaction center, this π-stacking interaction is disrupted in PS-II by an in plane tilt of the macrocycle. It is likely that this tilt was needed to localize the hole state. As noted by Rutherford and Faller (Rutherford et al., 2002) the monomeric nature of the P_{680}^+ state probably was one key element in the evolution of PS-II that allowed to reach a high enough redox potential for the splitting of water. Another interesting observation is that the higher the resolution of the x-ray data of PS-II became the smaller got the distance between the two "special pair" pigments in the x-ray crystallographic models. It seems that it is rather a rotation than a translation that has localized the state P_{680}^+.

The redox potentials of the reaction center chlorophylls in PS-II are so high that the usual photoprotection mechanism, i.e. the quenching of the physiologically dangerous triplet state populations of the chlorophylls by carotenoids would not work, as the carotenoids would simply be oxidized by the chlorophylls. Consequently, no carotenoids are found in van der Waals contact of the 4 strongly coupled reaction center chlorophylls in PS-II. An alternative mechanism concerns the quenching of triplets by Q_A^- (van Mieghem et al., 1995). As proposed by Noguchi (Noguchi, 2002) this quenching mechanism might be the reason why the triplets equilibrate between P_{D1} and Chl_{D1}, simply because the triplets at Chl_{D1} can be quenched efficiently because of the close distance to Q_A^-. Nevertheless, the mean *in vivo* lifetime of a PS-II reaction center is only about half an hour at high light (Kim et al., 1993; Barber, 1994). During that time the D1-protein gets irreversibly damaged and is subsequently replaced by an intact protein. At least two different possibilities are discussed for the molecular mechanism behind the damage (Barber, 1994). One possibility is an oxidation of pigments (or parts of the protein) by the highly oxidizing P_{680}^+ and a subsequent degradation of the unstable cationic states. Another possibility of damage proposed (Vass et al., 1992; Barber, 1994; Noguchi, 2002) is that Q_A gets doubly reduced and doubly protonated and leaves its binding pocket in the protein. Now, the chlorophyll triplets can no longer be quenched by Q_A^- and their lifetime increases by two orders of magnitude (van Mieghem et al., 1995). The chlorophyll triplets react with triplet oxygen to form the poisonous singlet oxygen that damages the D1-protein. In both cases,

the unidirectional electron transfer in Photosystem II is of physiological relevance, because it localizes the triplet formation and the creation of oxidizing equivalents to the D1-branch, thereby limiting the photophysical damage to this branch. A mechanism to prevent D2 oxidative damage probably is the controlled hole transfer from P_{D1}^{+} to cyt$b559$ via Car_{D2} (Schlodder et al., 2008) and a subsequent charge recombination with reduced Q_B (Buser et al., 1992). In addition, based on calculations of excitation energy and primary electron transfer in PS-II core complexes, I will show in the next chapter that for closed reaction centers the rate constant for primary electron transfer slows down to an extent that a considerable part of the excitation energy returns to the antenna and the subsequently formed triplet energy of the Chls is quenched by the carotenoids there (Raszewski et al., 2008).

Chapter 5

Excitation energy and primary electron transfer in Photosystem II core complexes

In this chapter a structure-based modeling and analysis of the primary photophysical reactions in photosystem II (PS-II) core complexes is presented. The modeling is based on a description of stationary and time-resolved optical spectra of the CP43, CP47 and D1-D2-cyt$b$559 subunits and whole core complexes. It shows that the decay of excited states in PS-II core complexes with functional (open) reaction centers (RCs) is limited by the excitation energy transfer from the CP43 and CP47 core antennae to the RC occurring with a time constant of 40-50 ps at room temperature. The chlorophylls responsible for the low energy absorbance bands in the CP43 and CP47 subunits are assigned and their signatures in hole burning, fluorescence line narrowing and triplet-minus-singlet spectra are explained. The different locations of these trap states in the CP43 and CP47 antennae with respect to the reaction center lead to a dramatic change of the transfer dynamics at low temperatures. The calculations predict that, compared to room temperature, the fluorescence decay at 77 K should reveal a faster transfer from CP43 and a much slower and highly dispersive transfer from CP47 to the RC. A factor of 3 increase in the fastest decay time constant of fluorescence that was reported to occur when the RC is closed (the plastoquinone Q_A is reduced) is understood in the present model by assuming that the intrinsic rate constant for primary electron transfer decreases from $(100\ \mathrm{fs})^{-1}$ for open RCs to $(6\ \mathrm{ps})^{-1}$ for closed RCs, leading to a reduction of the primary electron acceptor $\mathrm{Pheo_{D1}}$, in 300 fs and 18 ps, respectively. The model suggests that the reduced Q_A switches the photosystem into a photoprotective mode in which a large part of the excitation energy of the RC returns to the CP43 and CP47 core antennae, where the physiologically dangerous triplet energy of the chlorophylls can be quenched by the carotenoids. Experiments are suggested to test this hypothesis. The ultrafast primary electron transfer inferred for open RCs provides further support for the accessory chlorophyll $\mathrm{Chl_{D1}}$ to be the primary electron donor in photosystem II.

This chapter is organized in the following way. First an overview of the problems addressed in this chapter is given. Next, the calculation of the stationary spectra of the CP43 and CP47 subunits and comparison with experimental data are used to determine site energies of the pigments in these subunits. These site energies are tested afterwards in the calculation of time-resolved optical spectra among with comparison with experimental data of the CP43 and CP47 complexes. Next, these parameters are used to to calculate the fluorescence decay of the PS-II core complexes. The intrinsic rate constant of the primary charge separation is obtained from the comparison of the calculation of the fluorescence decay with the experimental data. In order to find the bottleneck of the excited state decay, different compartment models are studied. In

the end calculation on the closed RCs are preformed to explain the variable fluorescence.

5.1 Overview

Different views about the relative time scale of exciton transfer and charge separation

Despite a long history of experimental studies on the primary excitation energy and charge transfer reactions in PS-II, different views exist about the kinetic and mechanistic details. At the extreme there is the so-called excited state radical pair equilibrium (ERPE) model (Schatz et al., 1987, 1988; Barter et al., 2001; Miloslavina et al., 2006; Holzwarth et al., 2006) that assumes the equilibration of excited states in the whole core complex to be fast compared to the primary electron transfer reaction in the RC. This trap limited model was used to explain the variable fluorescence observed for open and closed reaction centers (Schatz et al., 1987, 1988) and for PS-II complexes of different size (Barter et al., 2001). Holzwarth and coworkers in early experiments observed (Schatz et al., 1987, 1988) that the fastest component detected for the fluorescence decay of PS-II core complexes slows down from 80 ps for open RCs to 220 ps for closed RCs, i.e., by a factor of almost three. The main 40 ps time constant observed in recent time resolved fluorescence (Miloslavina et al., 2006) and pump-probe spectra (Holzwarth et al., 2006) on PS-II core complexes with open RCs was explained within the ERPE model by reversible electron transfer, assuming that the equilibration time of excited states in the whole system is about 1.5 ps and that primary charge separation, i.e., the reduction of $\mathrm{Pheo}_{\mathrm{D1}}$ takes about 3 ps.

The ERPE model was challenged by studies on PS-II containing membranes (BBY particles) (Broess et al., 2006) and PS-II core complexes (Jennings et al., 2000; Pawlowicz et al., 2007), which reported evidence for relatively slow excitation energy transfer. From recent time resolved visible pump/ mid-infrared probe studies (Pawlowicz et al., 2007) a 20-30 ps time constant for exciton relaxation between CP43, CP47 and the RC (Pawlowicz et al., 2007) was inferred. The same technique was applied to D1-D2-cyt$b$559 RC complexes and it was concluded that the reduction of $\mathrm{Pheo}_{\mathrm{D1}}$ occurs in 600-800 fs (Groot et al., 2005). In this case electron transfer in the RC is much faster than excitation energy transfer to the RC and the decay of excited states is limited by the transfer to the trap. Alternative to this transfer-to-the-trap limited model, from time-resolved fluorescence data of RC-CP47-complexes it was concluded that the decay of excited states is neither trap nor transfer-to-the-trap limited, but that primary charge separation and excitation energy transfer occur on the same time scale (Andrizhiyevskaya et al., 2004).

Objectives and theoretical aspects

A main aspect of this chapter is to provide an answer to the question: *What is the bottleneck for the decay of excited states in PS-II core complexes?* Besides the controversial interpretations of experimental studies discussed above, there have been calculations by Vasiliev and coworkers on this point (Vasilev et al., 2001, 2002). The latter have led to the conclusion that the decay is limited by the transfer to the trap. However, localized excited states were assumed and the site energies used in the calculations were assigned without calculations of optical spectra. In addition the energy transfer calculations were based on a preliminary structural model (Vasilev et al., 2001) where about 50 % of the transition dipole moments were incorrectly assigned, with nearly perpendicular directions with respect to the true orientations that were resolved in the recent structural study (Loll et al., 2005). All of these shortcomings have to be overcome in order to provide a definite answer to the above question. There are two main problems for the theory: 1) to take into account, both, the excitonic as well as the exciton-vibrational coupling in an appropriate way and 2) to assign realistic site energies to the 35 Chl a and 2 Pheo a molecules that are bound in the PS-II core complex.

If one of the two types of couplings in 1) dominates, there are standard theories to describe

the spectra and the excitation energy transfer. In the case of strong excitonic coupling, the excited states will be delocalized and the excitons relax between these delocalized states, as described by Redfield theory (e.g. ref Renger et al. (2001)) or Modified Redfield theory (Zhan et al., 1998; Yang et al., 2002; Renger et al., 2003). In the other limit, localized states are excited and Förster theory (Förster, 1948) describes the transfer between these states. One aspect, often overlooked, is that the excited states are not only localized by static disorder but also by the dynamic modulation of transition energies. Even if two pigments have the same site energy their excited states are only delocalized if the excitonic coupling is comparable or larger than the nuclear reorganization energy of the local optical transitions. This aspect is particularly important if one of the two pigments represents a sink for the excitation energy, for example, because electron transfer starts from this pigment. Without dynamical localization the excitation energy of the other pigment would be immediately quenched, independent of the strength of excitonic coupling between the two pigments, if they happen to have the same site energy. Dynamical localization, in the case of weak excitonic coupling, requires excitation energy transfer to the sink before the quenching.

Unfortunately, at present there exists no lineshape theory that can describe life time broadening and vibrational sidebands (Renger et al., 2002) and, in addition, a dynamic localization of exciton states (Renger et al., 2004). However, the latter may be treated implicitly by assuming that delocalized excited states can only be formed between pigments that are coupled stronger than their local reorganization energy of the exciton-vibrational coupling (Yang et al., 2003). If such domains are defined, exciton transfer between the domains is described by generalized Förster theory (Fetisova et al., 1996; Sumi, 1999; Mukai et al., 1999; Scholes et al., 2000; Jang et al., 2004; Müh et al., 2007), whereas the exciton relaxation within the domains is treated by Redfield theory or Modified Redfield theory.

Concerning point 2), an estimation of the site energies can be obtained from a fit of optical spectra of the subunits. The site energies of the RC pigments were previously determined and verified from a description of a large number of optical spectra of D1-D2-cyt$b$559 complexes (as described in previous chapters 3.24)(Raszewski et al., 2005).

In this chapter, the site energies of the CP43 and CP47 subunits are determined from a fit of their experimental linear optical spectra (Groot et al., 1999; de Weerd et al., 2002; Groot et al., 1995; Alfonso et al., 1994) and verified by calculations of time resolved pump-probe spectra and comparison with experimental data (de Weerd et al., 2002a).

Experimental facts about low energy absorbance bands in CP43 and CP47

Important information about the low-energy states, the so-called trap states in the CP43 and CP47 subunits was obtained from high-resolution spectroscopy in the frequency domain (Groot et al., 1999; de Weerd et al., 2002; Groot et al., 1995; Alfonso et al., 1994; van Dorsson et al., 1987; Jankowiak et al., 2000; Hughes et al., 2006). Excitation dependent fluorescence line narrowing spectra (Groot et al., 1999) gave first evidence that in CP43 at low temperatures there are two emitting states with different inhomogeneous distributions. From the vibrational fine structure of the excitation dependent emission it was inferred that one of the two low energy states is due to Chls with a hydrogen bond between their 13^1-keto group and the protein, whereas the other state showed signatures of six-coordinated Chls that do not form such hydrogen bonds. From the Stark and triplet-minus-singlet (T-S) spectra evidence about partially delocalized excited states in CP43 was reported (Groot et al., 1999).

The two quasi-degenerate low energy states in CP43 were further characterized by non-photochemical hole burning (NPHB) and triplet bottleneck hole burning spectra by Jankowiak *et al.* (Jankowiak et al., 2000) who termed these states A- and B-states. Interestingly, the A-state was found to mainly contribute to the triplet bottleneck spectrum, whereas the B-

state was detected, instead, in the NPHB spectrum (Jankowiak et al., 2000). These findings were explained by assuming a longer life time of the triplet state of A and that most of the excitation energy from higher energy exciton states is trapped by the B-state (Jankowiak et al., 2000). Some evidence for excitonic coupling of the B-state pigments was reported from high energy satellite holes at 673 nm and 678 nm (Jankowiak et al., 2000). Recently, Hughes et al. (2006) investigated CP43-complexes with NPHB and non-wavelength selective photoconversion spectroscopy. They proposed a different intrinsic photoconversion efficiency of the A- and the B-state due to the the strong hydrogen bond of the B-state Chls reported earlier by Groot et al. (1999) This explanation allows both low energy states to participate equally in excitation energy transfer to the RC, whereas Jankowiak et al. (2000) inferred from the narrow zero-zero linewidths in their NPHB data that the two states are uncoupled and therefore located in different layers in the membrane. From circular dichroism difference spectra, Hughes et al. (2006) reported evidence that the B-state is excitonicaly correlated with higher energy states at 677 nm and 682 nm.

The low energy states of CP47 were studied in great detail by de de Weerd et al. (2002) From a Gaussian band fitting of the absorption and linear dichroism spectra, it was concluded that the low-energy state around 690 nm is due to a monomeric Chl with a distinct orientation of its Qy-transition relative to the membrane plane (with an angle larger than 35°), and that the next higher excited state around 683 nm carries the oscillator strength of approximately 3 Chls. The finding about the 690 nm emitting Chl supported earlier investigations of van Dorsson et al. (1987) which provided evidence that the low energy fluorescing state in PS-II belongs to CP47. From polarized emission measurements, de Weerd et al. (2002) obtained additional evidence for a single emitting state at 690 nm. The depolarized 683 emission was interpreted by assuming that at least two isoenergetic states with non-parallel transition dipole moments contribute. From the vibrational fine structure in the FLN spectra it was inferred that there is a strong hydrogen bond between the 13^1-keto group of the 690 nm monomeric Chl and the protein, whereas the Chls contributing to the 683 nm states form less strong hydrogen bonds (de Weerd et al., 2002). Additional evidence for the monomeric nature of the 690 nm state was reported from the relative decrease of a 80 cm^{-1} mode at long wavelengths in the emission. This mode is thought to represent intermolecular vibrations modulating the coupling between pigments (Peterman et al., 1998). Interestingly, the T-S spectra did show no bleaching at 690 nm but only the 683 nm state appeared and some higher energy satellites that were taken as evidence for the delocalized nature of the 683 nm state (de Weerd et al., 2002). Two alternatives were offered for the absence of a 690 nm bleaching in the T-S spectra: either an artifact due to the high excitation power leading to a permanent bleaching of this state, or an efficient quenching of the triplet state formed at the 690 nm Chl by a nearby carotenoid (de Weerd et al., 2002).

The fluorescence of the 690 nm state that gives rise to an emission maximum at 695 nm, was used as a marker for the presence of PS-II core complexes in thylakoid membranes in mutation experiments on various histidines in CP47 by Shen and Vermaas (Shen et al., 1994). When His B114 was mutated to Tyr, the 695 nm band was completely lost and also no O_2 evolution was detectable. Whereas a mutation of His B114 to Gln led to a 70 % reduction in the amplitude of the 695 nm emission and O_2 evolution and in addition to a blue shift of the emission to 693 nm. These results were taken as evidence that His B114 and the Chl it binds are important for assembly and function of PS-II (Shen et al., 1994).

In this chapter I will suggest the molecular identities of the above trap states in CP43 and CP47 and explain their signatures in the various spectra.

Time-resolved experiments on exciton transfer in CP43 and CP47

The excitation energy transfer in CP43 and CP47 was investigated by time-resolved absorption and fluorescence spectroscopy (de Weerd et al., 2002a) at 77 K. In both complexes, time constants of 0.2-0.4 ps and 2-3 ps were found that were attributed to exciton transfer between Chls in the same, stromal or lumenal, layer and that between pigments in different layers, respectively. In CP47, in addition, a slower 17-28 ps component was detected for transfer to the 690 nm trap state. The present calculations provide a structure-based analysis of these pump-probe spectra and also serve to check the exciton relaxation times predicted by the theory. It is important to note that no adjustable parameter is used to tune the transfer rates. This approach was successfully tested in calculations of exciton relaxation in smaller complexes before (Müh et al., 2007; Raszewski et al., 2005; Renger et al., 2002b; Adolphs et al., 2006; Renger et al., 2007).

5.2 Results

The calculations of stationary spectra of the CP43 and CP47 subunits and comparison with experimental data are used to determine the site energies of the pigments in these subunits and the Huang-Rhys factor of the exciton vibrational coupling. The Huang-Rhys factor and the site energies are tested afterwards in the calculation of time-resolved optical spectra and comparison with experimental data of the CP43 and CP47 complexes. Next, the parameters are used in calculations of the fluorescence decay of PS-II core complexes where the intrinsic rate constant of primary charge transfer is determined on the basis of a comparison of the calculations with the experimental fluorescence decay data. To find the bottleneck of the excited state decay, various compartment models are studied by assuming fast equilibration of excited states in these compartments. Finally, calculations are performed for PS-II core complexes with closed RCs to explain the variable fluorescence.

5.2.1 Stationary spectra of CP43 and CP47

A genetic algorithm, described in section 2.9 (Raszewski et al., 2005; Adolphs et al., 2006) was used to determine site energies of the Chls in the CP43 and CP47 subunits from a fit of their linear optical spectra. In Figure 5.1, the linear absorption, linear dichroism and fluorescence spectra of the CP43-complex at 77 K, calculated for the optimized site energies in Table 5.1 are compared with experimental data (Groot et al., 1999). From the temperature dependence of the

Table 5.1: Site energies in the CP43-complex, optimized by a fit of the linear optical spectra in Figure 5.1. The three Chls with the lowest site energies and the respective values are highlighted.

Chl	33	34	35	**37**	41	42	**43**
λ/nm	667	673	670	**678**	661	670	**676**
Chl	44	**45**	46	47	48	49	
	673	**676**	665	665	670	667	

absorption spectrum in the upper part of Figure 5.1, a Huang-Rhys factor $S \approx 0.5$ is inferred which is comparable to the $S = 0.65$ estimated for the reaction center pigments previously (see chapter 3.2)(Raszewski et al., 2005). A width Δ_{inh}=180 cm^{-1} (fwhm) of the Gaussian distribution function for the site energies gave the best fit. The same $S = 0.5$ and Δ_{inh}=180 cm^{-1} are used for the Chls in CP47, since both core antenna subunits have a similar structure. The optical spectra of the CP47-complex, calculated with the optimized site energies in Table

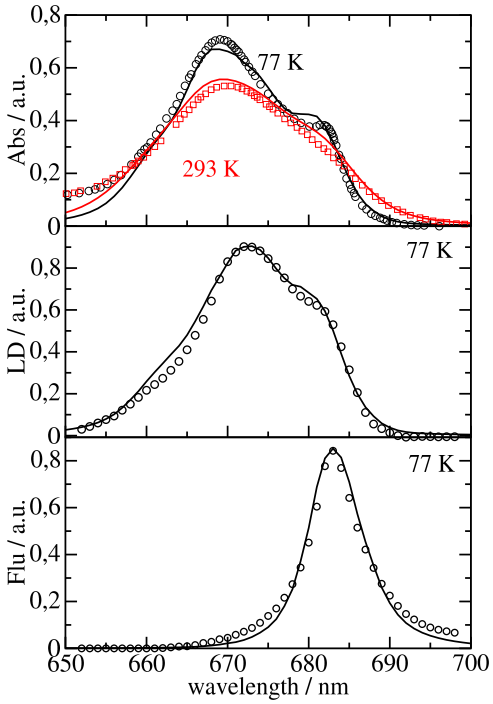

Figure 5.1: The absorption (Abs), linear dichroism (LD) and fluorescence (Flu) spectra of the CP43-complex at 77 K and 293 K (Abs) calculated with the site energies in Table 5.1 are compared with experimental data.(Groot et al., 1999) The calculations are shown as lines and the experimental data as symbols.

5.2 are compared in Figure 5.2 with experimental data at 77 K (linear absorption (de Weerd et al., 2002), linear dichroism (de Weerd et al., 2002) and fluorescence (Groot et al., 1995)) and at 293 K (circular dichroism (Alfonso et al., 1994)).

The wavelengths corresponding to the site energies in Tables 5.1 and 5.2 vary between 664 nm and 688 nm. The three lowest site energies in CP43 belong to Chls 37, 43 and 45 (using the numbering of Loll *et al.* (Loll et al., 2005)), whereas the low energy pigments in CP47 are Chls 11, 24 and 29. The low energy Chls in CP43 are located relatively close to the RC as seen in Figure 5.3, whereas those of CP47 are distributed over the whole complex (Fig. 5.4).

Table 5.2: Site energies and corresponding wavelengths in the CP47-complex, optimized by a fit of the linear optical spectra in Figure 5.2. The three Chls with the lowest site energies and the respective values are highlighted.

Chl	**11**	12	13	14	15	16	17	21
λ/nm	**681**	664	676	669	675	672	661	668
Chl	22	23	**24**	25	26	27	28	**29**
λ/nm	675	655	**680**	664	673	672	668	**688**

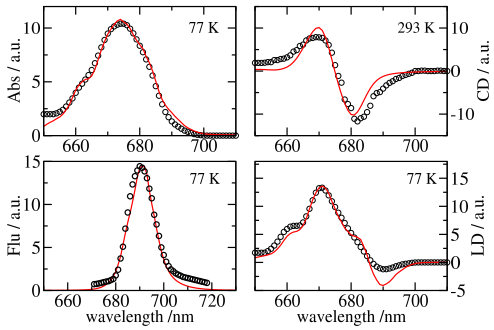

Figure 5.2: The absorption (Abs), circular dichroism (CD), fluorescence (Flu), and linear dichroism (LD) spectra of the CP47-complex at 77 K (Abs, Flu, LD) and 293 K (CD), calculated with the site energies in Table 5.2 are compared with experimental data for Abs and LD (de Weerd et al., 2002), Flu (Groot et al., 1995) and CD (Alfonso et al., 1994). The calculations are shown as lines and the experimental data as symbols.

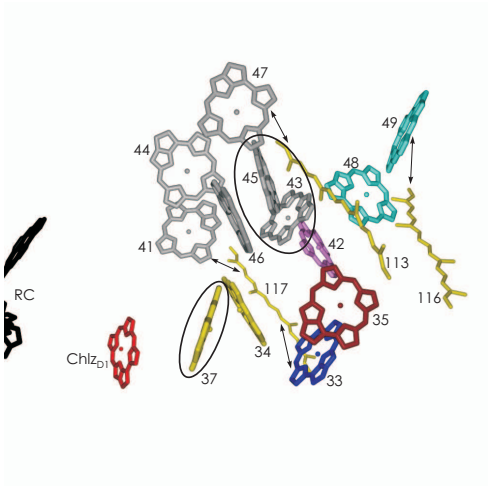

Figure 5.3: Arrangement of pigments in the CP43-complex. The pigments are numbered as in ref (Loll et al., 2005). Chls with the same color belong to the same exciton domain. A cutoff energy of 36 cm^{-1} was used in the definition of the domains. If two pigments are coupled stronger than this value they belong to the same domain. Arrows indicate a van der Waals contact between the conjugated π-systems of a carotenoid and a Chl. The three encircled Chls are those with the lowest site energy (trap states). In addition a small part of the reaction center including $Chlz_{D1}$ is shown.

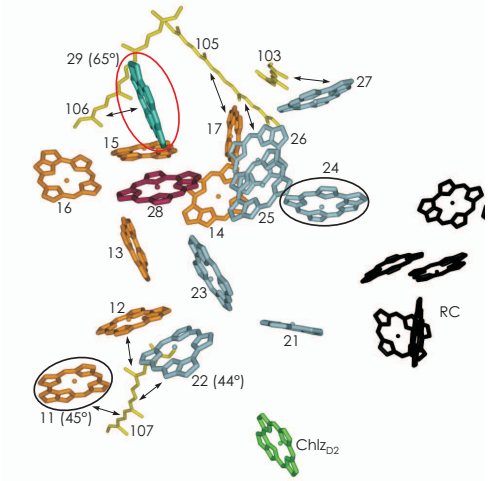

Figure 5.4: Arrangement of pigments in the CP47-complex. The pigments are numbered as in ref (Loll et al., 2005). Chls with the same color belong to the same exciton domain. A cutoff energy of 36 cm^{-1} was used in the definition of the domains. If two pigments are coupled stronger than this value they belong to the same domain. Arrows indicate a van der Waals contact between the conjugated π system of a carotenoid and a Chl. The three encircled Chls are those with low site energies (trap states), the one with the lowest site energy is encircled in red. Angles of Chl transition dipoles with respect to the membrane plane that are larger than 35° (corresponding to $\theta < 55°$) are shown in parentheses. In addition, part of the RC including $Chlz_{D2}$ is shown.

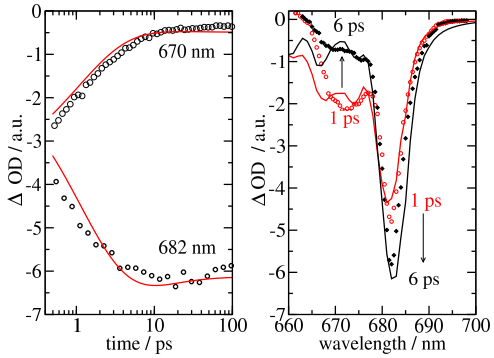

Figure 5.5: The 77 K pump-probe spectra of the CP43-complex, calculated using the site energies and the Huang-Rhys factor from the fit of the linear spectra in Figure 5.1, are compared with experimental data.(de Weerd et al., 2002a) The CP43-complex was excited with a 60 fs pump-pulse, centered at 671 nm. The left part of the figure contains the pump-probe signal at two different probe wavelengths in dependence on the delay time between the pulses and the right part the pump-probe spectrum at two different delay times. The experimental data are shown as symbols and the calculations as solid lines.

Chl 24 is the only low energy Chl of CP47 that is close to the RC. Two of the low energy pigments in CP43 (Chls 43 and 45) are part of a large exciton domain of six strongly coupled Chls and one, Chl 37, forms a dimer domain with Chl 34. In CP47 all three low energy pigments are located in different domains. Two of them, Chls 11 and 24, are part of large domains, each containing seven Chls, in the lumenal and stromal layer, respectively and Chl 29 has a localized excited state. It is the red-most pigment in the whole PS-II core complex and gives rise to a negative LD signal at low energies (long wavelengths).

5.2.2 Time-resolved spectra of CP43 and CP47

The site energies of the CP43 and CP47 subunits determined above from the fit of stationary spectra together with the Huang-Rhys factor $S = 0.5$ and the inhomogeneous width $\Delta_{\text{inh}} = 180$ cm^{-1} were used to calculate time-resolved pump-probe spectra. In Figures 5.5 and 5.6 the pump-probe signals calculated for different probe wavelengths and delay times after excitation by a 60 fs pump-pulse centered at 671 nm (CP43) or 670 nm (CP47) are compared with experimental data (de Weerd et al., 2002a). In the case of CP43, quantitative agreement between calculated and measured spectra is obtained. The pump-probe signal reflects exciton transfer/relaxation from high to low energies that occurs on a sub-ps and ps timescale and is finished in about 6 ps. In CP47, in addition to these fast components, there are longer relaxation times detected and calculated in Figure 5.6. These slow processes last until about 100 ps in the experiment, and somewhat longer in the calculations. Except for these deviations, there is a good qualitative agreement between the calculated and measured spectra for CP47. The exciton relaxation processes in CP43 and CP47 and their relative amplitudes are illustrated in the LFD maps of time-dependent emission in Figures 5.7 and 5.8. In CP43, there are two main relaxation components of about 200 fs and 2 ps. In CP47, besides the two main components of 250 fs and 700 fs, dispersive decay behavior is calculated with time constants ranging from 5 ps to 100 ps. The latter changes qualitatively at room temperature (Fig. 5.9). A main slow component at 10 ps appears, whereas the faster components are not changed qualitatively.

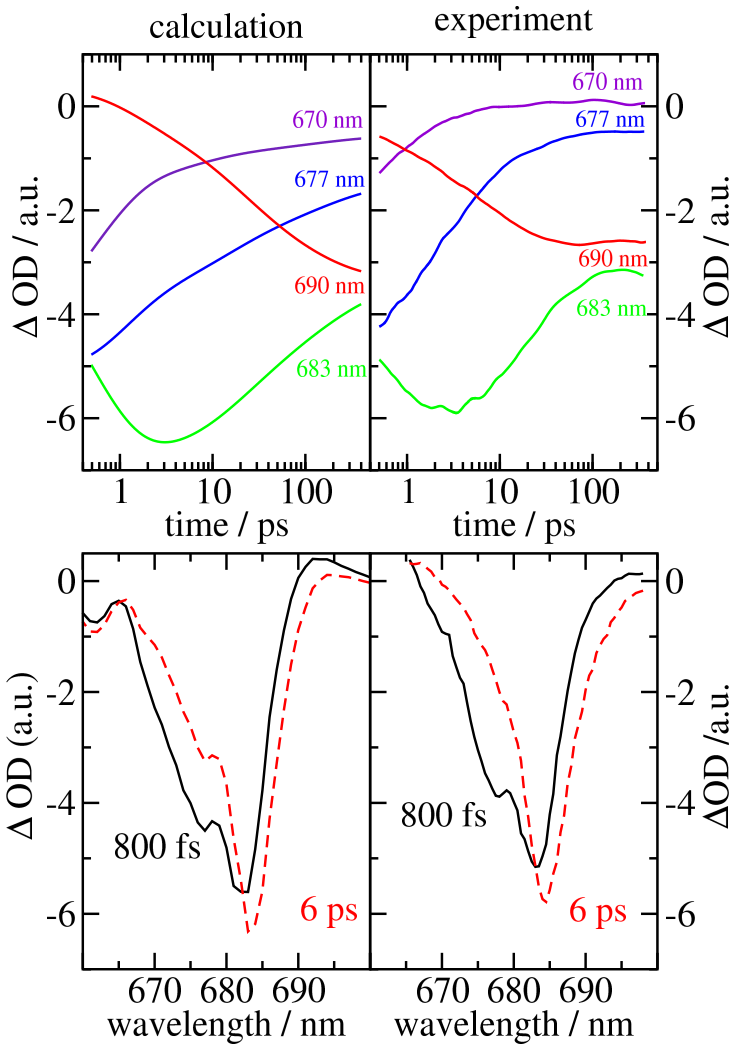

Figure 5.6: The 77 K pump-probe spectra of the CP47-complex calculated using the site energies from the fit of the linear spectra in Figure 5.2 are compared with experimental data.(de Weerd et al., 2002a) The CP47-complex was excited with a 60 fs pump-pulse, centered at 670 nm. The upper part of the figure contains the pump-probe signal at four different probe wavelengths in dependence on the delay time between the pulses and the lower part the pump-probe spectrum for two different delay times. The calculations are shown in the left and the experimental data in the right part.

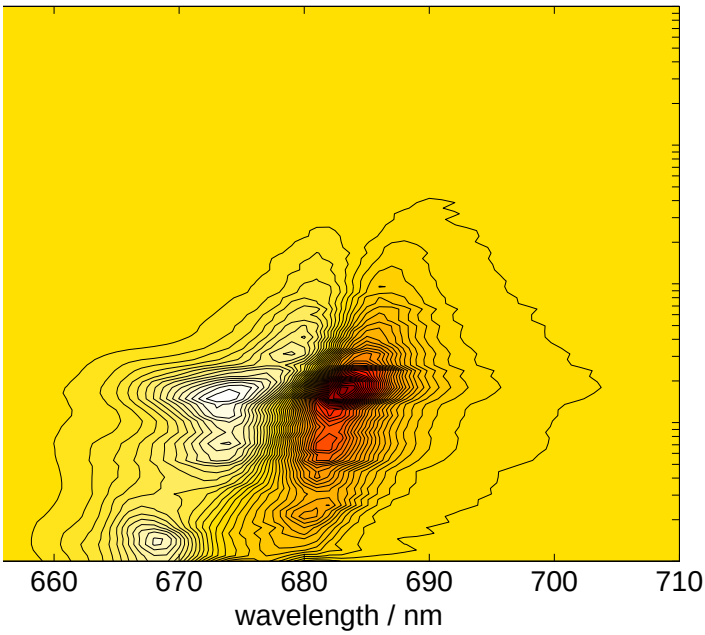

Figure 5.7: The life time density map of time dependent emission of the CP43-complex at 77 K, calculated assuming excitation with a 60 fs pulse at 671 nm.

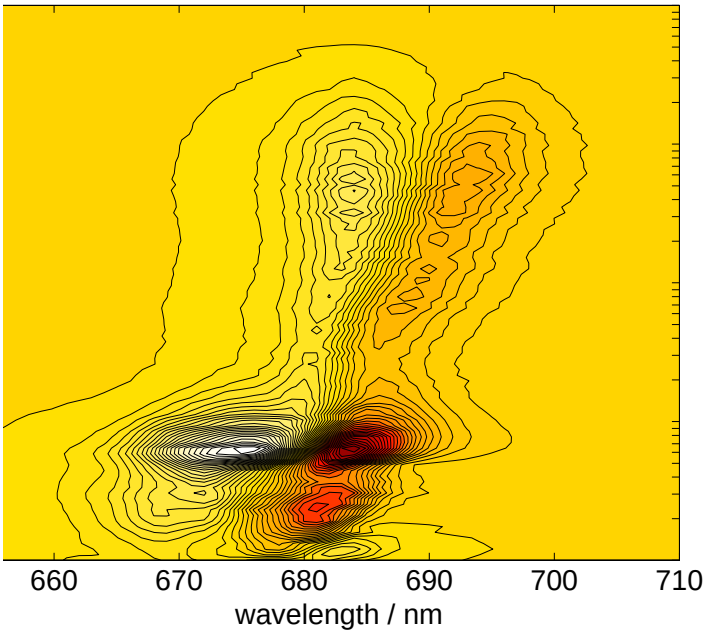

Figure 5.8: The life time density map of time dependent emission of the CP47-complex at 77 K, calculated assuming excitation with a 60 fs pulse at 670 nm.

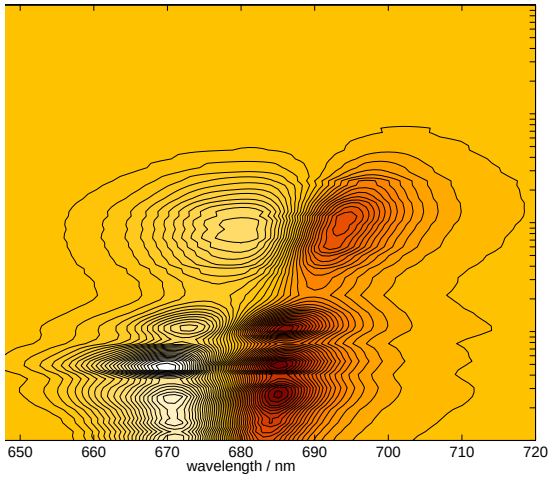

Figure 5.9: Fluorescence life time density map of the CP47-complex at 300 K, calculated assuming excitation with a 60 fs pulse at 670 nm.

5.2.3 Time-dependent fluorescence of PS-II core complexes

The site energies, determined from the linear spectra and tested in the simulations of non-linear spectra, were applied to calculate the time-dependent fluorescence of PS-II core complexes at 300 K. The experimental frequency integrated and time-resolved fluorescence (Miloslavina et al., 2006), detected after excitation with a 100 fs optical pulse that was centered at 663 nm, can be described by assuming an intrinsic rate constant for primary charge separation of $k_{\mathrm{intr}} = (100\ \mathrm{fs})^{-1}$, as seen in Figure 5.10.

To find the bottleneck for the decay of excited states, the fluorescence decay was calculated in simplified models, in which fast equilibration of excitation energy in certain compartments is assumed. The fluorescence decays obtained in these models are compared in Figure 5.10 with the full calculation and the experimental data. If fast exciton relaxation is assumed in the domains of strongly coupled Chls (Fig. 5.11) virtually the same result as in the calculation without this assumption is obtained for the fluorescence decay in Figure 5.10 (the red dashed and black solid curves). The respective inverse disorder averaged rate constants $\langle k_{a\to b}\rangle^{-1}_{\mathrm{dis}}$ (with the $k_{a\to b}$ in eq 2.58) in Figure 5.11 show that the fastest transfer between exciton domains in different layers in CP43 and CP47 occurs with time constants of 2-7 ps at 77 K and room temperature. The disorder average was performed with respect to the site energies of the pigments, in the same way as for the optical spectra, explained below eq 2.20. If fast exciton relaxation is assumed in the whole CP43, CP47, and RC subunits, there are still only very minor deviations with respect to the complete calculation, as seen in Figure 5.10. Since $\mathrm{Chlz}_{\mathrm{D1}}$ equilibrates faster with CP43 than with the RC and, similarly, $\mathrm{Chlz}_{\mathrm{D2}}$ with CP47, these two Chlz were included in the compartment of the respective antenna subunit. The disorder averaged inverse rate constants for this three compartment model and a five compartment model, where the Chlz are in separate compartments are shown in Figure 5.12. The inter-compartment rate constants were obtained from eq 2.60, and averaged over disorder in site energies. The time constant for exciton transfer between the CP47-$\mathrm{Chlz}_{\mathrm{D1}}$ compartment and the RC at room temperature is 50 ps and that between CP43-$\mathrm{Chlz}_{\mathrm{D2}}$ and the RC is 41 ps. If fast exciton equilibration in the whole PS-II core complex is assumed, as in the ERPE model, large deviations with respect to the complete calculation are obtained (the blue dotted line in Fig. 5.10).

An analysis of the excitation energy transfer and trapping dynamics in PS-II core complexes

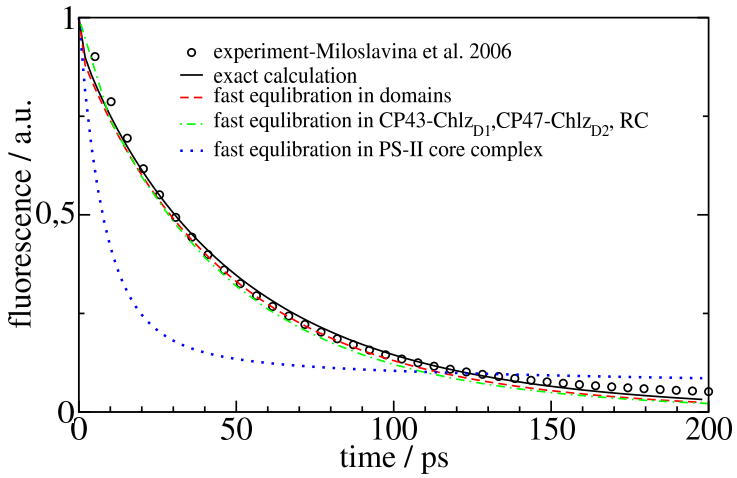

Figure 5.10: Frequency integrated fluorescence decay of PS-II core complexes at 300 K calculated in different models, compared to experimental data (Miloslavina et al., 2006). The PS-II core complex was excited with a 100 fs optical pulse, centered at 663 nm. The experimental data were reconstructed from Table 1 of ref (Miloslavina et al., 2006).

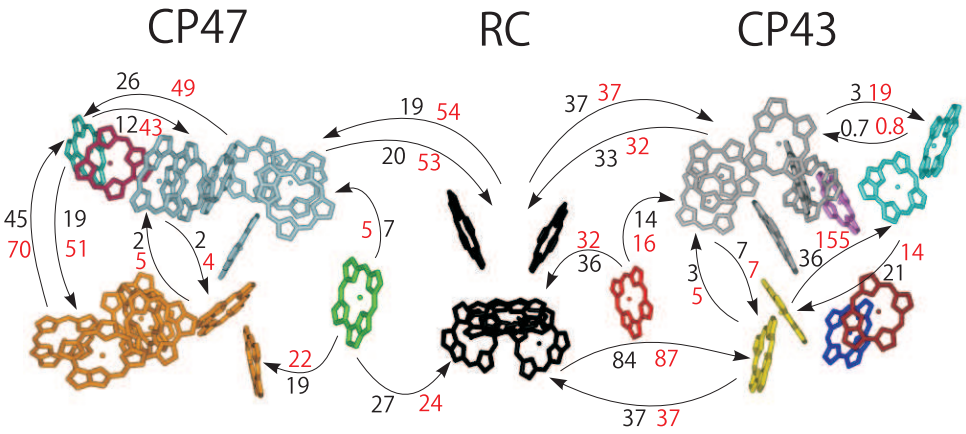

Figure 5.11: Disorder averaged inverse rate constants in units of ps for important transfer paths between exciton domains in the PS-II core complex, assuming fast intra domain exciton relaxation, at 300 K (black numbers) and 77 K (red numbers). Chls with the same color belong to the same exciton domain.

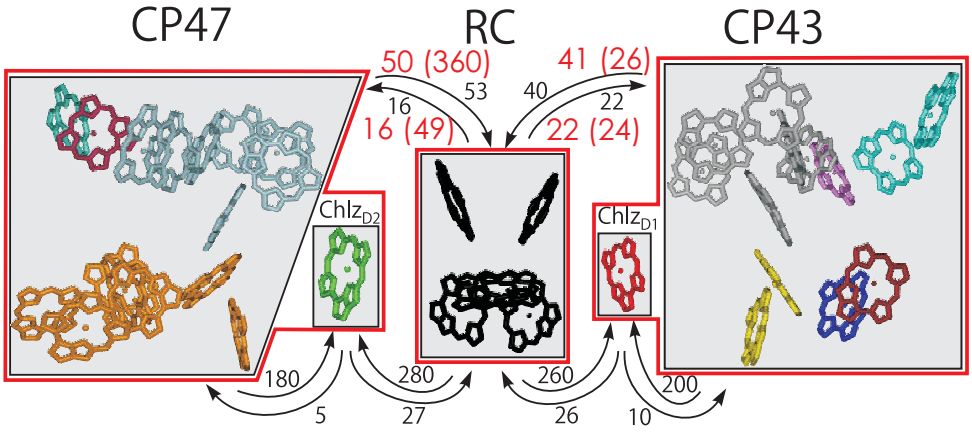

Figure 5.12: Disorder averaged inverse rate constants in units of ps for exciton transfer between compartments in the PS-II core complex assuming fast intra compartment exciton relaxation. The numbers in black refer to a five compartment model, containing CP43, CP47, RC, Chlz$_{D1}$ and Chlz$_{D2}$ for T = 300 K. The numbers in red were obtained for a three compartment model with the compartments CP43-Chlz$_{D1}$, CP47-Chlz$_{D2}$, RC at T = 300 K and 77K (numbers in parentheses).

is given in Fig. 5.13 by means of the fluorescence LFD map, calculated either with or without electron transfer (including charge recombination reactions). The LFD map without electron transfer was calculated to analyze the time constants of exciton relaxation/ transfer in the system. Several components ranging from sub ps to 200 ps are found (components A to F in Figure 5.13). These components reflect intra-domain exciton relaxation (A, B), exciton transfer between the domains in one subunit (B), exciton transfer to the trap state of CP47 and exciton equilibration between CP43, CP47 and RC (C), exciton transfer between CP43 and CP47 via the RC (D), exciton transfer from CP43 to RC and CP47 to RC and trapping in the RC (E), and electron transfer between RP2 and RP3 and recombination (F).

The disorder averaged inverse rate constants in Fig. 5.12, show that at room temperature excitation energy transfer between CP47 and RC and between CP43 and RC occurs with similar time constants of 40-50 ps. However, at 77 K a striking decrease of the rate constant $k_{\mathrm{CP47}\rightarrow\mathrm{RC}}$ is obtained: It slows down by an order of magnitude (red numbers in parentheses in Figure 5.12). To understand the origin of this temperature dependence, the probability distributions of the different time constants were calculated, including also the time constant $\tau_{\mathrm{RC}\rightarrow\mathrm{RP1}} = (k_{\mathrm{RC}\rightarrow\mathrm{RP1}})^{-1}$ (eq 2.59) for primary electron transfer. As shown in Figure 5.14, the maxima of the distribution functions of the time constants of the primary electron transfer and excitation energy transfer between CP43 and RC move towards shorter times at 77 K, but their widths does not change qualitatively.

In contrast, the rate of excitation energy transfer from CP47 to the RC becomes highly dispersive, the width of the distribution of the respective time constant widens by an order of magnitude and the maximum shifts from 50 ps at 300 K to 200 ps at 77 K. If the site of Chl 29 in CP47 is increased such that the corresponding wavelength decreases from 688 nm to 670 nm (which corresponds to the site energy of the equivalent Chl 49 in CP43), a large part of the dispersive behavior is lost, as seen in Figure 5.15 (red curve) and the average time constant for transfer from CP47 to the RC decreases from 400 ps in the native system to 100 ps in the modified system. Increasing the site energy of another CP47 trap state, the one at Chl 11, has only a minor effect on the transfer efficiency to the RC (the blue line in Figure 5.15). However upshifting the site energies of both these CP47 trap states results in a cooperative effect, i.e., the maximum of the distribution function for the CP47 → RC transfer shifts furthest towards shorter times (the green line in Figure 5.15).

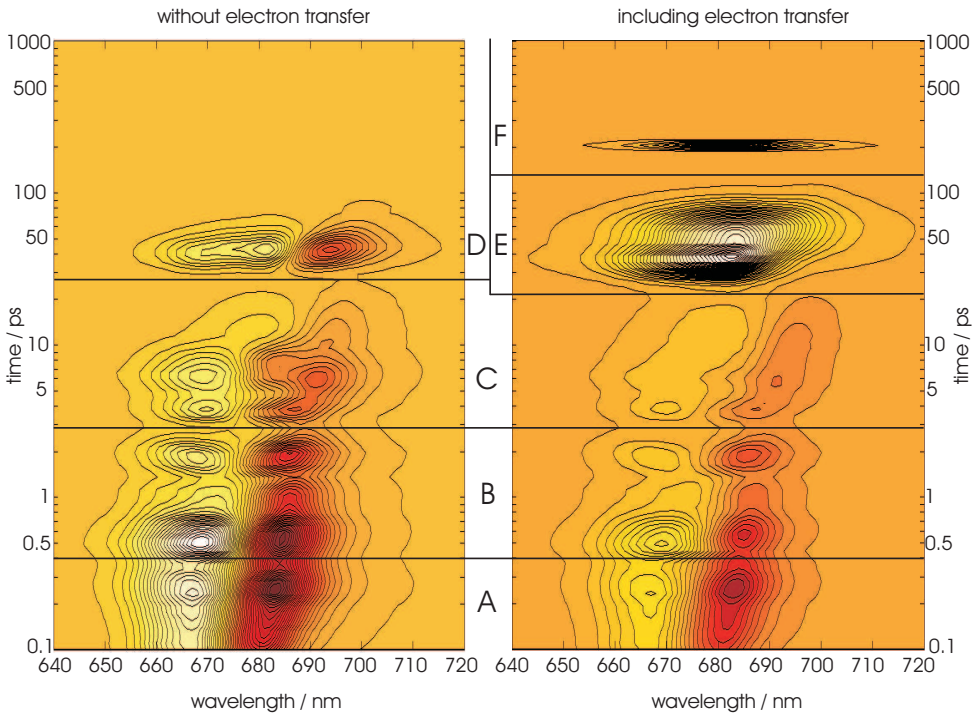

Figure 5.13: Lifetime density maps of time dependent emission of PS-II core complexes calculated with and without including electron transfer, assuming excitation by a 100 fs pulse at 660 nm, T = 300 K.

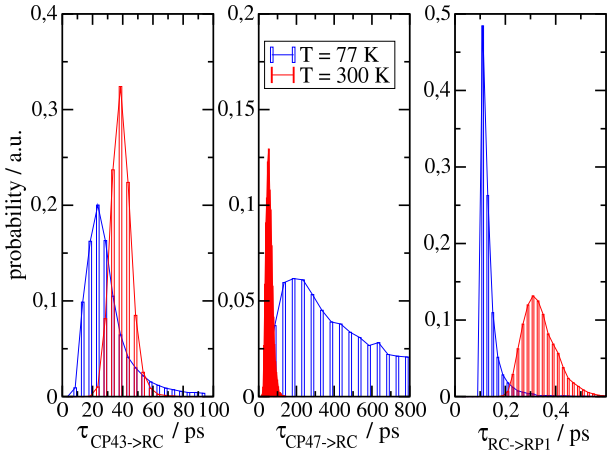

Figure 5.14: Probability distribution of time constants for transfer from CP43 to RC (left), from CP47 to RC (middle) and primary electron transfer (right) at T = 77 K (blue) and T = 300 K (red). The rate constants were obtained in the three compartment model, i.e. $Chlz_{D1}$ was included in the CP43 compartment and $Chlz_{D2}$ in that of CP47.

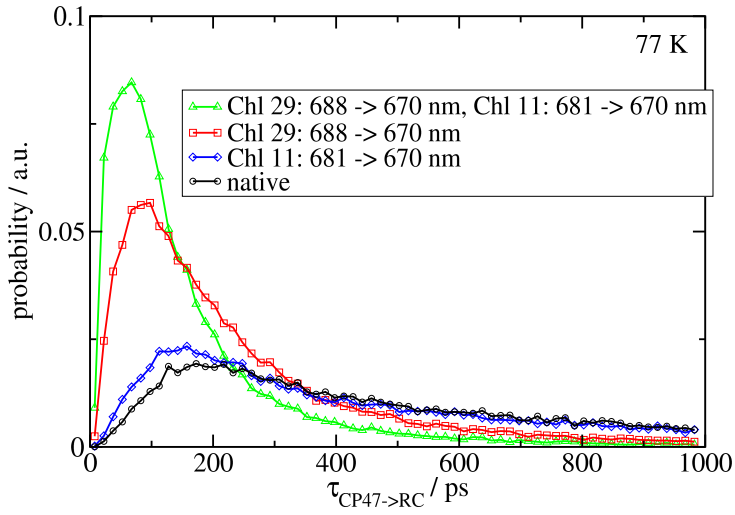

Figure 5.15: Probability distribution of time constants for transfer from CP47 to RC at T = 77 K for native system (as in Fig. 5.14, middle part) compared to that for modified systems where the site energies of two trap states were increased as indicated in the figure.

5.3 Discussion

5.3.1 Trap states in CP43 and CP47

For the analysis of the antenna trap states, the exciton state pigment distribution function $d_m(\omega)$ (eq 3.2) introduced previously is shown in Figure 5.16 for the three pigments with the lowest site energies in CP43 and CP47 (compare Tables 5.1 and 5.2). Whereas in CP43 all three low energy pigments contribute at the lowest excitation energy of the subunit, in CP47 just Chl 29 has a contribution. In addition, all of the functions d_m except for the one of Chl 29 indicate a certain delocalization of the excitons by multiple maxima or at least shoulders.

In CP43, two of the three pigments, Chls 43 and 45, belong to the same domain, whereas Chl 37 is part of a dimer domain with Chl 34 (see Fig. 5.3). Hence, there are two degenerate low energy exciton transitions around 682 nm which represent the lowest excited states of the two domains in the lumenal (containing Chls 34 and 37) and stromal layer (containing Chls 41, 43-47). These characteristics fit very nicely to the A- and B-states identified in NPHB and triplet bottleneck spectra (Groot et al., 1999; Jankowiak et al., 2000; Hughes et al., 2006), discussed in the Introduction. The B-state is identified as the low energy exciton state of the stromal domain with 6 pigments (shown in grey in Figure 5.3), whereas the A-state is the low energy exciton state of the Chl 34-37 dimer on the lumenal side (shown in yellow in Figure 5.3). Whereas there is a van der Waals contact between Chls and carotenoids for Chls 41 and 47 of the large domain, there is no such connections for Chls 34 and 37 in the dimer. This difference could be the reason, why the A-state does show a strong triplet bottleneck signal and the B-state does not (Jankowiak et al., 2000). The hydrogen bonds predicted by Groot et al. (1999) on the basis of the vibrational fine structure of the emission most likely are formed between the 13^1-keto group of the low energy Chls 43 and 45 of the B-state domain and His C164 and Ser C275, respectively.

Concerning the larger hole burning efficiency of the B-state, at first glance, both explanations discussed in the introduction (sec.5.1) could apply. Since the B-state domain is three times larger than the dimeric A-state domain it can collect more excitation energy, as suggested by Jankowiak et al. (2000). On the other hand, the hydrogen bonds to Chls 43 and 45, discussed above, could explain the higher photoconversion of the B-state, as proposed by Krausz and

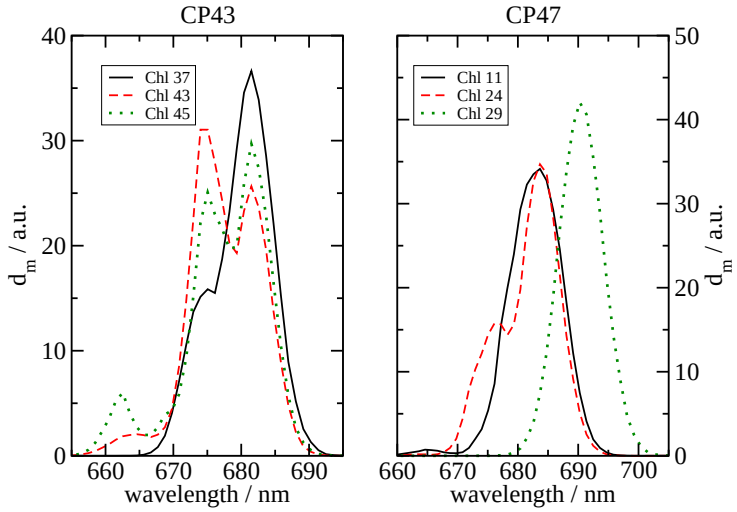

Figure 5.16: Exciton states pigment distribution function $d_m(\omega)$ (eq 3.2) for the three low energy pigments in CP43 (left) and CP47 (right).

coworkers (Hughes et al., 2006), since no such hydrogen bonds exist for Chls 34 and 37 in the A-state domain. As seen in Figure 5.11, both layers of the membrane are well connected by excitation energy transfer. Hence, the present calculations are in favor of the proposal of Krausz and coworkers (Hughes et al., 2006). A possible explanation of the narrow 0-0 lineshape measured in hole burning (Jankowiak et al., 2000) is that at low temperature those complexes are selected from the ensemble in the sample which have non-degenerate low energy exciton states and where the energy gap between the two antenna trap states (A and B) is large compared to the thermal energy. In this case the excited states of the pigments in the exciton state with the lowest energy have a long lifetime and therefore exhibit a high hole burning efficiency.

The coupling between the A-state Chls 37 and 34 is seen as a shoulder of the function d_{37} in Figure 5.16 around 672 nm. In the experiment this shoulder is found at somewhat shorter wavelengths (higher energies) around 669 nm (Groot et al., 1999; Jankowiak et al., 2000) indicating that the site energy of Chl 34 might be slightly higher than determined here from a fit of the linear spectra. Concerning the excitonic coupling in the B-state domain, Jankowiak et al. (2000) found correlations between the B-state at 683 nm and other exciton transitions at 678 and 673 nm. The correlation between 683 nm and 673 nm involve Chls 43 and 45, as shown in Figure 5.16.

In agreement with de Weerd et al. (2002), the present calculations show that the lowest excited state of CP47 is localized on a monomeric Chl, namely Chl 29. From the 16 Chls in CP47 only Chls 11, 22 and 29 have an angle between their transition dipole moment and the membrane plane larger than 35° and therefore could be responsible for the negative LD signal observed at low energies. Chls 11 and 22 are part of two large exciton domains in the lumenal and stromal layer of the membrane, respectively. Hence, the only localized excited state with negative LD is the one of Chl 29.

The 2 nm blue shift of the low-temperature fluorescence that occurred after mutation of His B114 (Shen et al., 1994), which turned out to be the axial ligand of Chl 29 (Loll et al., 2005), to Gln provides further support for the present assignment. Chl 29 forms a hydrogen bond to Thr H5 of the H-subunit, in agreement with the prediction of a strong hydrogen bond of the low energy Chl from the FLN spectra (de Weerd et al., 2002). The absence of a 690 nm bleaching in the T-S signal (de Weerd et al., 2002) could very well be due to the quenching of the triplet energy of Chl 29 by Car 106 (see Fig. 5.4). From the three low energy pigments in CP47, only

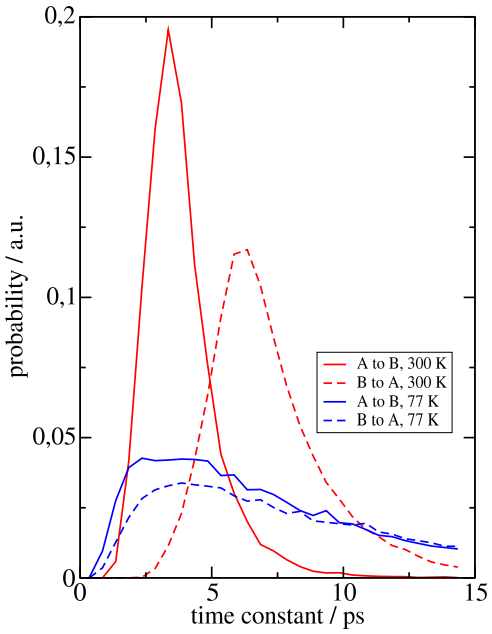

Figure 5.17: Probability distribution for the inter-layer exciton transfer between the lumenal and stromal trap state domains in the CP43-complex at 77 K and 300 K. The lumenal dimeric trap state domain is labeled by A and the stromal hexameric trap state domain by B.

Chl 24 is not in van der Waals contact with a carotenoid. Therefore, it can be expected to be the main contributor to the T-S signal. As suggested from anisotropy measurements (de Weerd et al., 2002), the 683 nm state consists of more than one exciton transition. Chls 11 and 24 which are located in different domains contribute to different exciton transitions at this wavelength (Fig. 5.16).

5.3.2 Excitation energy transfer in the CP43 and CP47 subunits

The experimentally found 0.2-0.4 ps and 2-3 ps time constants (de Weerd et al., 2002a) for exciton relaxation in CP43-complexes are well reproduced by the calculations of the pump-probe spectra in Figure 5.5 and the LFD map in Figure 5.7. As described above, there are two trap states in CP43, one in the lumenal and one in the stromal layer. The 200 fs time constant reflects exciton relaxation in the domains and exciton transfer between the domains in the same layer to the trap state domain. As seen in Figure 5.11, the disorder averaged transfer times between the trap state domain in the stromal and the one in the lumenal layer are 6 ps and 8 ps which appear to be somewhat too slow to explain the main 2 ps equilibration time constant in the LFD map in Figure 5.7. The latter is understood by taking into account, instead of the average value, the maxima of the probability distribution of these time constants which are both about 4 ps (Fig. 5.17).

The resulting 2 ps equilibration time explains also the pump-probe spectra in Figure 5.5.

The LFD map of CP47 in Figure 5.8 contains strong 500 fs -800 fs components that appear to be somewhat too fast for exciton relaxation between the lumenal and stromal layers as judged by the transfer times in Figure 5.11, which would yield a relaxation time of about 2 ps. As in the case of CP43, the distribution of this interlayer transfer times in CP47 is asymmetric (data not shown). If one uses the maxima of the distributions, one arrives at an equilibration time of about 1 ps, which is still slightly too slow to explain the fast components in the LFD map. Obviously, the latter are dominated by contributions from intra-domain exciton relaxation to

the degenerate 683 nm trap states in each of the two domains in the lumenal and stromal layer. From these two traps states a largely dispersive transfer to the 690 nm trap state at Chl 29 occurs with time constants that have a strongly asymmetric distribution at 77 K with maxima in the 20-60 ps range. This behavior is reflected in the measured and calculated pump-probe signal in Figure 5.6. The 683 nm signal first becomes more negative up to a delay time of 2 ps and then starts to increase up to 100 ps in the experiment and somewhat longer in the calculations. The rise of the negative signal reflects excitation energy transfer to the 683 nm trap states and, therefore, increased SE at this wavelength. The decay of this signal at larger times and the parallel growth of the negative signal at 690 nm is due to excitation energy transfer to the trap state at Chl 29.

5.3.3 Excited state decay in PS-II core complexes

Having determined the site energies from linear optical spectra and having tested them in the calculation of time resolved spectra, provides a solid ground to investigate excitation energy transfer and trapping in PS-II core complexes. The measured main 40-50 ps decay component of the fluorescence (Miloslavina et al., 2006) can only be described by assuming that charge recombination reactions occur on a slower time scale. Assuming a faster recombination would cause a too slow decay of the fluorescence in contradiction with the experimental data. This finding enables one to describe the decay by using only one adjustable parameter, namely the k_{intr} for primary electron transfer. A quantitative description of the experimental data is obtained in Figure 5.10 for $k_{\mathrm{intr}} = (100\ \mathrm{fs})^{-1}$. Due to the partial delocalization of exciton states in the RC and the fast equilibration of exciton state populations prior to electron transfer, the first radical pair state is created with a time constant of about 300 fs, as seen in the right part of Figure 5.14 (see also eqs 2.55 and 2.59). This time constant is an order of magnitude faster than the 3 ps inferred from pump-probe spectra in the visible spectral range (Holzwarth et al., 2006), and about a factor of 2 faster than the 600-800 fs from mid IR-vis pump-probe data (Groot et al., 2005) on D1-D2-cyt$b$559 complexes. If real, the discrepancy by a factor of two between the latter result and the present calculations might reflect a conformational difference between D1-D2-cyt$b$559 and PS-II core preparations that could change the electron transfer coupling matrix element between $\mathrm{Chl_{D1}}$ and $\mathrm{Pheo_{D1}}$, or lead to a slight change of the driving force of the reaction. In fact, a 4 nm red shift of the site energy of $\mathrm{Chl_{D1}}$ in PS-II core complexes as compared to that in D1-D2-cyt$b$559 complexes described in previous chapters, could have the same origin. On the other hand, using an intrinsic rate constant of $k_{\mathrm{intr}} = (200\ \mathrm{fs})^{-1}$ that corresponds to a Pheo reduction with a time constant of 600 fs, as reported in ref (Groot et al., 2005), results only in a slightly less satisfying description of the measured fluorescence decay as seen in Fig. 5.18.

However, the present model is not consistent with a time constant of 3 ps for Pheo reduction (Fig. 5.18). In bacterial reaction centers, electron transfer starting at the accessory bacteriochlorophyll was found to occur an order of magnitude faster (< 400 fs) than electron transfer starting at the special pair (3 ps) (van Brederode et al., 1997, 1999). Taking into account the high similarity in arrangements of $\mathrm{Chl_{D1}}$ and $\mathrm{Pheo_{D1}}$ and its bacterial counterparts, as described in details in previous chapter, the present finding of ultrafast primary electron transfer provides further support for $\mathrm{Chl_{D1}}$ as the primary electron donor in PS-II.

The direct detection of the ultrafast intrinsic rate constant of $(100\ \mathrm{fs})^{-1}$ for primary charge separation, inferred here, is difficult, because it is impossible to excite the primary donor $\mathrm{Chl_{D1}}$ exclusively in PS-II core complexes. It would, therefore, be helpful to repeat the earlier experiments on ultrafast electron transfer starting at the accessory bacteriochlorophyll in bacterial reaction centers (van Brederode et al., 1997, 1999) with a higher time resolution to pinpoint the exact value of this rate constant. In the present treatment, k_{intr} was just treated as a fit param-

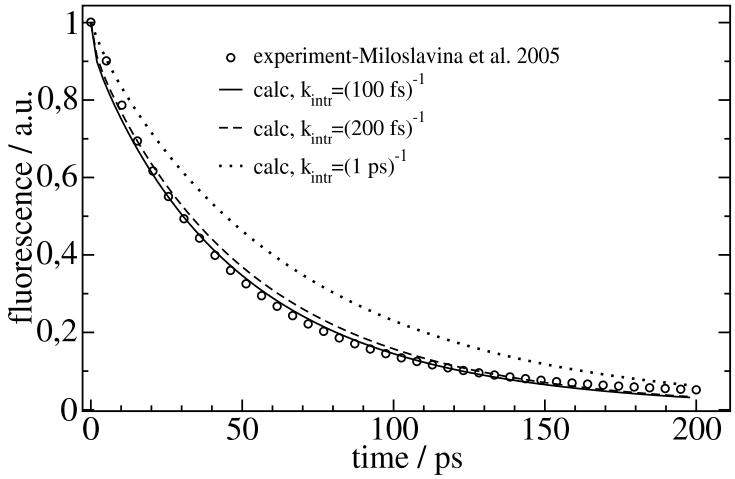

Figure 5.18: Frequency integrated fluorescence decay of PS-II core complexes, calculated for different k_{intr} in comparison to experimental data (Miloslavina et al., 2006).

eter without using any mechanistic description of the electron transfer reaction. The assumed dependence of $k_{M\rightarrow RP1}$ on $|c^{(M)}_{\mathrm{Chl_{D1}}}|^2$ in eq 2.55 seems to suggest a second order perturbation theory in the electronic coupling, i.e., a non-adiabatic reaction. However, because of the low site energy of $\mathrm{Chl_{D1}}$, the $|c^{(M)}_{\mathrm{Chl_{D1}}}|^2$ is essentially non-zero only for one exciton level that is strongly localized on the primary donor (Raszewski et al., 2005, 2007). Hence, the square of the coefficient just ensure that primary electron transfer starts at $\mathrm{Chl^*_{D1}}$. The fast time constant of 100 fs for primary electron transfer, inferred here, provides some indications that the electron transfer reaction occurs beyond the non-adiabatic limit, i.e., in a more adiabatic way, where the rate constant is determined by the vibrational motion in an adiabatic surface that reflects a certain delocalization between the initial and the final states of the primary electron transfer reaction in eq 2.56. Indeed, there are some independent experimental facts that point in this direction: (i) Krausz et al. (2005) reported experimental evidence about quinone reduction after long wavelength excitation (down to 730 nm) at cryogenic temperatures. A possible explanation of this phenomenon could be that due to the quantum mechanic mixing of $\mathrm{Chl^*_{D1}}$ and $\mathrm{Chl^+_{D1}Pheo^-_{D1}}$ the latter state borrows some oscillator strength from the former and therefore can be directly excited (Renger et al., 2004). (ii) To explain their unconventional Stark spectra, Frese et al. (2003) suggested that the low energy exciton state in PS-II RCs is mixed with a charge transfer state. (iii) The temperature dependence of the site energy of $\mathrm{Chl_{D1}}$, inferred from the calculation of optical difference spectra (see chapter 4) Raszewski et al. (2007) could reflect a temperature dependent localization of a mixed excited/ charge transfer state (Renger et al., 2004).

In order to find the bottleneck for the decay of excited states in PS-II core complexes, calculations were performed, assuming fast exciton relaxation in certain compartments. The respective inverse rate constants are given in Figs. 5.11 and 5.12. As seen in Figure 5.10, the simplest model that still describes the decay of excited states is a three compartment model, where it is assumed that exciton relaxation in CP43-$\mathrm{Chlz_{D1}}$, CP47-$\mathrm{Chlz_{D2}}$ and in the RC is fast compared to the transfer between these compartments. The time constants obtained in a five compartment model with Chlz in extra domains in Figure 5.12 show that $\mathrm{Chlz_{D1}}$ and $\mathrm{Chlz_{D2}}$ in terms of light harvesting function belong to the CP43 and CP47 subunits, respectively, rather than to the RC. The transfer times of 50 ps and 41 ps between CP43(-$\mathrm{Chlz_{D1}}$) and RC and CP47(-$\mathrm{Chlz_{D2}}$) and RC (Fig. 5.12) are found to represent the main decay components of excited states in the LFD map of PS-II core complexes in Figure 5.13. Because of the one order of magnitude faster primary electron transfer, nearly every excitation that reaches the RC is

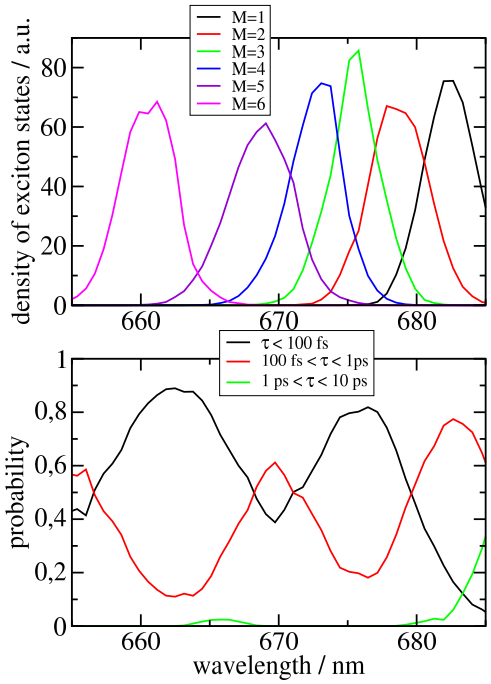

Figure 5.19: *Upper part:* density of exciton states $d_M(\omega)$ formed by the six strongly coupled RC pigments. *Lower part:* probabilities to find an exciton state in the RC with a life time in a certain range, as indicated in the figure, T = 300 K.

irreversibly trapped. This result shows that the decay of excited states in PS-II is limited by the transfer to the trap, i.e., the RC. Note that the rate constants for excitation energy transfer between the compartments are no free parameters, but are obtained from the individual intra-domain rate constants, calculated from a microscopic theory.

In the 3- and 5-compartment models, primary electron transfer was assumed to start from an equilibrated exciton manifold in the RC. The close agreement in Fig. 5.10 between the full calculation that does not assume such an equilibration of excitons prior to charge transfer and the compartment calculations indicates that exciton relaxation in the RC at 300 K occurs on an ultrafast sub 100 fs time scale. Independent support for this result is obtained by a direct calculation of the life times of exciton states in the RC as seen in Fig. 5.19.

The assumption of a fast equilibration of excited states in the whole PS-II core complex prior to electron transfer leads to large deviations with respect to the calculation without restrictions (Fig. 5.10). These deviations provide additional evidence that the excited state decay in PS-II is not trap-limited. Charge recombination reactions do not play the dominant role for the main decay component of excited states as assumed in the ERPE model. Nevertheless, there is an influence on a longer time scale as seen in Fig. 5.10, where the neglect of charge recombination causes the deviations between the calculated and measured data at 150 ps and longer times.

Including charge recombination removes this deviation (Fig. 5.20) and leads to an additional decay component that is seen in the LFD map in Fig. 5.13 at about 200 ps. This time constant is close to the 180 ps transfer time constant (Holzwarth et al., 2006) assumed in the calculations for the irreversible RP1 → RP3 transfer.

The remaining parameters of the charge recombination model are given in the Fig. 5.20. The minor deviations between the experimental data and the calculations without charge recombination reactions in Figure 5.10 do not allow to determine these parameters faithfully. These values were just adopted from the literature. However, there is an important restriction on the value

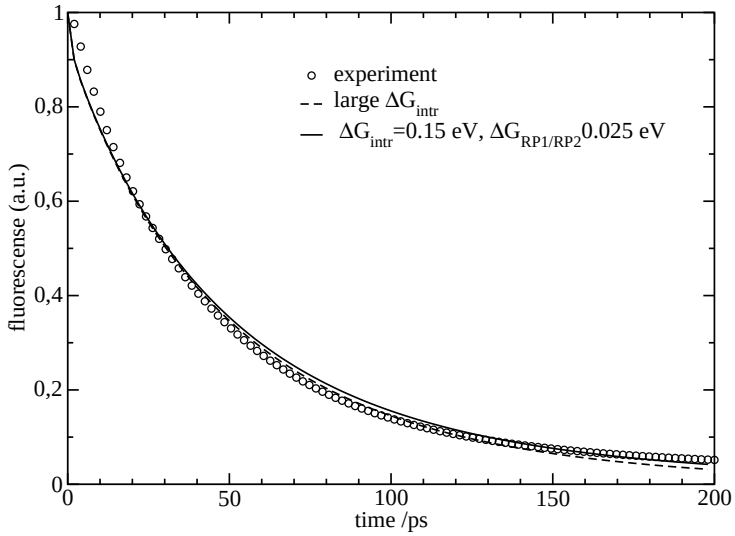

Figure 5.20: Fluorescence decay calculated for open reaction centers with and without including back-electron transfer reactions in comparison to experimental data Miloslavina et al. (2006).

used for the difference in standard free energy $\Delta G^{(0)}$ between the excited state of the RC from which electron transfer starts and the charge separated state RP2=P^+_{D1} $Pheo^-_{D1}$. According to the present calculations, this $\Delta G^{(0)} = \Delta G_{\rm intr} + \Delta G_{\rm RP1/RP2}$ must be about 175 meV or larger in order to avoid significant charge recombination. A significantly smaller $\Delta G^{(0)}$ would slow down the decay of excited states such that the experimental data could not be described without scaling the excitation energy transfer rate constants. The latter were determined from independent experiments and calculations and therefore cannot be adjusted. From measurements of the recombination fluorescence, values for $\Delta G^{(0)}$ of 110 meV (Booth et al., 1990) in D1D2cyt$b$559 complexes and 170 meV (Hillmann et al., 1995a) in PS-II core complexes were reported. The latter is very similar to the present estimate and to the $\Delta G^{(0)} = 170 - 190$ meV determined for the bacterial reaction centers of *Rh. spaeroides* and *Rh. rubrum* (Woodbury et al., 1986).

Although at room temperature the CP43 to RC and the CP47 to RC transfer times are very similar, there are important differences concerning the locations of low energy exciton states in the two antenna subunits. Whereas in CP43 the trap states in the lumenal and the one in the stromal layer are situated close to the RC, i.e. tuned for efficient excitation energy transfer, in CP47 the low-energy trap state at 690 nm at Chl 29 is at a large distance to the RC. The different energetics and locations of the trap states in CP43 and CP47 obtained in the present study can be investigated by low-temperature time resolved spectroscopy. The calculations predict an acceleration of the CP43 to RC transfer at low temperatures and a slowing down of the transfer between CP47 and the RC. The latter should become highly dispersive, as seen in Fig. 5.14. Hence the excited state decay at 77 K, due to the accelerated CP43-RC transfer, should on hand contain a 25 ps time constant (Fig. 5.14) that is smaller than the 40-50 ps observed at room temperature and on the other hand multiple slower components in the sub ns range with a maximum amplitude at around 200 ps, as judged from the maximum of the distribution function of the CP47-to-RC transfer time constant in Fig. 5.14. The antenna trap state at Chl 29 in CP47 is mainly responsible for the slow and dispersive transfer from CP47 to the RC at 77 K, as seen in Fig. 5.15. Due to the localized excited state and the low site energy of Chl 29 the excitation energy is efficiently trapped at this site. At low temperatures, the small thermal energy allows only for a slow uphill transfer of the excitation energy from the excited Chl 29 to the exciton states in the neighborhood. The rate constant for this transfer depends

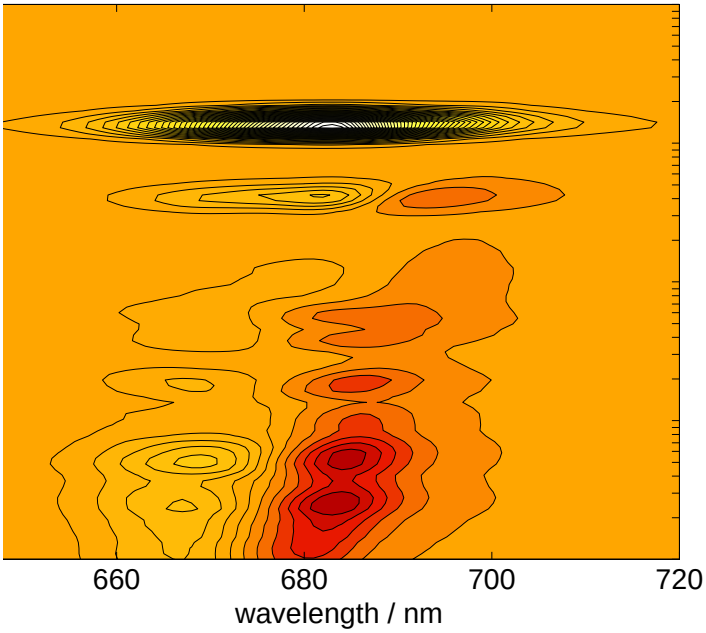

Figure 5.21: Lifetime density map of time-dependent emission of PS-II core complexes with closed RCs, assuming excitation with a 100 fs pulse at 660 nm, T = 300 K.

critically on the energy differences and therefore varies widely for the different realizations of disorder in site energies, explaining the dispersive nature of the transfer.

An about 3 times slower fast component of fluorescence decay in closed RCs (220 ps) compared to open RCs (80 ps) was measured (Schatz et al., 1987). This variable fluorescence for open and closed reaction centers was explained in the ERPE model by assuming that the extra electron on the reduced Q_A slows down the primary electron transfer by a factor of about 6 (Schatz et al., 1988). In the present model, the variable fluorescence is explained by decreasing k_{intr} from $(100\ \mathrm{fs})^{-1}$ in open RCs to $(6\ \mathrm{ps})^{-1}$ in closed RCs, i.e. by a factor of 60. In this case, the primary electron transfer converting an excited state of the RC to a charge separated state takes 18 ps. This time constant now is very similar to those for excitation energy transfer from RC to CP43 (20 ps) and from RC to CP47 (16 ps) (see Fig. 5.12). Hence, an excitation arriving at the RC will be trapped with a probability of one third compared to a probability of almost one for open RCs, explaining the factor three decrease of the fastest time constant in the fluorescence decay for closed RCs seen in the LFD map calculated for closed RCs in Fig. 5.21 compared to that calculated for open RCs in Fig. 5.13.

Because of the smaller trapping probability in closed RCs, excitation energy can be exchanged between CP43 and CP47 via the RC, a process that is not possible for open RCs. As the LFD map calculated without electron transfer in the left part of Fig. 5.13 shows, this transfer takes about 40 ps. Indeed this energy transfer component is seen in the LFD map for closed RCs in Fig. 5.21. Hence, the present model predicts, that an energy transfer component with a time constant of 40 ps should appear in the time-dependent emission of PS-II core complexes with closed RCs at room temperature. It is important to note that the time constant detected for the fast fluorescence decay of open RCs has decreased from 80 ps in early experiments (Schatz et al., 1987, 1988) to 40 ps measured recently (Miloslavina et al., 2006). A reason for the discrepancy could be the improved quality of recent PS-II core preparations. It would therefore be helpful to verify whether for recent preparations also a factor of three increase in the time constant for the

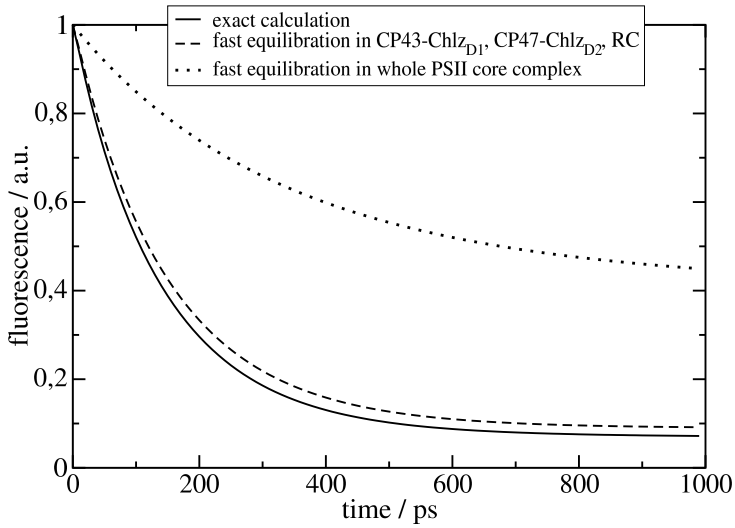

Figure 5.22: Fluorescence decay calculated for PS-II core complexes with closed RC. The solid line shows the exact calculation and the dashed and dotted lines calculations assuming fast exciton equilibration in certain compartments.

fluorescence decay results upon closing the RC. The prediction of the present model, concerning the appearance of a 40 ps energy transfer component, also holds if this factor would be only two.

As for open RCs, also in the case of closed RCs, the decay of excited states in PS-II core complexes can be well described by a three compartment model as shown in Fig. 5.22. However, the decay of excited states is not transfer-to-the trap limited in this case, since the decay is slower by about a factor of three than the excitation energy transfer from CP43 or CP47 to the RC.

Under light stress, when the RC is closed, still about one third of the excitation energy arriving at the RC will be trapped by electron transfer, as discussed above. Since the double reduction of Q_A is a slow process, the charge recombination of $^3[P^+_{D1}\ Pheo^-_{D1}]$ leads to the formation of $^3Chl_{D1}$ and $^3P_{D1}$. Because of the high oxidative power of the Chls in the RC, no carotenoids are located in their vicinity that could quench the physiologically harmful triplet energy. Instead, in the RC the latter is quenched by Q_A^- (van Mieghem et al., 1995; Noguchi, 2002). The present study suggests that Q_A^-, in addition, redirects the excitation energy back to the antennae with the same goal, namely, the quenching of triplet energy. Chl 29, that has the lowest site energy in the PS-II core complex and is in van der Waals contact with a carotenoid, can be expected to play an important role in this photoprotective process. The importance of Chl 29 for the function of PS-II is also evident from the fact that upon mutation of its axial ligand His B114 to Tyr, PS-II activity is lost (Shen et al., 1994).

Chapter 6

Summary

The aim of this work was to find answers for the following questions: what is the primary electron donor in PS2 and what is the *bottleneck* for the decay of excited states? These two questions triggered additional questions:

- What are the values of the site energies of the pigments in PS2?
- On which pigment(s) does the triplet state stabilize in the RC?
- On which pigment(s) of the RC does the hole stabilize after charge separation?
- What is the identity of the excitation energy trap states in the antenna complexes CP43 and CP47?
- Why is energy relaxation after light excitation in the CP43 complex about five times faster than in the CP47 complex at low temperatures?
- Is it possible to describe the spectroscopic properties of PS2 from different species with the same set of parameters?

A genetic algorithm was used to obtain the site energies of the RC pigments in D1-D2-cyt$b559$ complexes. These parameters were further used for a description of several independent experiments performed on the same complex. The site energies obtained, are almost symmetric in the two branches, except for the one of $\mathrm{Chl_{D1}}$, the latter being lower by about 30 meV than the one of its D2-counterpart $\mathrm{Chl_{D2}}$. The lowest exciton state of the RC is dominated by the excited state of $\mathrm{Chl_{D1}}$, which has the lowest site energy of all reaction center pigments. The same procedure was applied to the antenna complexes CP43 and CP47. The lowest exciton state in PS2 core complexes is dominated by Chl29 of the CP47 complex. In the CP43 complex two low-energy exciton states were found, allowing the identification of the low-energy trap states.

From the calculations of T-S spectra of the D1-D2-cyt$b559$ complex at different temperatures strong evidence was obtained for the stabilization of the triplet state at $\mathrm{Chl_{D1}}$ at low temperatures and a thermal distribution of the triplet energy between $\mathrm{P_{D1}}$ and $\mathrm{Chl_{D1}}$ at higher temperatures. An energy difference of 10 meV was obtained for the two triplet states, $^3\mathrm{P_{D1}}$ and $^3\mathrm{Chl_{D1}}$. Based on the assignment of the site energies for D1-D2-cyt$b559$ complexes, several independent experiments performed on PS2 core complexes were described. Calculation of the difference absorption spectra of PS2 core complexes clearly show that after primary charge separation the hole stabilizes at $\mathrm{P_{D1}}$. From the calculations of T-S difference spectra at different temperatures strong evidence is given for the stabilization of the triplet state at $\mathrm{Chl_{D1}}$ at low temperatures and a thermal distribution between $\mathrm{P_{D1}}$ and $\mathrm{Chl_{D1}}$ at higher temperatures. An energy difference of 11 meV was obtained between the two triplet states, $^3\mathrm{P_{D1}}$ and $^3\mathrm{Chl_{D1}}$ in PS2

core complexes which is practically identical to the energy difference in D1-D2-cyt$b559$ complexes.

Using a simple model for primary electron transfer a measured temperature dependence of the fast phase can only be explained if Chl_{D1} is assumed to be the primary electron donor in PS2.

The site energy of Chl_{D1} is even more red shifted in PS2 core complexes than in D1-D2-cyt$b559$ complexes. Additionally to the temperature dependence of the site energy of Chl_{D1}, also the site energy of P_{D1} shows such a dependence. The lowest excited state is strongly localized on Chl_{D1} and consequently primary electron transfer at low temperatures starts from this pigment, as discussed above for D1-D2-cyt$b559$ complexes. At physiological temperatures the energy gap between the lowest excited state dominated by Chl_{D1} and the "special pair" is reduced from 10 nm at 5K to 6 nm. At room temperature, after exciton equilibration different local excited states are populated. Nevertheless still the dominant contribution comes from Chl_{D1}, which is twice as large as that of P_{D1}, making it likely that also at room temperature the primary charge separation is initiated from Chl_{D1}.

A set of site energies was provided that describes the stationary and time- resolved spectra of the CP43 and CP47 subunits of PS2. In particular, the low-energy trap states in these subunits were identified, which are important for light-harvesting and photo-protection, because they determine the direction of excitation energy flow and the sites where Chl triplet states form under light stress. On this basis, the decay of excited states in PS2 core complexes was modeled. The main 40-50 ps decay component of excited states measured at room temperature can only be described by assuming that the primary electron transfer is ultrafast ($(300fs)^{-1}$ corresponding to an intrinsic rate constant of $(100fs)^{-1}$) and that the free energy difference between the equilibrated exciton states in the RC and the second radical pair state is about 175 meV or larger, so that charge recombination reactions are slow. The calculations demonstrate clearly that the *bottleneck* for the decay of excited states in PS-II core complexes with open RCs is due to the transfer from the CP43 and CP47 subunits to the RC, i.e. the decay is transfer-to-the-trap limited. The kinetics of the PS2 is summarized in Fig. 6.1 where the minimal three compartment model is shown, that is inferred in the present work, with the resulting excitation energy and primary electron transfer time constants.

Evidence is presented that the parameters used for the description of the spectra of *T. elongatus* describe as well the spectroscopic properties of different species. Small variations of the site energy of Chl_{D1} were observed in such cases.

The present model suggests a mode switch from a light harvesting mode for open RCs to a photoprotective mode for closed RCs. For the latter, the rate constant for primary electron transfer slows down to an extent that it becomes comparable to the rate for excitation energy transfer from the RC to the core antennae. In this case a considerable part of the excitation energy of the reaction center will return to the antennae and the triplet energy of chlorophyll can be quenched by the carotenoids there. The overall design principle seems to be a RC that is higher in free energy than the antenna, giving rise to fast exit channels for the excitation energy, that are activated only when the RC is closed. This principle is a compromise between high energy transfer efficiency and photochemical stability of the system.

The following predictions of the present model can be tested by experiments: (i) The main decay component of the fluorescence changes from 40-50 ps at room temperature to 25 ps at 77 K, reflecting faster transfer from CP43 to the RC. In addition, a wide distribution of transfer times with a maximum at 200 ps appears at 77 K, reflecting slower and highly dispersive transfer from CP47 to the RC. (ii) The fluorescence decay for closed RCs at room temperature contains a 40 ps excitation energy transfer component that is due to transfer between CP43 and CP47 via the RC.

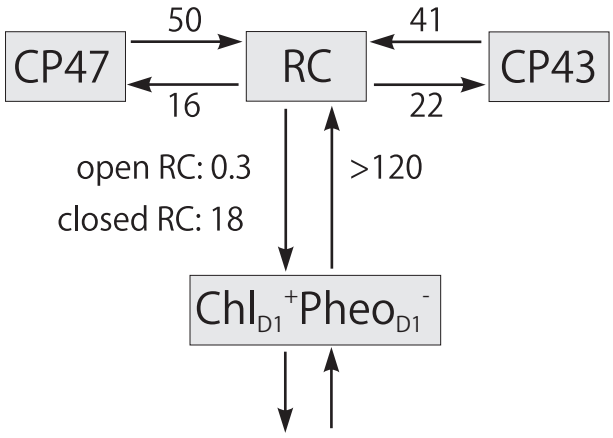

Figure 6.1: Summary of disorder averaged excitation energy transfer and primary charge transfer time constants (in units of ps) obtained in the present model. The excitation energy transfer time constants were obtained in the three compartment model, T = 300 K.

Summarizing, the proposed model fully explains the spectroscopic properties of the PS2 core complexes and its subunits as it was shown by a description of a large number of independent experiments. Moreover the model has predictive power, which was demonstrated for the mutant studies of the $Q_A^- - Q_A$ spectra. The predictive power can be further tested as proposed above. The site energies obtained for the RC pigments of *T. elongatus* can be used to explain spectroscopic properties of PS2 core complexes of different species, not only bacteria but also higher plants, as it was shown for $Q_A^- - Q_A$ spectra of pea and spinach and mutant studies of *Synechocystis*. The present calculations clearly show that Chl_{D1} is the primary electron donor in PS2 and that the decay of the excited states is limited by the excitation energy transfer from the antenna complexes CP43 and CP47 to the RC.

Chapter 7

Zusammenfassung

Das Ziel dieser Arbeit war, Antworten auf die folgenden Fragen zu finden: Was ist der primäre Elektronen-Donator im Photosystem 2 (PS2) und was ist der *Engpass* für den Zerfall von Anregungszuständen? Diese beiden Fragen geben Anlass zu weiteren Fragen:

- Welche Werte haben die lokalen Übergangsenergien der Pigmente im PS2?
- Auf welchem Pigment (welchen Pigmenten) stabilisiert sich der Triplettzustand im Reaktionszentrum (RZ)?
- Auf welchem Pigment (welchen Pigmenten) des Reaktionszentrums stabilisiert sich das Loch nach der Ladungstrennung?
- Welche Identität haben die Anregungsenergie-Senken in den Antennen-Komplexen CP43 und CP47?
- Warum ist bei tiefer Temperatur die Energie-Relaxation nach Lichtanregung im CP43-Komplex etwa fünfmal schneller als im CP47-Komplex?
- Ist es möglich die spektralen Eigenschaften von PS2-Komplexen verschiedener Arten mit dem gleichen Parametersatz zu beschreiben?

Ein genetischer Algorithmus wurde benutzt um die lokalen Übergangsenergien der RZ-Pigmente in D1-D2-cyt$b$559-Komplexen zu erhalten. Diese Parameter wurden im weiteren zur Beschreibung verschiedener unabhängiger Experimente an dem gleichen Komplex benutzt. Die erhaltenen Übergangsenergien sind annähernd symmetrisch für die beiden Äste, mit Ausnahme der von $\mathrm{Chl_{D1}}$, welche rund 30 meV niedriger ist als die Übergangsenergie ihres Gegenübers im D2-Ast, $\mathrm{Chl_{D2}}$. Der niedrigste Anregungszustand des Reaktionszentrums wird bestimmt durch den angeregten Zustand von $\mathrm{Chl_{D1}}$, welcher die niedrigste Übergangsenergie von allen RZ-Pigmenten hat. Das gleiche Verfahren wurde auf die Antennenkomplexe CP43 und CP47 angewendet. Der niedrigste Anregungszustand im PS2-*core*-Komplex wird bestimmt durch das Chl-29 des CP47-Komplexes. Im CP43-Komplex wurden zwei niedrig-energetische Anregungszustände gefunden, welche die Identifikation der Energie-Senke ermöglichen.

Berechnungen von T−S-Spektren des D1-D2-cyt$b$559-Komplexes für verschiedene Temperaturen wiesen überzeugend darauf hin, dass der Triplettzustand sich bei niedriger Temperatur auf $\mathrm{Chl_{D1}}$ stabilisiert, und sich bei höherer Temperatur thermisch auf $\mathrm{P_{D1}}$ und $\mathrm{Chl_{D1}}$ verteilt. Für die beiden Triplettzustände $^3\mathrm{P_{D1}}$ und $^3\mathrm{Chl_{D1}}$ wurde eine Energiedifferenz von 10 meV berechnet. Auf der Zuordnung der Übergangsenergien für den D1-D2-cyt$b$559-Komplex basierend, wurden verschiedene unabhängige Experimente am PS2-*core*-Komplex beschrieben. Die Berechnung des Absorptions-Differenzspektrums des PS2-*core*-Komplexes zeigt klar, dass sich das Loch nach der

primären Ladungstrennung auf P_{D1} stabilisiert. Berechnungen von T−S-Differenzspektren für verschiedene Temperaturen weisen stark darauf hin, dass sich der Triplettzustand bei niedrigen Temperaturen auf Chl_{D1} stabilisiert, und bei höheren Temperaturen thermisch auf P_{D1} und Chl_{D1} verteilt. Für die beiden Triplettzustände $^3P_{D1}$ und $^3Chl_{D1}$ des PS2-*core*-Komplexes ergab sich eine Energiedifferenz von 11 meV, was praktisch identisch mit der Energiedifferenz im D1-D2-cyt*b*559-Komplex ist.

Unter Verwendung eines einfachen Modells für den primären Elektronentransfer kann die gemessene Temperaturabhängigkeit der schnellen Phase nur erklärt werden, wenn angenommen wird, dass Chl_{D1} der primäre Elektronen-Donator im PS2 ist.

Die Übergangsenergie von Chl_{D1} ist im PS2-*core*-Komplex sogar stärker rot-verschoben als im D1-D2-cyt*b*559-Komplex. Nicht nur die Übergangsenergie von Chl_{D1} ist temperaturabhängig, sondern auch die von P_{D1}. Der niedrigste Anregungszustand ist stark lokalisiert auf Chl_{D1}, daher beginnt der primäre Elektronentransfer bei tiefen Temperaturen an diesem Pigment, wie zuvor schon für den D1-D2-cyt*b*559-Komplex diskutiert wurde. Bei physiologischen Temperaturen reduziert sich die Energiedifferenz zwischen dem niedrigsten Anregungszustand, bestimmt durch Chl_{D1}, und dem "*special pair*" von 10 nm (bei 5 K) auf 6 nm (bei 300 K). Bei Raumtemperatur sind nach Äquilibrierung der Anregungsenergie die lokalen Anregungszustände aller RZ-Pigmente besetzt. Dennoch kommt der dominante Beitrag immer noch von Chl_{D1}, welcher doppelt so groß ist wie der von P_{D1}, was es wahrscheinlich macht, dass auch bei Raumtemperatur die primäre Ladungstrennung von Chl_{D1} ausgeht.

Ein Satz von Übergangsenergien wurde bestimmt, der die stationären and zeitaufgelösten Spektren der PS2-Untereinheiten CP43 und CP47 beschreibt. Insbesondere die Energie-Senken dieser Untereinheiten wurden identifiziert. Diese sind wichtig für Lichtsammlung und Lichtschutz, weil sie sowohl die Richtung des Anregungsenergieflusses bestimmen, als auch die Stellen, an denen sich Chl-Triplettzustände bilden, wenn Licht-Stress herrscht. Darauf basierend wurde der Zerfall der Anregungszustände im PS2-*core*-Komplex modelliert. Die Hauptzerfallskomponente (40-50 ps) der Anregungszustände, gemessen bei Raumtemperatur, kann nur unter der Annahme erklärt werden, dass der primäre Elektronentransfer ultraschnell ist (100 $(fs)^{-1}$) und die freie-Energie-Differenz zwischen den äquilibrierten Anregungszuständen im RZ und dem zweiten Radikalpaar-Zustand ungefähr 175 meV oder größer ist, so dass die Ladungs-Rekombinationsreaktionen langsam ablaufen. Die Berechnungen zeigen klar, dass der Energietransfer von den Untereinheiten CP43 und CP47 zum RZ den Engpass für den Zerfall der Anregungszustände im PS2-*core*-Komplex mit geöffnetem RZ darstellt. Die primäre Ladungs- und Energietransferkinetik des PS2-Komplexes ist in Abbildung 6.1 zusammenfassend dargestellt. In dieser Abbildung ist das minimale kinetische Modell, das in der vorliegenden Arbeit abgeleitet wurde, mit den resultierenden Anregungsenergien und Zeitkonstanten des primären Elektronentransfers, gezeigt.

Es wurde gezeigt, dass die Parameter, die für die Beschreibung der Spektren von *T. elongatus* benutzt wurden, ebenfalls die Eigenschaften der Spektren verschiedener anderer Spezies beschreiben. In diesen Fällen wurden kleine Variationen der Übergangsenergie von Chl_{D1} beobachtet.

Das aktuelle Modell legt ein Umschalten vom Lichtsammel-Modus bei offenem RZ in einen Lichtschutz-Modus bei geschlossenem RZ nahe. Für letzteren reduziert sich die Ratenkonstante für primären Elektronentransfer auf eine Größe, die vergleichbar ist mit der Rate des Anregungsenergietransfers vom RZ zu den *core*-Antennen. In diesem Fall wird ein beträchtlicher Anteil der Anregungsenergie des RZ zu den Antennen zurückkehren und die Triplett-Energie des Chlorophylls kann durch die Karotinoide in den Antennen gelöscht werden. Das Bauprinzip scheint ein RZ mit höherer freier Energie als die der Antennen vorzusehen, was zur Folge hat, dass es schnelle Ausgangskanäle für die Anregungsenergie gibt, welche nur aktiv sind, wenn das RZ geschlossen ist. Dieses Prinzip ist ein Kompromiss zwischen hoher Effizienz des Energi-

etransfers und photochemischer Stabilität des Systems.

Die folgenden Vorhersagen des gegenwärtigen Modells können durch Experimente überprüft werden: (i) Die Hauptzerfallskomponente der Fluoreszenz ändert sich von 40-50 ps bei Raumtemperatur auf 25 ps bei 77 K, was den schnelleren Transfer von CP43 zum RZ wiederspiegelt. Zusätzlich tritt bei 77 K eine breite Verteilung mit einem Maximum bei 200 ps auf, welche den langsameren und stark dispersiven Transfer von CP47 zum RZ wiedergibt. (ii) Der Fluoreszenz-Zerfall bei geschlossenem RZ und Raumtemperatur enthält einen 40 ps Anregungenergietransfer-Beitrag, infolge des Transfers zwischen CP43 und CP47 über das RZ.

Zusammenfassend kann gesagt werden, dass das vorgeschlagene Model die spektralen Eigenschaften des PS2-*core*-Komplexes und seiner Untereinheiten vollständig erklärt, wie durch die Beschreibung einer großen Anzahl von unabhängigen Experimenten gezeigt wurde. Darüberhinaus ist das Modell vorhersagefähig, wie anhand der Mutanten-Studie der $Q_A^- - Q_A$-Spektren gezeigt wurde. Die Vorhersagekraft kann überprüft werden wie oben vorgeschlagen. Die Übergangsenergien, die für die RZ-Pigmente von *T. elongatus* erhalten wurden, können verwendet werden um die Eigenschaften der Spektren des PS2-*core*-Komplexes verschiedener Spezies zu erklären, und zwar nicht nur von Bakterien, sondern auch von höheren Pflanzen, wie anhand der $Q_A^- - Q_A$-Spektren von Erbsen und Spinat, sowie Mutanten-Studien an *Synechocystis* gezeigt wurde. Die vorliegenden Rechnungen zeigen deutlich, dass Chl_{D1} der primäre Elektronendonor im PS2-Komplex ist, und dass der Zerfall der Anregungszustände limitiert ist durch den Anregungsenergietransfer von den Antennenkomplexen CP43 und CP47 zum Reaktionszentrum.

Bibliography

Adolphs, J., and T. Renger. 2006. How proteins trigger excitation energy transfer in the FMO complex of green sulfur bacteria. *Biophys. J.* 91:2778–2797.

Adolphs, J., F. Müh, M. E. Madjet, and T. Renger. 2007. Calculation of Pigment Transition Energies in the FMO Protein: From Simplicity to Complexity and Back. *Photosynth. Res.* in press.

Adolphs, J.; Müh, F.; Madjet, M. E.; Renger, T. *Photosynth. Res.* **2008**, *95*, 197.

Alfonso, M.; Montoya, G.; Cases, R.; Rodriguez, R.; Picorel, R. *Biochemistry* **1994**, *33*, 10494.

Andrizhiyevskaya, E. G.; Frolov, D.; van Grondelle, R.; Dekker, J. P. *Phys. Chem. Chem. Phys.* **2004**, *6*, 4810.

Årsköld, S. P, M. V. Masters, B. J. Prince, P. J. Smith, R. J. Pace and E. Krausz. 2003. Optical Spectra od Syneochocystis and Spinach Photosystem II Preparations at 1.7K: Identification of the D1–Pheophytin Energies and Stark Shifts. *J. AM. CHEM. SOC.* 125:13063–12074

Barber, J. 1994. Molecular basis of the vulnerability of photosystem ii to damage by light. *Aust. J. Plant Physiol.* 22:201–208.

Barter, L. M. C.; Bianchietti, M.; Jeans, C.; Schilstra, M. J.; Hankamer, B.; Diner, B. A.; Barber, J.; Durrant, J. R.; Klug, D. R. *Biochemistry* **2001**, *40*, 4026.

Barter, L. M. C., J. R. Durrant, and D. R. Klug. 2003. A quanititative structure-function relationship for the photosystem II reaction center: Supermolecular behavior in natural photosyntesis. *Proc. Natl. Acad. Sci. USA*. 100:946–951.

Bayliss, N. S. 1950. The effect of the electrostatic polarization of the solvent on electronic absorption spectra in solution. *J. Chem. Phys.* 18:292–296.

Biesiadka, J., B. Loll, J. Kern, K. D. Irrgang, and A. Zouni. 2004. Crystal structure of cyanobacterial photosystem II at 3.2 Å resolution: a closer look at the Mn-cluster. *Phys. Chem. Chem. Phys.* 6:4733–4736.

J. Biesiadka, private communication.

Booth, P. J.; Crystall, B.; Giorgi, L. B.; Barber, J.; Klug, D. R.; Porter, G. *Biochim. Biophys. Acta* **1990**, *1016*, 141.

van Brederode, M. E., M. R. Jones, F. van Mourik, I. H. M. van Stokkum, and R. van Grondelle. 1997. A New Pathway for Transmembrane Electron Transfer in Photosynthetic Reaction Centers of *Rhodobacter sphaeroides* Not Involving the Excited Special Pair. *Biochemistry.* 36:6855–6861.

van Brederode, M. E., M. E. van Brederode, and R. van Grondelle. 1999. New and unexpected routes for ultrafast electron transfer in photosynthetic reaction centers. *FEBS Lett.* 455:1–7.

van Brederode, M. E., F. van Mourik, I. H. M. van Stokkum, M. R. Jones, and R. van Grondelle. 1999. Multiple pathways for ultrafast transduction of light energy in the photosynthetic reaction center of *rhodobacter sphaeroides*. *Proc. Natl. Acad. Sci. USA*. 96:2054–2059.

Broess, K.; Trinkunas, G.; van der Wei-de Wit, C. D.; Dekker, J. P.; van Hoek, A.; van Amerongen, H.; *Biophysical J.* **2006**, *91*, 3776.

Buser, C. A., B. A. Diner, and G. W. Brudvig. 1992. Photooxidation of cytochrome *b*559 in oxygen-evolving photosystem ii. *Biochemistry* 31:11449–11459.

Chang, J. C. 1977. Monopole effects on electronic excitation interactions between large molecules. I. Application to energy transfer in chlorophylls. *J. Chem. Phys.* 67:3901–3904.

Creemers, T. M. H., C. A. De Caro, R. W. Visschers, R. van Grondelle, and S. Völker. 1999. Spectral Hole Burning and Fluorescence Line Narrowing in Subunits of the Light-Harvesting Complex LH1 of Purple Bacteria. *J. Phys. Chem. B.* 103:9770–9776.

Dashdorj, N., W. Xu, P. Martinsson, P. R. Chitnis, and S. Savikhin. 2004. Electrochromic shift of chlorophyll absorption in photosystem i from *synechocystis* sp. pcc 6803: A probe of optical and dielectric properties around the secondary electron acceptor. *Biophys. J.* 86:3121–3130.

Dekker, J. P., and R. van Grondelle. 2000. Primary charge separation in photosystem II. *Photosynth. Res.* 63:195–208.

Diner, B. A., and F. Rappaport. 2002. Structure, dynamics, and energetics of the primary photochemistry of photosystem II of oxygenic photosysnthesis. *Annu. Rev. Plant Biol.* 53:551–580.

Diner, B. A., E. Schlodder, P. J. Nixon, W. J. Coleman, F. Rappaport, J. Laverge, W. F. J. Vermaas, and D. A. Chisholm. 2001. Site-directed mutations at D1-His198 and D2-His197 of photosystem II in *synechosystis* PCC 6803: sites of primary charge separation and cation and triplet stabilization. *Biochemistry.* 40:9265–9281.

Doer67 Doering, G., H. H. Stiel, and H. T. Witt. 1967. A second chlorophyll reaction in the electron chain of photosynthesis-registration by the repetitive excitation technique. *Z. Naturforsch.* 22:639–644.

Van Dorsson, R. J.; Plijter, J. J.; Dekker, J. P.; Den Ouden, A.; Amesz, J. *Biochim. Biophys. Acta* **1987**, *890*, 134.

Durrant, J. R., L. B. Giorgi, J. Barber, D. R. Klug, and G. Porter. 1990. Characterization of triplet states in isolated photosystem II reaction centres: oxygen quenching as a mechanism for photodamage. *Biochemistry.* 42:9205–9213.

Durrant, J. R., G. Hastings, D. M. Joseph, J. Barber, G. Porter, and D. R. Klug. 1992. Subpicosecond equilibration of excitation energy in isolated photosystem II reaction centers. *Proc. Natl. Acad. Sci. USA.* 89:11632–11636.

Durrant, J. R., D. R. Klug, S. L. S. Kwa, R. van Grondelle, G. Porter, and J. P. Dekker. 1995. A mulitmer model for P680, the primary electron donor of photosystem II. *Proc. Natl. Acad. Sci. USA.* 92:4798 4802.

Eccles, J., and B. Honig. 1983. Charged amino-acids as spectroscopic determinants for chlorophyll *in vivo*. *Proc. Natl. Acad. Sci. USA* 80:4959–4962.

Fenimore, P. W., H. Frauenfelder, B. H. McMahon, and R. D. Young. 2004. Bulk-solvent and hydration-shell fluctuations, similar to α- and β-fluctuations in glasses, control protein motions and functions . *Proc. Natl. Acad. Sci. USA*. 101:14408–14413.

Ferreira, K. N., T. M. Iverson, K. Maghlaoui, J. Barber, and S. Iwata. 2004. Architecture of photosynthetic oxygen-evolving center. *Science*. 303:1831–1838.

Fetisova, Z., A. Freiberg, K. Mauring, V. Novoderezhkin, A. Taisova, and K. Timpmann. 1996. Excitation energy transfer in chlorosomes of green bacteria: theoretical and experimental studies. *Biophys. J.* 71:995–1010.

Förster T. *Ann. Phys.* **1948**, *2*, 55.

Frese, R. N., M. Germano, F. L. de Weerd, I. H. M. van Stokkum, A. Y. Shuropatov, V. A. Shuvalov, H. J. van Gorkom, R. van Grondelle, and J. P. Dekker. 2003. Electric field effects on the chlorophylls, pheophytins, and β-carotens in the reaction center of photosystem II. *Biochemistry*. 42:9205–9213.

Germano, M., A. Y. Shkuropatov, H. Permentier, R. A. Khatypov, V. A. Shuvalov, A. J. Hoff, and H. J. van Gorkom. 2000. Selective replacment of the active and inactive pheophytion in reaction centers of photosystem II by 13^1-deoxo-13^1-hydroxy-pheophytin *a* and comparison of their 6 K absorption spectra. *Photosyn. Res.* 64:189–198.

Germano, M., A. Y. Shkuropatov, H. Permentier, R. Wijn de, A. J. Hoff, V. A. Shuvalov, and H. J. van Gorkom. 2001. Pigment organization and their interactions in reaction centers of photosystem II: optical spectroscopy at 6K of reaction centers with modified pheophytin composition. *Biochemistry*. 40:11472–11482.

Greenfield, S. R., M. Seibert, Govindjee, and M. R. Wasielewski. 1997. Direct measurments of the effective rate constant for primary charge separation in isolated photosystem II reaction centers. *J. Phys. Chem. B*. 101:2251–2255.

Greenfield, S. R., M. Seibert, Govindjee, and M. R. Wasielewski. 1999. Time-resolved absorption changes of the pheophytin Q_x band in isolated photosystem II Towards complete cofactor arrangement in the 3.0 Å resolution structure of photosystem IIeaction centers at 7 K: energy transfer and charge separation. *J. Phys. Chem. B*. 103:8364–8374.

Groot, M. L., E. J. G. Peterman, P. J. M. van Kan, I. H. M. van Stokkum, , J. P. Dekker, and R. van Grondelle. 1994. Temperature–Dependent Triplet and Fluorescence Quantum Yields of the Photosystem II Reaction Center Described in a Thermodynamic Model. *Biophys. J.* 67:318–330.

Groot, M. L., Peterman, E. J. G., van Stokkum, I. H. M., Dekker, J. P., van Grondelle, R. 1995. Triplet and fluorescing states of the CP47 antenna complex of photosystem II studied as a function of temperature. *Biophys. J.* 68:281–290

Groot, M. L., J. P. Dekker, , R. van Grondelle, F. T. H. Den Hartog, and S. Völker. 1996. Energy Transfer and Trapping in Isolated Photosystem II Reaction Centers of Green Plants at Low Temperature. A Study by Spectral Hole Burning. *J. Phys. Chem.* 100:11488–11495.

Groot, M., F. van Mourik, C. Eijckelhoff, I. H. M. van Stokkum, J. P. Dekker, and R. van Grondelle. 1997. Charge separation in the reaction center of photosystem II studied as a function of temperature. *Proc. Natl. Acad. Sci. USA*. 94:4389–4394.

Groot, M. L., R. N. Frese, F. L. de Weerd, K. Bromek, Å. Pettersson, E. J. G. Petwrman, I. H. M. van Stokkum, R. van Grondelle and J. P. Dekker. 1999. Spectroscopic Properties of the CP43 Core Antenna Protein of Photosystem II. *Biophys. J.* 77:3328–3340.

Groot, M.-L.; Pawlowicz, N. P.; Van Wilderen, L. J. G. W.; Breton, J.; Van Stokkum, I. H. M.; van Grondelle, R. Initial electron donor and acceptor in isolated photosystem II reaction centers identified with femtosecond mid-IR spectroscopy. *Proc. Natl. Acad. Sci. USA* 102:13087–13092.

Heinz, H., U. W. Suter, and E. Leontidis. 2001. Simple and accurate computations of solvatochromic shifts in $\pi \rightarrow \pi^*$ transitions of aromatic chromophores. *J. Am. Chem. Soc.* 123:11229–11236.

Hillmann B.,K. Brettel, F. van Mieghem, A. Kamowski, A. W. Rutherford and E. Schlodder. 1995 Charge Recombination Reaction in Photosystem II. 2. Transient Absorbance Difference Spectra and Their Temperature Dependence. *Biochemistry* 34:4814–4827

Hillmann, B.; Moya, I.; Schlodder, E. *in Photosynthesis: from Light to Biosphere*, Proc. X Int. Congr. Photosynthesis (1995), (Mathis, P. ed.), Vol. 1, pp. 603-606, Kluwer Academic Publishers, Dodrecht.

Holzwarth, A. R., M. G. Müller, M. Reus, M. Nowaczyk, J. Sander and M. Rögner 2006 Kinetics and mechanism of electron transfer in intect photosystem II and in the isolated reaction center: Pheophytin is the primary electron donor. *Proc. Natl. Acad. Sci. USA*. 103:6895–6900.

Huber, H., M. Meyer, H. Scheer, W. Zinth, and J. Wachtveitl. 1998. Temperature dependence of the primary electron transfer reaction in pigment-modified bacterial reaction centers. *Photos. Res.* 55:153–162.

Hughes, J. L., R. Picorel, M. Seibert and E. Krausz 2006 Photophysical Behavor and Assigment of the Low-Energy Chlorophyll States in the CP43 Proximal Antenna Protein of Higher Plant Photosystem II. *Biochemistry* 45:12345–12357

Ishikita, H., W. Saenger, J. Biesiadka, B. Loll, and E.-W. Knapp. 2006. How photosynthetic reaction centers control oxidation power in chlorophyll pairs P680, P700, and P870. *Proc. Natl. Acad. Sci. USA* 103:9855–9860.

Jang, S.; Newton, M. D.; Silbey, R. J. *Phys. Rev. Lett.* **2004**, *92*, art. no. 218301.

Jankowiak, R., M. Ratsep, M. Picorel, M. Seibert, and S. G. J. 1999. Excited states of the 5-chlorophyll photosystem II reaction center. *J. Phys. Chem. B.* 103:9759–9769.

Jankowiak, R., D. Tang, G. J. Small, and M. Seibert. 1989. Transient and Persistent Hole Burning of the Reaction Center of Photosystem-II. *J. Phys. Chem.* 93:1649–1654.

Jankowiak, R., V. Zazubuvich, M. Rätsep, S. Matsuzaki, M. Alfonso, R. Picorel, M. Seibert and G. J. Small. 2000. The CP43 Core Antenna Complex of Photosystem II Posseses Two Quasi–Degenerate and Weakly Coupled Q_{rmy}–Trap States *J. Phys. Chem. B* 104:11805–11815.

Jennings, R. G.; Elli, G.; Garlaschi, F. M.; Santabarbara, S.; Zucchelli, G. *Photosynth. Res.* **2000**, *66*, 225.

Jordan, P.; Fromme, P.; Witt, H. T.; Klukas, O.; Saenger, W.; Krauss, N. *Nature* **2001**, *411*, 909.

van Kan, P. J. M., S. C. M. Otte, F. A. M. Kleinherenbrink, M. C. Nieveen, T. J. Aartsma, and H. J. van Gorkom. 1990. Time-resolved spectroscopy at 10 K of the Photosystem II reaction center; deconvolution of the red absorption band. *Biochim. Biophys. Acta.* 1020:146–152.

Kamlowski, A., L. Frankemoller, A. van der Est, D. Stehlik, and A. R. Holzwarth. 1996. Evidence for Delocalization of the Triplet State $^3P_{680}$ in the D_1D_2cytb_{559}-Complex of Photosystem II. *Ber. Bunsenges. Phys. Chem.* 100:2045–2051.

Kern, J.; Renger, G. *Photosynth. Res.* **2007**, *94*, 183.

Kim, J. H., J. A. Nemson, and A. Melis. 1993. Photosystem II Reaction Center Damage and Repair in *Dunaliella salina* (Green Alga). *Plant Physiol.* 103:181–189.

Knox, R. S., and B. Q. Spring. 2003. Dipole strengths in the chlorophylls. *Photochem. Photobiol.* 77:497–501.

Konermann, L., and A. R. Holzwarth. 1996. Analysis of the absorption spectrum of photosystem II reaction centers: temperature dependence, pigment assignment and inhomogeneous broadening. *Biochemistry.* 35:829–842.

Konermann, L., I. Yruela, and A. R. Holzwarth. 1997. Pigment Assignment in the Absorption Spectrum of the Photosystem II Reaction Center by Site-Selection Fluorescence Spectroscopy. *Biochemistry.* 36:7498–7502.

Krausz, E., J. L. Hughes, P. Smith, R. Pace and S. Peterson Åsköld. 2005. Oxygen-evolving Photosystem II core complexes: a new paradigm based on the spectral identification of the charge-separating state, the primary acceptor and assigment of low-temperature fluorescence. *Photchem. Photbiol. Sci.* 4:744–753

Krawczyk, S. 1991. Electrochromism of Chlorophyll-a Monomer and Special Pair Dimer. *Biochim. Biophys. Acta.* 1056:64–70.

Kriegl, J. M., and G. U. Nienhaus. 2003. Structural, dynamic, and energetic aspects of long-range electron transfer in photosynthetic reaction centers. *Proc. Natl. Acad. Sci. USA* 101:123–128.

Krüger, B. P., G. D. Scholes, and G. R. Fleming. 2005. Calculation of couplings and energy transfer pathways between pigments of LH2 by the *ab-initio* transition density cube method . *J. Phys. Chem. B* 4:744–753.

Kwa, S. L. S., C. Eijckelhoff, v. Grondelle, and J. P. Dekker. 1994. Site-Selection Spectroscopy of the Reaction Center Complex of Photosystem II. 1. Triplet-minus-Singlet Absorption Difference: Search for a Second Exciton Band of P-680†. *J. Phys. Chem.* 98:7702–7711.

Lax, M. 1952. The Franck-Condon Principle and Its Application to Crystals. *J. Chem. Phys.* 20:1752.

Leegwater, J. A., J. R. Durrant, and D. R. Klug. 1998. Exciton equilibration induced by phonons: Theory and application to PS II . *J. Phys. Chem. B* 102:5378–5386.

Leeson, D. T., and D. A. Wiersma. 1995. Real time observation of low-temperature protein motions. *Phys. Rev. Lett.* 74:2138–2141.

Lockhart, D. J., and P. S. Kim. 1992. Internal Stark effect measurement of the electric field at the amino terminus of an α helix. *Science* 257:947–951.

Longuet-Higgens, H. C., and J. A. Pople. 1957. Electronic spectral shifts of nonpolar molecules in nonpolar solvents. *J. Chem. Phys.* 27:192–194.

Loll, B., Kern, J., Saenger, W., and Biesiadka, J. Towards complete cofactor arrangement in the 3.0 Å resolution structure of photosystem II *Nature 2005* 438:1040.

Madjet, M. E., A. Abdurahman, and T. Renger. 2006. Intermolecular Coulomb couplings from *ab initio* electrostatic potentials: Application to optical transitions of strongly coupled pigments in photosynthetic antennae and reaction centers . *J. Phys. Chem. B* 110:17268–17281.

May, V., and O. Kühn. 2000. Charge and Energy Transfer Dynamics in Molecular Systems: A Theoretical Introduction. *Wiley–VCH, Berlin, 2000.* :103–113, 137, 203, 233.

McMahon, B. H., J. D. Müller, C. A. Wraight, and G. U. Nienhaus. 1998. Electron transfer and protein dynamics in the photosynthetic reaction center. *Biophysical J.* 74:2567–2587.

Merry, S. A. P., S. Kumazaki, Y. Tachibana, D. M. Joseph, G. Porter, K. Yoshihara, J. Barber, J. P. Durrant, and D. R. Klug. 1996. Sub-picosecond Equilibration of Excitation Energy in Isolated Photosystem II Reaction Centers Revisited: Time–Dependent Ansisotropy. *J. Phys. Chem.* 100:10469–10478.

Miloslavina, Y., M. Szczepaniak, M. G. Müller, J. Sander, M. Nowaczyk, M. Rögner, and A. R. Holzwarth. 2006. Charge separation kinetics in intact photosystem ii core particles is trap-limited. a picosecond fluorescence study. *Biochemistry* 45:2436–2442.

van Mieghem, F., K. Brettel, B. Hillmann, A. Kamlowski, A. W. Rutherford, and E. Schlodder. 1995. Charge recombination reactions in photosystem II. 1. Yields, recombination pathways, and kinetics of the primary pair. *Biochemistry.* 34:4789–4813.

van Mieghem, F. J. E., K. Satoh, and A. W. Rutherford. 1991. A chlorophyll tilted 30° relative to the membrane in the photosystem II reaction center. *Biochim. Bioph. Acta.* 1058:379–385.

Müh, F., F. Lendzian, R. Mason, J. C. Williams, J. P. Alenn, and W. Lubitz. 1985. Pigment-protein interactions in bacterial reaction centers and their influence on oxidation potential and spin density distribution of the primary donor. *J. Phys. Chem. B* 106:3226–3236.

Müh, F., M. E. Madjet, J. Adolphs, A. Abdurahman, B. Rabenstein, H. Ishikita, E.-W. Knapp, and T. Renger. 2007. α-helices direct excitation energy flow in the Fenna-Matthews-Olson protein. *Proc. Natl. Acad. Sci. USA* 104:16862–16867.

Müller, M. G.; Niklas, J.; Lubitz, W.; Holzwarth, A. R. *Biophys. J* **2003**, *85*, 3899.

Mukai, K.; Abe, S.; Sumi, H. *J. Phys. Chem. B* **1999**, *103*, 6096.

Nienhaus, G. U., H. Frauenfelder, and F. Parak. 1991. Structural fluctuations in glass-forming liquids: Mössbauer spectroscopy on iron in glycerol. *Phys. rev. B* 43:3345–3350.

Noguchi, T. 2002. Dual role of triplet localization on the accessory chlorophyll in the photosystem II reaction center: photoprotection and photodamage of the D1 protein. *Plant Cell Physiol.* 43:1112–1116.

Noguchi, T., Y. Inoue, and K. Satoh. 1993. FT-IR studies on the triplet state of P680 in the photosystem II reaction center: triplet equilibrium within a chlorophyll dimer. *Biochemistry.* 32:7186–7195.

Noguchi, T., T. Tomo, and Y. Inoue. 1998. Fourier Transform Infrared Study of the Cation Radical of P680 in the Photosystem II Reaction Center: Evidence for Charge Delocalization on the Chlorophyll Dimer. *Biochemistry.* 37:13614–13625.

Noguchi, T., T. Tomo, and C. Kato. 2001. Triplet formation on a monomeric chlorophyll in the photosystem II reaction center as studied by time-resolved infrared spectroscopy. *Biochemistry.* 40:2176–2185.

Novoderezhkin, V. I., E. G. Andrizhiyewskaya, J. P. Dekker, and R. Van Grondelle. 2005. Pathways and timescales of primary charge separation in the photosystem II reaction center as revealed by a simultaneos fit of time-resolved fluorescence and transient absorption. *Biophys. J.* 89:1464–1481.

Novoderezhkin, V. I., J. P. Dekker, and R. Van Grondelle. 2007. Mixing of Exciton and Charge-Transfer States in Photosystem II reaction Centers: Modeling of Stark Spectra with Modified Redfield Theory. *Biophys. J.* 93:1293–1311.

Ohta, K., M. Yang, and G. R. Fleming. 2001. Ultrafast exciton dynamics of *J*-aggregates in room temperature solution studied by third–order nonlinear optical spectroscopy and numerical simulation based on exciton theory. *J. Chem. Phys.* 115:7609–7621.

Parak, F., E. W. Knapp, and D. Kucheida. 1982. Protein dynamics: Mössbauer spectroscopy on deoxymyoglobin crystals. *J. Mol. Biol.* 161:177–194.

Pawlowicz, N. P.; Groot, M.-L.; Van Stokkum, I. H. M.; Breton, J.; van Grondelle, R. *Biophysical J.* **2007**, *93*, 2732.

Peterman, E. J. G., H. van Amerongen, R. van Grondelle, and J. P. Dekker. 1998. The nature of the excited state of the reaction center of photosystem II of green plants: A high resolution fluorescence spectroscopy study. *Proc. Natl. Acad. Sci. USA.* 95:6128–6133.

Prokhorenko, V., and A. R. Holzwarth. 2000. Primary processes and structure of the photosystem II reaction center: a photon echo study. *J. Phys. Chem. B.* 104:11563–11578.

Rasmussen, B. F., A. M. Stock, D. Ringe, and G. A. Petsko. 1992. Crystalline ribonuclease a loses function below the dynamical transition at 220 k. *Nature* 357:423–424.

Raszewski, G., W. Saenger, and T. Renger. 2005. Theory of optical spectra of Photosystem II reaction centers: Location of the triplet state and the identity of the primary electron donor. *Biophys. J.* 88:986–998.

Raszewski, G.; Diner, B. A.; Schlodder, E.; Renger, T. *submitted.*

Raszewski, G., and T. Renger. 2008. Light-harvesting in photosystem ii core complexes is limited by the transfer to the trap: Can the core complex turn into a photoprotective mode? *J. Am. Chem. Soc.,* in press.

Renger, T.; May, V. *Photochem. Photobiol.* **1997**, *66*, 618.

Renger, T.; May, V.; *J. Phys. Chem. A* **1998**, *102*, 4381.

Renger, T. and V. May. 2000. Simulations of Frequency-Domain Spectra: Structure-Function Relationships in Photosynthetic Pigment-Protein Complexes. *Phys. Rev. Lett.* 84:5228–5231.

Renger, T.; May, V.; Kühn, O. *Phys. Rep.* **2001**, *343*, 138.

Renger, T. and R. A. Marcus. 2002a. On the relation of protein dynamics and exciton relaxation in pigment-protein complexes: an estimation of the spectral density and a theory for the calculation of optical spectra. *J. Chem. Phys.* 116:9997–10019.

Renger, T. and R. A. Marcus. 2002b. Photophysical properties of PS-2 reaction centers and a discrepancy in exciton relaxation times. *J. Phys. Chem. B.* 106:1809–1819.

Renger, T.; Marcus, R. A. *J. Phys. Chem. B* **2002**, *106*, 1809.

Renger, T. and R. A. Marcus. 2003. Variable-range hopping electron transfer through disordered bridge states: application to DNA. *J. Phys. Chem. A.* 107:8404–8419.

Renger, T. 2004. Theory of optical spectra involving charge transfer states: Dynamic localization predicts a temperature dependent optical band shift. *Phys. Rev. Lett.* in press.

Photosystem II: The light-driven water plastoquinone oxidoreductase, T. Wydrzynski, K. Satoh, eds., Springer 2005, Dordrecht.

Renger, T.; Trostmann, I.; Theiss, C.; Madjet, M. E.; Richter, M.; Paulsen, H.; Eichler, H. J.; Knorr, A.; Renger, G. *J. Phys. Chem. B* **2007**, *111*, 10487.

Rigby, S. E. J., J. H. A. Nugent, and P. J. O'Malley. 1994. Endor and special triple resonance studies of chlorophyll cation radicals in photosystem 2. *Biochemistry* 33:10043–10050.

Rutherford, A. W., and P. Faller. 2002. Photosystem ii: evolutionary perspectives. *Phil Trans. R. Soc. Lond. B* 358:245–253.

Schatz, G.H.; Brock, H.; Holzwarth, A. R. *Proc. Natl. Acad. Sci. USA* **1987**, *84*, 8414.

Schatz, G.H.; Brock, H.; Holzwarth, A. R. *Biophys. J* **1988**, *54*, 397.

Scholes, G. D; Fleming, G. R. *J. Phys. Chem. B* **2000**, *104*, 1854.

Shen, G.; Vermaas, W. F. J. *Biochemistry* **1994**, *33*, 7379.

Shkuropatov, A. Y., R. A. Khatypov, V. A. Shkuropatova, M. G. Zvereva, T. G. Owens, and V. A. Shuvalov. 1999. Reaction centers of photosystem II with a chemically-modified pigment composition: exchange of pheophytins with 13^1-deoxo-13^1-hydroxy-pheophytin *a*. *FEBS Lett.* 450:163–167.

Shkuropatov, A. Y., R. A. Khatypov, T. S. Volshchukova, V. A. Shkuropatova, T. G. Owens, and V. A. Shuvalov. 1997. Spectral and photochemical properties of borohydride-treated D1-D2-cytochrome *b*-559 complex of photosystem II. *FEBS Lett.* 420:171–174.

Schlodder, E., T. Renger, G. Raszewski, W. J. Coleman, P. J. Nixon, R. O. Cohen, and B. Diner. 2008. Site-directed mutations at d1-thr179 of photosystem ii in *synechocystis* sp. pcc 6803 modify the spectral properties of the accessory chlorophyll in the d1-branch of the reaction center. *Biochemistry,* in press.

Smith, J., K. Kuczera, and M. Karplus. 1990. Dynamics of myoglobin: Comparison of simulation results with neutron scattering spectra. *Proc. Natl. Acad. Sci. USA* 87:1601–1605.

Steffen, M. A., K. Lao, and S. G. Boxer. 1994. Dielectric asymetry in the photosynthetic reaction center. *Science.* 264:810–816.

Stewart, D. H., Nixon, P. J., Diner, B. A., and Brudvig, G. W. 2000. Assignment of the Q_Y absorbance bands of photosystem II chromophores by low temperature optical spectroscopy of wildtype and mutant reaction centers. *Biochemistry* 39:14583-14594.

Sumi, H. 1999. Theory on Rates of Excitation-Energy Transfer between Molecular Aggregates through Distributed Transition Dipoles with Application to the Antenna System in Bacterial Photosynthesis. *J. Phys. Chem. B.* 103:252–260.

Tang, D., R. Jankowiak, M. Seibert, C. F. Yocum, and G. J. Small. 1990. Excited-State Structure and Energy-Transfer Dynamics of Two Different Preparations of the Reaction Center of Photosystem II: A Hole-Burning Study. *J. Phys. Chem.* 94:6519–6522.

Vacha, F., D. M. Joseph, J. R. Durrant, A. Telfer, D. R. Klug, G. Porter, and J. Barber. 1995. Photochemistry and spectroscopy of a five-chlorophyll reaction center of photosystem II isolated by using a Cu affinity column. *Proc. Natl. Acad. Sci. USA*. 92:2929–2933.

Vacha, F., M. Durchan, and P. Siffel. 2002. Excitonic interactions in the reaction centre of photosystem II studied by using circular dichroism. *Biochim. Bioph. Acta.* 1554:147–152.

Vasilev, S.; Orth, P.; Zouni, A.; Owens, T. G.; Bruce, D. *Proc. Natl. Acad. Sci. USA* **2001**, *98*, 8602.

Vasilev, S.; Lee, C.I.; Brudvig, G. W.; Bruce, D. *Biochemistry* **2002**, *41*, 12236.

Vass, I., S. Styring, T. Hundal, A. Koivuniemi, E.-M. Aro, and B. Andersson. 1991. Reversible and irreversible intermediates during photoinhibition of photosystem ii: Stable reduced q_a promote chlorophyll triplet formation. *Proc. Natl. Acad. Sci. USA* 89:1408–1412.

Gaozhong Shen and Wim F. J. Vermaas. 1994 Mutation of Chlorophyll Ligands in the Chlorophyll-Binding CP47 Protein As Studied in a Synechocystis sp. PCC 6803 Photosystem I-less Background. *Biochemistry.* 33:7379–7388

Vermeglio, A. and Clayton, R. K. 1977. Kinetics of ElectronTransfer Between Primary and SecondaryElectron Acceptor in Reaction Centers from *Rhodopseudomonas Sphaeroides. Biochimica et Biophysica Acta* 46:159–165.

de Weerd, F. L., I. H. van Stokkum, H. van Amerongen, J. P. Dekker and R. van Grondelle. 2002. Pathways for Energy Transfer in the Core Light-Harvesting Complexes CP43 and CP47 of Photosystem II. *Biophys. J.* 82:1586–1507

de Weerd, F. L., M. A. Palacios, E. G. Andrizhiyevskaya, J. P. Dekker and R. van Grondelle. 2002. Identifying the Lowest Electronic States of the Chlorophylls in the CP47 Core Antenna Protein of Photosystem II. *Biochemistry.* 41:15224–15233

Woodbury, N. W., Parson, W. W. *Biochim. Biophys. Acta* **1986**, *850*, 197.

Yang, M.; Fleming, G. R. *Chem. Phys.* **2002**, *275*, 355.

Yang, M.; Damjanovic, A.; Vaswani, H. M.; Fleming, G. R. *Biophys. J.* **2003**, *85*, 140.

Yu, I. S. 1993. Electrodeless measurement of rf dielectric constant and loss. *Meas. Sci. Technol.* 4:344–348.

Zech, S. G., J. Kurreck, H.-J. Eckert, G. Renger, W. Lubitz, and R. Bittl. 1980. Pulsed EPR measurements of the distance between P_{680}^+ and Q_A^- in photosystem II. *Biophys. Chem.* 12:83–91.

Zhang, W. M., T. Meier, V. Chernyak, and S. Mukamel. 1998a. Exciton-migration and three-pulse femtosecond optical spectroscopies of photosynthetic antenna complexes. *J. Chem. Phys.* 108:763–7774.

Zhang, W. M., T. Meier, V. Chernyak, and S. Mukamel. 1998b. Simulation of three-pulse-echo and fluorescence depolarization in photosynthetic aggregates. *Philos. Trans. R. Soc. London, Ser. A*. 356:405–419.

Zollfrank, J., J. Friedrich, J. Vanderkooi, and J. Fidy. 1991. Conformational relaxation of a low-temperature protein as probed by photochemical hole burning. *Biophysical J.* 59:305–312.

Zouni, A., H. T. Witt, J. Kern, P. Fromme, N. Krauss, W. Saenger, and P. Orth. 2001. Crystal structure of photosystem II from *Synechococcus elongatus* at 3.8 Å resolution. *Nature*. 409:739–743.

Appendix

Table 7.1: Coupling in RC

	P_{D2}	Chl_{D1}	Chl_{D2}	$Pheo_{D1}$	$Pheo_{D2}$	$Chlz_{D1}$	$Chlz_{D2}$
P_{D1}	150	-42	-55	-6	17	0	1
P_{D2}		-56	-36	20	-2	1	1
Chl_{D1}			7	46	-4	3	0
Chl_{D2}				-5	37	0	2
$Pheo_{D1}$					3	-4	0
$Pheo_{D2}$						0	-4
$Chlz_{D1}$							0

Table 7.2: Coupling in CP43

	34	35	37	41	42	43	44	45	46	47	48	49
33	-7	0	-2	-3	12	16	1	-9	3	-2	0	1
34		-25	60	1	-6	-8	3	19	-12	10	-6	-1
35			-20	-2	0	-5	-3	-4	-11	-4	13	4
37				2	4	2	6	-2	21	3	-3	4
41					-13	-76	-11	18	-2	-1	1	-4
42						20	10	-25	11	4	-6	9
43							-10	64	-3	-6	24	-24
44								6	56	29	-16	9
45									-50	78	3	-8
46										-59	-9	10
47											-15	9
48												-41

Table 7.3: Coupling in CP47

	12	13	14	15	16	17	21	22	23	24	25	26	27	28	29
11	-49	-12	4	-2	-4	-1	4	-6	-2	-2	3	-2	-1	-2	-1
12		-83	20	5	-6	-5	5	-20	-13	-4	6	-9	-2	4	-2
13			0	-6	-59	-3	-8	32	15	2	-10	4	-2	-1	-3
14				-47	-13	65	5	-11	-6	-1	21	-35	8	-3	0
15					72	-20	-2	1	-5	-3	-6	-7	-4	13	11
16						7	-3	8	-4	6	-4	9	4	1	9
17							0	4	1	6	-2	17	3	-2	2
21								-17	-83	-16	20	-5	-3	3	-1
22									48	99	-16	10	4	-2	6
23										-13	52	0	-6	32	-7
24											-12	56	37	-18	8
25												-64	95	25	2
26													-63	-3	2
27														-12	13
28															-8

Table 7.4: Coupling betwenn RC and CP43

	P_{D1}	P_{D2}	Chl_{D1}	$Pheo_{D1}$	$Chlz_{D1}$
37	-4				8
41	-4	4	8	-10	
43					6
44	4			6	

Table 7.5: Coupling betwenn RC and CP47

	Chl_{D2}	$Pheo_{D2}$	$Chlz_{D2}$
11			-4
12			-5
21	8	-12	-6
23			-7
24		6	

Acknowledgment

Thank You very much

- Thomas Renger for fruitful discussions, understandable explanations, pleasant collaboration and the faithful supervision of my thesis.
- Walter Knapp for hosting me in his group.
- Jacek Biesiadka, Bernhard Loll and Wolfram Saenger for providing crystal structure of Photosystem II prior to publication and for helpful discussions.
- All members of AG Knapp/Renger for their assistance and help.

Publications

Raszewski G and Renger T. 2008. Light harvesting in photosystem II core complexes is limited by the transfer to the trap: Can the core complex turn into a photoprotective mode? JOURNAL OF THE AMERICAN CHEMICAL SOCIETY 130 (13):4431–4446

Raszewski G, Diner BA, Schlodder E and Renger T. 2008. Spectroscopic properties of reaction center pigments in photosystem II core complexes: Revision of the multimer model. BIOPHYSICAL JOURNAL *in press* (avaliable on line)

Schlodder E, Renger T, Raszewski G , Coleman WJ, Nixon PJ, Cohen RO, Diner BA. 2008. Site-directed mutations at D1-Thr179 of photosystem II in Synechocystis sp PCC 6803 modify the spectroscopic properties of the accessory chlorophyll in the D1-branch of the reaction center. BIOCHEMISTRY 47(10):3143–3154

Raszewski G, Saenger W, Renger T. 2005. Theory of optical spectra of photosystem II reaction centers: Location of the triplet state and the identity of the primary electron donor. BIOPHYSICAL JOURNAL 88(2):986–998

Bzowska A, Koellner G, Wielgus-Kutrowska B, Stroh A, Raszewski G, Holy A, Steiner T, Frank J. 2004. Crystal structure of calf spleen purine nucleoside phosphorylase with two full trimers in the asymmetric unit: Important implications for the mechanism of catalysis. JOURNAL OF MOLECULAR BIOLOGY 342(3):1015–1032

Loll B, Raszewski G, Saenger W, Biesiadka J. 2003. Functional role of C^{α}–H$\cdots$O hydrogen bonds between transmembrane alpha-helices in photosystem I. JOURNAL OF MOLECULAR BIOLOGY 328(3):737–747

Koellner G, Stroh A, Raszewski G, Holy A, Bzowska A. 2003. Crystal structure of calf spleen purine nucleoside phosphorylase in a complex with multisubstrate analogue inhibitor with 2,6-diamino-purine aglycone. NUCLEOSIDES NUCLEOTIDES & NUCLEIC ACIDS 22(5-8): 1699-170